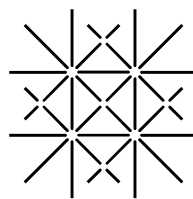


Excitation and Breakup of $\pi^+ \pi^-$ -Atoms at High Energies

INAUGURALDISSERTATION

zur
Erlangung der Würde eines Doktors der Philosophie
vorgelegt der
Philosophisch-Naturwissenschaftlichen Fakultät
der Universität Basel

von
Marc Schumann
aus Deutschland



UNI
BASEL

Basel, 2003

Genehmigt von der Philosophisch-Naturwissenschaftlichen Fakultät
auf Antrag der Herren Professoren:

Prof. Dr. Dirk Trautmann, Universität Basel
Prof. Dr. Jürg Schacher, Universität Bern

Basel, den 8. Juli 2003

Prof. Dr. Marcel Tanner, Dekan

For my wife Desirée

Abstract

The DIRAC collaboration at CERN currently aims at measuring the lifetime of ponium ($\pi^+\pi^-$ -atoms) with an accuracy of 10%. This is a crucial test of Chiral Perturbation Theory which predicts the lifetime to be (2.9 ± 0.1) fs. To be able to determine if the theory is correct is very important for our understanding of the low energy limit of the Standard Model of particle physics. To be able to extract the lifetime from the measurement of the breakup probability, theoretical input is needed to describe the Coulomb interaction with the target atoms. The first order Born approximation of ponium–target atom interaction has, by now, been calculated completely. The main task of this work is to evaluate higher order corrections to the excitation cross-sections in Glauber theory. It has been found that they are non-negligible for heavy target materials (up to 15% difference compared to the Born approximation). Due to the apparent importance of higher order terms, a coupled channel calculation was performed to investigate the accuracy of the Glauber approximation. Finally, a Monte Carlo simulation of ponium moving through the target was done to investigate the influence of the different cross-sections of ponium–target interaction. It was found that for small and medium Z , the lifetime of ponium depends very little on the choice of the cross section, but for large Z targets, the differences become quite important.

Zusammenfassung

Das Experiment DIRAC, das momentan am CERN durchgeführt wird, hat zum Ziel, die Lebensdauer von Ponium (einem $\pi^+\pi^-$ -Atom) mit einer Genauigkeit von mindestens 10% zu bestimmen. Diese Messung ist ein entscheidender Test der chiralen Störungstheorie, mit deren Hilfe eine Lebensdauer von (2.9 ± 0.1) fs vorhergesagt worden ist. Für unser Verständnis des Standardmodells der Teilchenphysik bei niedrigen Energien ist es sehr wichtig zu wissen, ob diese Theorie richtig ist. Um die Lebensdauer von Ponium aus der Messung der Ionisationswahrscheinlichkeit bestimmen zu können, wird eine theoretische Beschreibung der Coulomb-Wechselwirkung des Poniums mit den Targetatomen benötigt. Diese Wechselwirkung ist in erster Bornscher Näherung schon vollständig berechnet worden. Die Hauptaufgabe der vorliegenden Arbeit ist es, Korrekturen höherer Ordnung zu den Anregungsquerschnitten in der Glauber Näherung zu bestimmen. Diese Korrekturen dürfen nicht vernachlässigt werden, da sie für schwere Target-Atome die Wirkungsquerschnitte bis etwa 15% verringern können. Zur Überprüfung der Genauigkeit der Glauber Theorie wurde eine ‘gekoppelte Kanäle’ (coupled channel) Rechnung durchgeführt. Letztlich wurde in einer Monte-Carlo Simulation eines Poniums im Target ausgeführt. Hierbei wurde der Einfluss der verschiedenen Wirkungsquerschnitte auf die Lebensdauerbestimmung aus der Ionisationswahrscheinlichkeit untersucht. Das Ergebnis ist, dass für leichte und mittelschwere Targets, die Lebensdauer von Ponium nur sehr gering von der Wahl der Wirkungsquerschnitte (und damit der Näherungsverfahren ihrer Berechnung) abhängt. Lediglich für schwere Targetatome mit großer Kernladungszahl Z treten größere Unterschiede auf, und es ist daher sinnvoll die Querschnitte, die Korrekturen der Glaubernäherung beinhalten, zu verwenden.

Acknowledgements

I would like to thank Prof. Dr. Dirk Trautmann for his tremendous support during the last few years in Basel, also Prof. Dr. Gerhard Baur for all the interesting and informative discussions that took place when he was able to make the trip from Jülich to visit us in Basel. A special thanks to Prof. Dr. Raoul Viollier for having made it possible for me to stay in Cape Town after my BSc Honours year.

Thanks also go to PD Dr. Kai Hencken and PD Dr. Thomas Heim, who I could talk to about any problems and who always provided new ideas and insights. Further thanks go to Dr. Cibran Santamarina for a great collaboration on the Monte Carlo simulation.

Furthermore, thanks to my parents for their ongoing support and encouragement during my long studies. And last, but not least, to my wife, Desirée, for coming with me to Switzerland and for her endless patience, support and also criticism when needed.

Contents

Abstract	iii
Zusammenfassung	iii
Acknowledgements	v
1 General introduction	1
2 The experiment DIRAC	3
2.1 Introduction	3
2.2 Theoretical motivation	3
2.3 Production of ponium	5
2.4 Measurement of the breakup probability	6
2.5 Preliminary results	9
3 The quantum mechanical scattering process	11
3.1 The scattering amplitude	11
3.2 The Born approximation	13
3.3 The eikonal approximation	14
3.3.1 The eikonal approximation in one dimension	15
3.3.2 The eikonal approximation in three dimensions	17
3.3.3 The eikonal scattering amplitude	18
3.4 The Glauber approximation	19
3.4.1 Scattering by a bound particle	19
3.4.2 Many-body scattering	22
3.4.3 Cross sections in the Glauber approximation	23
4 Calculations in the first order Born approximation	25
4.1 The leading term: the scalar potential	25
4.1.1 Theory	25
4.1.2 Radial form factors	29
4.1.3 Results	32
4.2 Coherent and incoherent atomic scattering	34
4.2.1 Formalism	34
4.2.2 Atomic form factors	37
4.2.3 Numerical method and results	41
4.3 Corrections due to the magnetic terms	43
4.3.1 Corrections from the non-relativistic Hamiltonian	43

4.4	Conclusions	45
5	Excitation cross sections in Glauber approximation	47
5.1	Introduction	47
5.2	Coulomb interaction between pionium and the target atoms	47
5.2.1	Born approximation	49
5.2.2	Glauber approximation	50
5.3	Results	52
5.3.1	Relative differences between Glauber and Born approximation	52
5.3.2	Estimation of the accuracy of the Glauber approximation	55
5.4	Conclusion	56
6	Coupled channel calculation	59
6.1	Theory	59
6.2	Matrix element V_{kj} for bound-bound transitions	60
6.3	Solving the coupled channel equation	64
6.4	Continuum states	66
6.4.1	Rescaling of the amplitudes	68
6.4.2	Weyl wave packets	70
6.5	Conclusion	71
7	Monte Carlo simulation	73
7.1	The simulation	73
7.1.1	Pionium production	73
7.1.2	Pionium annihilation	74
7.1.3	Electromagnetic interaction of pionium with the target	75
7.1.4	Pionium evolution in the target	76
7.2	Breakup probability calculation	77
7.2.1	Computational difficulties due to physical characteristics of the problem	78
7.2.2	Calculation procedure	80
7.3	Cross section sets	81
7.4	Results and conclusions	85
8	Conclusions and outlook	89
	Bibliography	91
	Lebenslauf	95

List of Figures

2.1	Creation of $\pi^+\pi^-$ -atoms and Coulomb $\pi^+\pi^-$ pairs.	6
2.2	Time of flight difference distribution.	7
2.3	Distribution of Coulomb pairs and fitted distributions for the background and distribution of n_A after subtracting background.	8
4.1	A relativistic heavy nucleus with charge Z is moving past a pionium atom.	26
4.2	The excitation probability P_{fi}^B as a function of the impact parameter b	33
4.3	The charge distribution determined from the analytical fit to the Dirac-Hartree-Fock-Slater ground state wave functions.	33
4.4	The total inelastic cross section from different initial states.	34
4.5	The lowest order Feynman diagram for the simultaneous excitation of projectile (pionium) and target (atom).	35
4.6	Electronic part F_{00} of the coherent atomic form factor and incoherent scattering function S_{inc} for Ti ($Z = 22$).	40
4.7	Various contributions to the integrand for the cross section vs. q_{\perp}	42
4.8	Integrand for incoherent (target-inelastic) cross section.	42
5.1	An atom is moving past a pionium atom at relativistic speed $v \approx c$	48
5.2	Comparison of the transition probabilities for the transition 1s–2p of the pionium due to the Coulomb interaction with a Ni ($Z = 28$) atom.	51
5.3	The Z -dependence of the relative correction δ_{fi} to the excitation cross sections for the three transitions 1s–2p, 2p–3d, and 2s–3p.	52
5.4	Comparison of the contributions of two- and three-photon exchange processes to the relative correction to the excitation cross section for a 1s–2p transition in Glauber theory.	55
5.5	The higher order corrections to the excitation cross-section.	56
6.1	Time evolution of the occupation probabilities of pionium states (Pt, $b = 1 a_{\pi}$).	65
6.2	Time evolution of the occupation probabilities of pionium states (Pt, $b = 3 a_{\pi}$).	65
6.3	Comparison of coupled channel calculation for bound states only with the results from the Born and Glauber approximation. Plotted is the transition probability from a pionium 1s to a 2p state. The target is Pt ($Z = 78$).	66

6.4	Comparison of a coupled channel calculation for bound states only, with the results from the Born and Glauber approximation. Plotted is the transition probability from a pionium 1s to a 2p state. The target is Ni ($Z = 28$).	67
6.5	Comparison of a coupled channel calculation for bound states only, with the results from the Born and Glauber approximation. Plotted is the transition probability from a pionium 1s to 3p and 4p states. The target is Pt ($Z = 78$).	67
6.6	Comparison of a coupled channel calculation for bound states only, with the results from the Born and Glauber approximation. Plotted is the transition probability from a pionium 1s to 3p and 4p states. The target is Ni ($Z = 28$).	68
6.7	The transition probabilities for pionium interacting with a Pt target as a function of t_0 , the time when a rescaling due to ionization is applied. The impact parameter $b = 1 a_\pi$	69
6.8	The transition probability from a 1s to a 2p state for pionium interacting with a Pt target, as a function of the impact parameter b	69
6.9	The transition probability from a 1s to a 2p state for pionium interacting with a Ni target, as a function of the impact parameter b	70
7.1	Laboratory momentum magnitude and angular distribution of low relative momentum $\pi^+\pi^-$ -atoms.	74
7.2	Annihilation, ionization, de-excitation and excitation probabilities per unit length.	77
7.3	Probabilities of finishing the evolution in a discrete state, by annihilation, or by ionization as a function of the parent state's principal quantum number.	79
7.4	The breakup, annihilation, and discrete probabilities as a function of lifetime, breakup and annihilation position distributions, and creation position of those atoms that leave the target in a bound state . .	82
7.5	Comparison of the <i>Born1</i> , <i>Born2</i> , and <i>Glauber</i> cross section sets for Titanium ($Z = 22$), Nickel ($Z = 28$), and Platinum ($Z = 78$). . . .	84
7.6	The breakup probability results for the three cross section sets and the three target materials.	87

List of Tables

5.1	Comparison of the relative differences of the accumulated excitation cross sections for various initial states.	54
7.1	Results for the different probabilities defined in (7.16), as calculated with the <i>Born2</i> cross section set for a sample of ten million pionic atoms in a 95 μm thick Nickel target.	81
7.2	Comparison of the breakup probability results for the Ti 251 μm , the Ni 95 μm and the Pt 28 μm targets. The lifetime value is assumed to be $3 \cdot 10^{-15}$ s in the calculations.	86

1 General introduction

The Standard Model of particle physics successfully describes the fundamental particles and forces. Within the Standard Model, quantum chromodynamics (QCD) is the theory for the dynamics of strongly interacting particles, the quarks and gluons [1, 2, 3, 4, 5]. One of the features of QCD is asymptotic freedom, which allows one to use perturbation theory for calculations involving particles interacting through high momentum transfers. The low-energy regime, however, can only be treated non-perturbatively. Using a special symmetry of the full QCD Lagrangian in the limit of massless quarks (chiral limit), one can write down a new effective theory, chiral perturbation theory, that describes the strong interaction at low energies, but now in terms of the pion-fields instead of the quark and gluons [6, 7, 8, 9].

While the Lagrangian of QCD in the chiral limit (massless quarks) is symmetric under chiral symmetry, the ground state is not. Therefore, there are Goldstone bosons, which are massless in the chiral limit and are pseudoscalars just as the pions. These Goldstone bosons do not interact at zero momentum, therefore the scattering lengths describing this interaction are zero in this limit. Weinberg [6] showed that the scattering lengths of the pions are related to the masses of the up and down quarks, and are therefore a measure of the chiral symmetry breaking.

The isoscalar and isotensor s-wave scattering lengths for pion-pion scattering (a_0 and a_2) have been evaluated with ever increasing accuracy [6, 9, 10, 11]. The difference between these scattering lengths squared turns out to be inversely proportional to the lifetime of ponium, the $\pi^+\pi^-$ -atom. As there is no experimental data accurate enough to verify or reject the results obtained from chiral perturbation theory, the experiment DIRAC (Dimeson Relativistic Atom Complex) has been designed to measure the lifetime of ponium and thus the difference of the scattering lengths [12]. The basic idea is to determine experimentally the breakup probability of ponium and then to use theoretical input regarding the electromagnetic interaction of ponium with the atoms in the target strip to determine the lifetime. In chapter 2 I will outline how the breakup probability is measured and in chapter 7 I will give details of how to determine the lifetime from the breakup probability.

The electromagnetic interaction of ponium with the target atoms has been an ongoing research interest in the Trautmann group since the inception of the experiment DIRAC. The ponium–target atom system is an ideal case to apply the semi-classical approximation, in which the $\pi^+\pi^-$ -atom is treated quantum mechanically and the target atom as a classical particle on a straight line trajectory. In a series of papers, the first order Born approximation has been completely evaluated for ponium–target atom scattering, including incoherent scattering off the target atom’s electrons and relativistic corrections [13, 14, 15]. I will give a review of these papers in chapter 4,

after a general overview on quantum mechanical scattering and the Born and Glauber approximation in chapter 3.

It was found by Afanasyev *et al* [16] that the total cross sections for ponium interacting with a target atom via the scalar part of the potential, calculated in Glauber approximation, differ from the ones found in Born approximation by up to about 10% for heavy targets. This indicates that higher order effects, such as multi-photon exchange, are important and must be included in the full calculation of the cross sections. To obtain a meaningful result for the lifetime from the experiment, it was expected that the cross sections could be calculated with an accuracy of 1% or better. The main task for this thesis was thus to calculate the excitation cross sections for ponium in the Glauber theory. In the case of the total cross sections the closure relation leads to a one-dimensional integral, that can be evaluated numerically with little effort. The excitation cross sections for a transition between arbitrary states cannot be simplified this way and extensive numerical calculations were required. The methods and results are discussed in chapter 5. They have already been published in [17].

Since the results obtained in Glauber and Born approximation differ by up to around 20% for the excitation cross sections, it is important to clarify which one is correct. This was attempted in a coupled channel calculation. The results are not conclusive as yet. The main problem is the coupling to the continuum which is a very delicate numerical problem. The details are given in chapter 6.

Finally, to relate the lifetime of ponium to its breakup probability a Monte Carlo simulation of the passage of ponium through the target material is performed. The results for the cross sections calculated in Born approximation and the ones combining the results of the Born approximation in first order with the Glauber approximation for higher order contributions are compared to another set of cross sections in first order sudden approximation using also a slightly different parameterization of the screened Coulomb potential [18]. The details of the simulation are given in chapter 7. The simulation is based on previous work by Santamarina [19]. The new results have been submitted for publication [20].

In the final chapter some conclusions are drawn from the work presented here and an outlook for possible future investigations are given.

2 The experiment DIRAC

2.1 Introduction

The aim of the experiment DIRAC is to measure the lifetime of the exotic atom, pionium, with an accuracy of 10% [12]. A 24 GeV/ c proton beam hits a target foil and produces (among many other particles) π^+ and π^- . Those pions with a low relative momentum ($q < 3$ MeV/ c) may form Coulomb-bound exotic atoms, pionium [21]. Moving through the target, pionium can decay via the strong interaction into two neutral pions (if it is still in a relative s-state), enter an excited state or even ionize due to the Coulomb interaction with the target atoms. The ionized pionium is detected by the experiment and from the accidental pairs that also enter the detector, one can calculate the initial number of pionium atoms. From the ration of ionized to produced pionium, one gets the breakup probability. With a Monte Carlo simulation of the evolution of pionium in the target, one can relate the breakup probability to the lifetime (see also chapter 7).

The lifetime is also related to the s-wave $\pi\pi$ -scattering lengths, a_0 and a_2 , with isospin zero and two, respectively. These scattering lengths are calculated using Chiral Perturbation Theory and the expected lifetime is $\tau = (2.9 \pm 0.1)$ fs [8, 9, 22, 23]. The purpose of this experiment is to test this very accurate prediction.

In this chapter, I will outline the motivation for the experiment in section 2.2, the production mechanism for pionium in section 2.3, and give a brief overview of the method of determining the breakup probability experimentally in section 2.4. Since the methods for determining the breakup probability accurately are continuously refined, this section can only give the main ideas behind the procedure. The chapter ends by stating some preliminary results for the lifetime measurement that have become available through presentations of members of the DIRAC collaboration.

2.2 Theoretical motivation

Quantum chromodynamics (QCD) is the non-Abelian gauge theory describing the strong interaction between colored quarks and gluons [1, 2, 3, 4, 5]. Its most important features are asymptotic freedom and color confinement. Due to asymptotic freedom one can successfully apply perturbation theory for interactions involving large momentum transfers. For low energy transfers, one needs to treat QCD non-perturbatively. There are two ways to proceed, lattice QCD, and chiral perturbation theory [7, 8, 9].

If one considers QCD with only the light quarks, up and down (and possibly strange) quarks, one notes that in the limit of zero quark masses, the Lagrangian of QCD is invariant under chiral $SU(2)_L \times SU(2)_R$ transformations, but the ground state of the theory is asymmetric under the action of this symmetry group. This is also called spontaneous breakdown of chiral symmetry. Thus the theory contains three massless pseudoscalar particles, the Goldstone bosons. The three lightest known hadrons, the pions, are also pseudoscalars, but not massless. Since the full QCD Lagrangian is not invariant under chiral symmetry because even the light quarks have a mass, these masses, m_u and m_d break the symmetry and provide the mass of the pions.

Massless (theoretical) Goldstone bosons with zero momentum do not interact at all, and the scattering length describing such an interaction are therefore zero in the chiral limit. Pions (π^+ and π^-) are anti-particles and do interact via the strong interaction. The scattering lengths describing the pion-pion interaction can therefore be seen as a measure of chiral symmetry breaking due to the fact that even the light quarks are not massless. The difference between the isoscalar and isotensor scattering length $\Delta = a_0 - a_2$, can be evaluated in chiral perturbation theory by a perturbation series in powers and logarithms of the pion mass,

$$\Delta = \Delta_0 (1 + \Delta_2 m_\pi^2 + \Delta_4 m_\pi^4 + \dots) . \quad (2.1)$$

Weinberg [6] showed that the leading term Δ_0 is given by

$$\Delta_0 = \frac{9m_\pi^2}{32\pi F_\pi^2} = 0.20 , \quad (2.2)$$

where m_π is the pion mass and $4\pi F_\pi \approx 1.2$ GeV set the scale. Δ_2 is found by evaluating one-loop diagrams [9]. Two-loop calculations have been performed recently [10]. The most accurate result to date, up to two-loop level using Roy equations [11], is

$$\Delta = 0.265 \pm 0.004 (1.5\%) . \quad (2.3)$$

The main decay channel for pionium is via the charge exchange

$$\pi^+ + \pi^- \rightarrow \pi^0 + \pi^0 \quad (2.4)$$

with a branching ratio of 96.6% [21]. Its lifetime is therefore inversely proportional to the width $\Gamma_{2\pi^0}$ of this decay channel. This width can be given in terms of constants that have been calculated in chiral perturbation theory [23]

$$\Gamma_{2\pi^0} = \frac{2}{9} \alpha^3 p^* A^2 (1 + K) \quad (2.5)$$

where α is the fine structure constant and

$$\begin{aligned} A &= (a_0 - a_2) + \epsilon \\ a_0 - a_2 &= 0.265 \pm 0.004 \\ \epsilon &= (6.1 \pm 1.6) \cdot 10^{-3} \\ K &= (1.15 \pm 0.03) \cdot 10^{-2} . \end{aligned} \quad (2.6)$$

Gasser et al. [23] found the lifetime of pionium to be

$$\tau_0 = (2.9 \pm 0.1) \text{ fs} . \quad (2.7)$$

2.3 Production of pionium

Pions are produced by interactions of the 24 GeV/ c protons of the CERN Proton Synchrotron with the nuclei of a target foil. They may combine to form pionium if their relative momentum is low, i.e. less than 3 MeV/ c . We can therefore give the probability of pionium production in terms of the double inclusive cross section ($d\sigma^0/d\mathbf{p}_1 d\mathbf{p}_2$) for the production of a π^+ and a π^- with small relative momentum and the pionium wavefunction at the origin,

$$\frac{d\sigma_{nlm}^A}{d\mathbf{P}} = (2\pi)^3 \frac{E}{M} |\psi_{nlm}(0)|^2 \left. \frac{d\sigma_s^0}{d\mathbf{p}_1 d\mathbf{p}_2} \right|_{\mathbf{p}_1=\mathbf{p}_2=\mathbf{P}/2}, \quad (2.8)$$

where \mathbf{P} , E , and M are momentum, energy and mass of the pionium in the laboratory system, respectively. The two terms on the right-hand side of the equation illustrate the final state interaction mechanism. The rightmost factor is the doubly inclusive cross section of π^+ and π^- pairs at equal momenta ($\mathbf{p}_1 = \mathbf{p}_2$) without considering the final state interaction, as indicated by the superscript 0. The subscript s means that only pions created from direct hadronic processes and decays of resonances with a very short lifetime are considered, because the Coulomb interaction of pions from long-lived sources (e.g. η , K_S^0 and Λ) is negligible and hence they do not contribute to the production of pionic atoms. The effect of the final state Coulomb interaction is to create a bound state with quantum numbers n , l , and m ; it is given by the squared wave function at the origin. Due to this factor, pionium can only be produced in an initial s -wave, since $|\psi_{nlm}(0)|^2 = 0$ for $l, m \neq 0$.

The doubly inclusive cross section can be obtained from the direct measurements of time correlated $\pi^+\pi^-$ pairs in DIRAC, according to the following reasoning:

- The final state Coulomb interaction for short-lived sources is given, as in the case of the creation of a bound state, by a multiplicative factor depending only on q , the magnitude of the relative momentum between the two pions. This is the so-called Coulomb or Gamow factor [24]

$$\frac{d\sigma_s}{d\mathbf{p}_1 d\mathbf{p}_2} = A_C(q) \frac{d\sigma_s^0}{d\mathbf{p}_1 d\mathbf{p}_2}; \quad A_C(q) = \frac{2\pi M_\pi \alpha / q}{1 - e^{-2\pi M_\pi \alpha / q}}, \quad (2.9)$$

where α is the fine structure constant.

- The contribution to the doubly inclusive cross section of pairs containing at least one pion from a long-lived source, $\omega_l(\mathbf{P})$, can be calculated with a hadron physics Monte Carlo simulation. In this case FRITIOF6 was used [25, 26, 27]. This function has been shown to depend only on P , the magnitude of the total momentum of the pion pair [28]. Taking this into account together with (2.9) one finds

$$\frac{d\sigma}{d\mathbf{p}_1 d\mathbf{p}_2} = \frac{d\sigma_s}{d\mathbf{p}_1 d\mathbf{p}_2} + \frac{d\sigma_l}{d\mathbf{p}_1 d\mathbf{p}_2} = A_C(q) \frac{d\sigma_s^0}{d\mathbf{p}_1 d\mathbf{p}_2} + \omega_l(P) \frac{d\sigma}{d\mathbf{p}_1 d\mathbf{p}_2}, \quad (2.10)$$

thus relating σ and σ_s^0 .

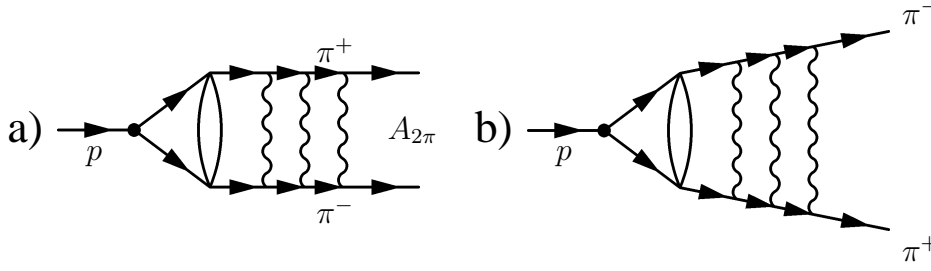


Figure 2.1: Creation of (a) $\pi^+\pi^-$ -atoms and (b) Coulomb $\pi^+\pi^-$ pairs in the collision of a proton with a target nucleus. Both bound and free $\pi^+\pi^-$ pairs shown here have final state Coulomb interactions distinguishing them from the not shown non-Coulomb pairs arising from the decay of long-lived particles.

- Finally, it was found that the P -dependence of the doubly inclusive cross section is not correlated to q , given that $q \ll 30 \text{ MeV}/c$.

These findings allow one to relate the P -dependence of σ and σ_s^0 by

$$\left. \frac{d\sigma_s^0}{d\mathbf{p}_1 d\mathbf{p}_2} \right|_{p_1=p_2=P/2} \propto \int_0^{q \sim 2 \text{ MeV}/c} (1 - \omega_l(P)) \frac{d\sigma}{d\mathbf{p}_1 d\mathbf{p}_2} d\mathbf{q}, \quad (2.11)$$

where the P distribution is obtained from the direct measurement of the laboratory momentum of low relative momentum $\pi^+\pi^-$ pairs in DIRAC. In figure 7.1 we show the distribution of the magnitude of the momentum P and the angular distribution relative to the proton beam axis for low relative momentum $\pi^+\pi^-$ pairs.

2.4 Measurement of the breakup probability P_{br}

Since the expected lifetime of pionium is very small, one can only observe $\pi^+\pi^-$ -atoms from the breakup due to Coulomb interaction with the target. We have shown in the previous section that the $\pi^+\pi^-$ pairs are produced either as free or bound states (pionium). The pionium may annihilate or get ionized into $\pi^+\pi^-$ pairs. The breakup probability will depend on the target material, its thickness, the pionium momentum and the lifetime. This will be detailed in chapter 7. Experimentally, one needs to know the number of produced $\pi^+\pi^-$ -atoms, N_A , and the number of ionized $\pi^+\pi^-$ pairs, n_A .

Using a time of flight measurement (see figure 2.2), one determines first the number of real $\pi^+\pi^-$ pairs by subtracting the accidental pairs detected in the intervals N1 ($-15.0 < \Delta t < -0.5 \text{ ns}$) and N4 ($7.0 < \Delta t < 17.0 \text{ ns}$). The intervals are chosen asymmetrically because of the slight asymmetry of the coincidence peak due to slower protons and kaons being detected in the positive arm of the spectrometer.

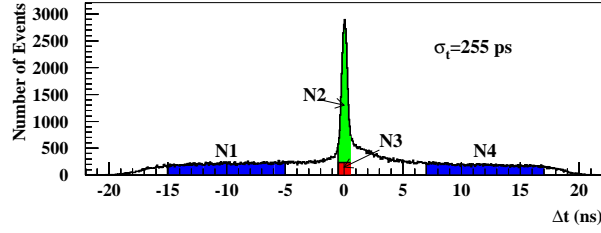


Figure 2.2: Time of flight difference distribution for oppositely charged hadrons. The regions N1 and N4 are used to determine the size of the accidental pair contribution N3 to the correlated pairs N2. (Reproduced from [29].)

For large relative momenta q , the real $\pi^+\pi^-$ pairs (i.e. the coincidence pairs N2) can be described by the sum of Coulomb and non-Coulomb free $\pi^+\pi^-$ pairs

$$\frac{dN^{\text{real}}}{dq} = \frac{dN_s^{\text{real}}}{dq} + \frac{dN_l^{\text{real}}}{dq}, \quad q > 4 \text{ MeV} \quad (2.12)$$

from short-lived (s) and long-lived (l) sources, respectively. On the other hand, it is known that

$$\frac{dN^{\text{acc}}}{dq} \sim \frac{dN_l^{\text{real}}}{dq} \sim \Phi(q), \quad (2.13)$$

while the Coulomb pairs stemming from short-lived sources are distributed according to

$$\frac{dN_s^{\text{real}}}{dq} \sim \Phi(q)A_c(q)(1 + kq), \quad (2.14)$$

where the Coulomb factor $A_c(q)$ (2.9) takes into account the Coulomb interaction and the term $(1 + kq)$ the strong interaction in the final state. Combining (2.13) and (2.14) we can approximate the distribution of real $\pi^+\pi^-$ pairs as

$$\frac{dN^{\text{real}}}{dq} = N\Phi(q) [(1 + kq)A_c(q) + f], \quad (2.15)$$

where N , k , and f are parameters found by fitting (2.15) to the measured distribution for $q > 3 \text{ MeV}$.

The number of $\pi^+\pi^-$ pairs that were ionized in the target can now be found by extrapolating the fitted distribution (2.15) to the region of $q < 2 \text{ MeV}$ and subtracting it from the total measured distribution in the same relative momentum region.

$$n_A = N_{\text{exp}}^{\text{real}} - \int_{q < 2 \text{ MeV}} dq \left(\frac{dN^{\text{real}}}{dq} \right). \quad (2.16)$$

Figure 2.3 shows the data of measured Coulomb pairs from the 2001-run of the DIRAC experiment using a Ni target. The left graph also indicates the background

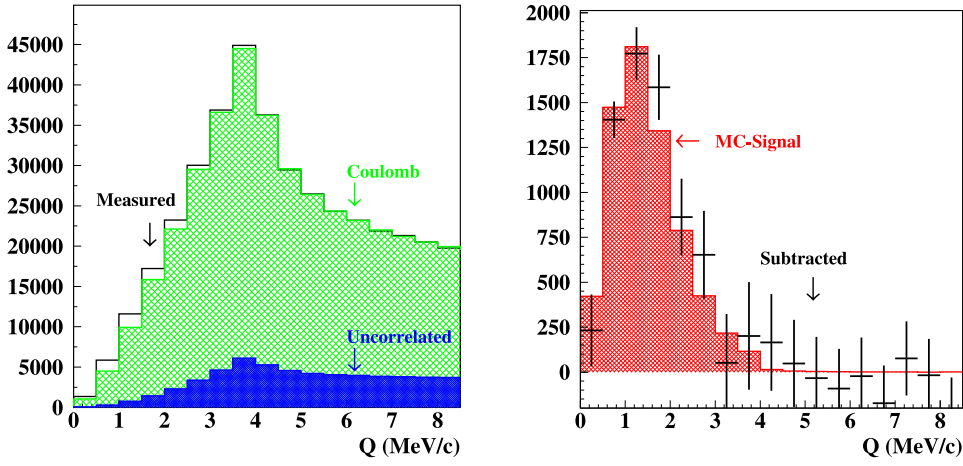


Figure 2.3: The left graph shows the measured distribution for the Coulomb pairs and the fitted Coulomb and uncorrelated background. The excess for small q corresponds to ionized pionium. The right figure shows the distribution of n_A after subtracting the background. The data is compared to a Monte Carlo simulation. Both graphs refer to data taken with a Ni target in 2001. (Reproduced from [30].)

from Coulomb pairs and from uncorrelated pairs that was fitted to the measured data according to the procedure outlined above. One can clearly see the small amount of signal excess for small q corresponding to the pionic pairs. The graph on the right shows the distribution of the pionic pairs after subtraction of the background [30]. The excess amounts to about 6800 ± 400 atomic pion pairs.

This is only the first ingredient for the measurement of the breakup probability $P_{br} = n_A/N_A$. The total number of $\pi^+\pi^-$ -atoms produced, is found by recognizing that in (2.8) and (2.9) both the number of produced $\pi^+\pi^-$ -atoms and the number of produced Coulomb pairs are proportional to the production cross section $d\sigma_s^0/d\mathbf{p}_1\mathbf{p}_2$ of two pions. Their ratio is therefore

$$\frac{N_A}{N_s^{\text{real}}} = K, \quad \text{for } q < 2 \text{ MeV}, \quad (2.17)$$

where

$$K = 0.62 \pm 0.01. \quad (2.18)$$

So finally, one can combine (2.16) and (2.17) to obtain a value for the breakup probability for a given target

$$P_{br} = \frac{n_A}{KN_s}. \quad (2.19)$$

This value can then be used to determine the lifetime of pionium with the help of the Monte Carlo simulation which is discussed in detail in chapter 7.

2.5 Preliminary results

Great care has been taken in the calibration of the detectors. This is very important as the momentum- and time-resolution needs to be very high. The momentum resolution, for example, can be verified by measuring the mass distribution of $p\pi^-$ pairs, which shows a sharp peak at the mass of the Λ (see for example [31]). As the experiment is ongoing, only preliminary results are available. The lifetime of ponium from measurements with a Ni target taken in 2000 and with a Ti target in 2000–2001 yield a combined value of (3.6 ± 0.9) fs [29]. Since then, data-taking has continued, especially with the Ni target. Ni is best suited for a lifetime of around 3 fs, since the curve relating the breakup probability and the lifetime of ponium is steepest for Ni around a lifetime of 3 fs (refer to 7.4).

3 The quantum mechanical scattering process

Before discussing the pionium-specific calculations of the excitation cross sections in the Born and Glauber approximation, I would like to give a general overview of quantum mechanical scattering and the Born- and Glauber-approximation in general.

The process of atom–atom scattering is governed by quantum mechanics. The usual approach is to consider a target atom in an initial state $|u_i\rangle$ that interacts with the potential of an incident projectile and is left in a final state $|u_f\rangle$ after the collision. In pionium–target-atom scattering, in the lab-frame the projectile is the pionium and the target is the atom in the target material. But since we are interested in the excitation of the $\pi^+\pi^-$ -atom, we have to boost the coordinate frame to the rest frame of pionium and look at the ‘target-atom’ as the projectile. The terminology is unfortunately somewhat confusing.

In this chapter we will outline the basic idea of a quantum mechanical scattering problem. Various approximation methods are commonly used this solve the problem. The Born, the eikonal and the Glauber approximation, which will be used in the following chapters, are introduced here.

3.1 The scattering amplitude

The simplest scattering problem is a spinless particle of mass m interacting with a localized potential $V(\mathbf{r})$ with a characteristic length scale (range) a . The energy of the incident particle is then $E = \hbar^2 k^2 / 2m$, where the wavevector \mathbf{k} describes the propagation of the incident wave.

We need to solve the Schrödinger equation

$$(\nabla^2 + k^2) \psi(\mathbf{r}) = \frac{2m}{\hbar^2} V(\mathbf{r}) \psi(\mathbf{r}), \quad (3.1)$$

and the solution needs to fulfill the requirement that asymptotically it can be written in terms of the incident wave plus an outgoing spherical wave with a scattering amplitude f , i.e.,

$$\psi(\mathbf{r}) \sim e^{i\mathbf{k}\cdot\mathbf{r}} + f(\mathbf{k}_f, \mathbf{k}_i) \frac{e^{ikr}}{r}. \quad (3.2)$$

The differential cross section is then given by the square of the scattering amplitude,

i.e.

$$\frac{d\sigma}{d\Omega} = |f(\mathbf{k}_f, \mathbf{k}_i)|^2 . \quad (3.3)$$

One possible ansatz to solve the Schrödinger equation (3.1) is to introduce a Green's function $G(\mathbf{r}, \mathbf{r}')$ that is defined as the solution of

$$(\nabla^2 + k^2) G(\mathbf{r}, \mathbf{r}') = \frac{2m}{\hbar^2} \delta^3(\mathbf{r} - \mathbf{r}') . \quad (3.4)$$

A general solution to the equation above is given by

$$G(\mathbf{r}, \mathbf{r}') = -\frac{2m}{4\pi\hbar^2} \frac{\alpha e^{ik|\mathbf{r}-\mathbf{r}'|} + \beta e^{-ik|\mathbf{r}-\mathbf{r}'|}}{|\mathbf{r} - \mathbf{r}'|} , \quad \alpha + \beta = 1 . \quad (3.5)$$

We are looking for a solution of the Schrödinger equation that behaves asymptotically as stated in (3.2), therefore we set $\alpha = 1$ and obtain

$$G(\mathbf{r}, \mathbf{r}') = -\frac{2m}{4\pi\hbar^2} \frac{e^{ik|\mathbf{r}-\mathbf{r}'|}}{|\mathbf{r} - \mathbf{r}'|} . \quad (3.6)$$

The solution to the Schrödinger equation (3.1) can now be expressed as an integral equation (Lippmann-Schwinger equation):

$$\psi(\mathbf{r}) = e^{i\mathbf{k}_i \cdot \mathbf{r}} + \int G(\mathbf{r}, \mathbf{r}') V(\mathbf{r}') \psi(\mathbf{r}') d^3r' . \quad (3.7)$$

To verify the asymptotic form of the solution of (3.7) we expand the terms in the integral for $r \gg r'$. Firstly, we have

$$|\mathbf{r} - \mathbf{r}'| \xrightarrow{r \gg r'} r - \frac{\mathbf{r} \cdot \mathbf{r}'}{r} . \quad (3.8)$$

As was mentioned at the beginning of this section, the potential V has a limited range (or at least falls off asymptotically faster than $1/r$), so that the integration of r' is of a limited range as well. Therefore, the assumption of $r \gg r'$ for large r is reasonable. If we now insert $G(\mathbf{r}, \mathbf{r}')$ of (3.6) into (3.7) and use the approximation (3.8) we obtain

$$\psi(\mathbf{r}) = e^{i\mathbf{k} \cdot \mathbf{r}} - \frac{2m}{4\pi\hbar^2} \int \frac{e^{ik|\mathbf{r}-\mathbf{r}'|}}{|\mathbf{r} - \mathbf{r}'|} V(\mathbf{r}') \psi(\mathbf{r}') d^3r' \quad (3.9)$$

$$\xrightarrow{r \gg r'} e^{i\mathbf{k} \cdot \mathbf{r}} - \frac{2m}{4\pi\hbar^2} \frac{e^{ikr}}{r} \int e^{-ik\frac{\mathbf{r} \cdot \mathbf{r}'}{r}} V(\mathbf{r}') \psi(\mathbf{r}') d^3r' . \quad (3.10)$$

Comparing equations (3.2) and (3.10) we read off the scattering amplitude

$$f(\mathbf{k}_f, \mathbf{k}_i) = -\frac{2m}{4\pi\hbar^2} \int e^{-i\mathbf{k}_f \cdot \mathbf{r}'} V(\mathbf{r}') \psi_{\mathbf{k}_i}(\mathbf{r}') d^3r' , \quad (3.11)$$

where we introduced $\mathbf{k}_f = k\mathbf{r}/r$ and $\mathbf{k}_i = \mathbf{k}$. The subscript \mathbf{k}_i on the wave function $\psi_{\mathbf{k}_i}$ indicates that $\psi_{\mathbf{k}_i}$ is found by solving the Lippmann-Schwinger equation for an initial plane wave with a wave vector \mathbf{k}_i .

We have now found an expression for the scattering amplitude, even though we still need to insert the wave function that solves the Schrödinger equation (3.1) or the Lippmann-Schwinger equation (3.9). However, the expression for the scattering amplitude has one major advantage, the integral contains the product $V(\mathbf{r})\psi(\mathbf{r})$. As noted above, V has a localized range and, therefore, to find $f(\mathbf{k}_f, \mathbf{k}_i)$, we only need to (approximately) know ψ over the range of the potential V .

Before we continue to the approximation methods, we show without proof two important identities fulfilled by the scattering amplitude.

1. Dynamical reversibility:

$$f(\mathbf{k}_f, \mathbf{k}_i) = f(-\mathbf{k}_i, -\mathbf{k}_f) . \quad (3.12)$$

2. Balancing symmetry, if $V(\mathbf{r}) = V(-\mathbf{r})$:

$$f(\mathbf{k}_f, \mathbf{k}_i) = f(-\mathbf{k}_f, -\mathbf{k}_i) = f(\mathbf{k}_i, \mathbf{k}_f) . \quad (3.13)$$

3.2 The Born approximation

The Born approximation is simply a perturbation series expansion of the scattering amplitude in powers of the scattering potential. We write as an ansatz

$$\psi_{\mathbf{k}_i}(\mathbf{r}) = \sum_{n=0}^{\infty} \phi_n(\mathbf{r}) , \quad (3.14)$$

where ϕ_0 is a plane wave

$$\phi_0(\mathbf{r}) = e^{i\mathbf{k}_i \cdot \mathbf{r}} \quad (3.15)$$

and

$$\phi_n(\mathbf{r}) = \int K_n(\mathbf{r}, \mathbf{r}') \phi_0(\mathbf{r}') d^3r' \quad n \geq 1 . \quad (3.16)$$

The kernel K is defined as

$$K_1(\mathbf{r}, \mathbf{r}') = G(\mathbf{r}, \mathbf{r}') V(\mathbf{r}') , \quad (3.17)$$

$$K_n(\mathbf{r}, \mathbf{r}') = \int K_1(\mathbf{r}, \mathbf{r}'') K_{n-1}(\mathbf{r}'', \mathbf{r}') d^3r'' \quad n \geq 2 . \quad (3.18)$$

Inserting the series expansion (3.14) into (3.11) and writing out the first few terms we obtain

$$f^B(\mathbf{k}_f, \mathbf{k}_i) = -\frac{2m}{4\pi\hbar^2} \left[\int e^{-i\mathbf{k}_f \cdot \mathbf{r}} V(\mathbf{r}) e^{i\mathbf{k}_i \cdot \mathbf{r}} d^3r + \iint e^{-i\mathbf{k}_f \cdot \mathbf{r}} V(\mathbf{r}) G(\mathbf{r}, \mathbf{r}') V(\mathbf{r}') e^{i\mathbf{k}_i \cdot \mathbf{r}'} d^3r d^3r' + \dots \right] . \quad (3.19)$$

We can now write the Born series for the scattering amplitude as

$$f^B(\mathbf{k}_f, \mathbf{k}_i) = \sum_{n=1}^{\infty} \bar{f}_n^B(\mathbf{k}_f, \mathbf{k}_i), \quad (3.20)$$

where

$$\bar{f}_1^B(\mathbf{k}_f, \mathbf{k}_i) = -\frac{2m}{4\pi\hbar^2} \int e^{-i\mathbf{k}_f \cdot \mathbf{r}} V(\mathbf{r}) e^{i\mathbf{k}_i \cdot \mathbf{r}} d^3r, \quad (3.21)$$

$$\bar{f}_n^B(\mathbf{k}_f, \mathbf{k}_i) = -\frac{2m}{4\pi\hbar^2} \int e^{-i\mathbf{k}_f \cdot \mathbf{r}} V(\mathbf{r}) K_{n-1}(\mathbf{r}, \mathbf{r}') d^3r' d^3r \quad (3.22)$$

$$= -\frac{2m}{4\pi\hbar^2} \int \dots \int e^{-i\mathbf{k}_f \cdot \mathbf{r}} V(\mathbf{r}) G(\mathbf{r}, \mathbf{r}') \dots V(\mathbf{r}^{(n-1)}) \\ \times e^{i\mathbf{k}_i \cdot \mathbf{r}^{(n-1)}} d^3r \dots d^3r^{(n-1)}, \quad (3.23)$$

where \bar{f}_n^B contains the potential V n times and the Green's function G , $(n-1)$ times. The Born approximation of order j is then defined as

$$f_j^B(\mathbf{k}_f, \mathbf{k}_i) = \sum_{n=1}^j \bar{f}_n^B(\mathbf{k}_f, \mathbf{k}_i). \quad (3.24)$$

The Born series can thus be seen as a multiple scattering series in which the particle interacts with the potential repeatedly and propagates freely in-between. For large enough energies and/or a sufficiently weak or screened potential, the series should converge. More specifically, the rate of convergence is dependent on the strength of the potential V and the time spent in the region of the potential which is a/v . The requirement for the convergence of the Born series is that the passage time a/v is much smaller than the time \hbar/V required for the potential to influence the projectile, i.e.

$$\frac{Va}{\hbar v} \ll 1. \quad (3.25)$$

In the following chapter (p. 25) we will apply the first order Born approximation to the pionium–target atom scattering.

3.3 The eikonal approximation

For projectiles with large enough energies and momenta, one can make an approximation using less stringent conditions than (3.25). Instead, two separate conditions are introduced which are easily fulfilled in usual high-energy experiments. The first requirement is that the magnitude of the potential is much less than the energy of the projectile,

$$\frac{V}{E} \ll 1, \quad (3.26)$$

and the second condition is that the de Broglie-wavelength of the projectile is much smaller than the typical range of the potential, i.e.

$$ka \gg 1 . \quad (3.27)$$

The second condition is also referred to as the semi-classical condition. Under these two conditions we can derive the high-energy or eikonal approximation [32, 33, 34].

3.3.1 The eikonal approximation in one dimension

The basic ideas of the high-energy approximation are already seen by examining a one-dimensional scattering process. This process is not very realistic, as the only possible outcomes are forward- and backward-scattering (which is even neglected), but it best illustrates the mathematical procedure [32]. There are many ways to approach this problem. We will examine two of them.

The Schrödinger equation in one dimension is given by

$$\left(\frac{d^2}{dx^2} + k^2 \right) \psi(x) = \frac{2m}{\hbar^2} V(x) \psi(x) . \quad (3.28)$$

Assuming the conditions (3.26) and (3.27) are met, back-scattering will be highly suppressed and we can make an ansatz for the wave function ψ

$$\psi(x) = e^{ikx} \varphi(x) , \quad (3.29)$$

where $\varphi(x)$ is a function that varies only slowly over a projectile wavelength. Inserting (3.29) in the Schrödinger equation (3.28) yields

$$\left(2ik \frac{d}{dx} + \frac{d^2}{dx^2} \right) \varphi(x) = \frac{2m}{\hbar^2} V(x) \varphi(x) . \quad (3.30)$$

Since φ is supposed to vary slowly over a wavelength $2\pi/k$ the first term in the brackets on the left-hand side of (3.30) will dominate. We obtain a simple differential equation for φ

$$\frac{d\varphi(x)}{dx} = -\frac{i}{\hbar v} V(x) \varphi(x) . \quad (3.31)$$

Since we assume no back-scattering, the wave function ψ is a plane wave for $x \rightarrow -\infty$, and we therefore get a boundary condition for the function φ

$$\lim_{x \rightarrow -\infty} \varphi(x) = 1 . \quad (3.32)$$

Equation (3.31) is easily solved and one obtains

$$\varphi(x) = \exp \left(-\frac{i}{\hbar v} \int_{-\infty}^x V(x') dx' \right) . \quad (3.33)$$

Another way to derive (3.33), which is useful in the three-dimensional case as well, and which shows more clearly where the assumptions (3.26) and (3.27) are used, is to start with the Lippmann-Schwinger equation in one dimension

$$\psi(x) = e^{ikx} + \int G(x-x') V(x') \psi(x') dx', \quad (3.34)$$

where the one dimensional Green's function can be written in Fourier space as

$$G(x-x') = -\frac{m}{\pi\hbar^2} \int_{-\infty}^{\infty} \frac{e^{ip(x-x')}}{p^2 - k^2 - i\varepsilon} d^3p, \quad \varepsilon \rightarrow 0^+. \quad (3.35)$$

After performing the integration one obtains

$$G(x-x') = -\frac{i}{\hbar v} e^{ik|x-x'|}. \quad (3.36)$$

Making the same ansatz as before, and inserting (3.29) into the Lippmann-Schwinger equation yields

$$\begin{aligned} \varphi(x) &= 1 - \frac{i}{\hbar v} \int_{-\infty}^{\infty} e^{ik|x-x'| - ik(x-x')} V(x') \varphi(x') dx' \\ &= 1 - \frac{i}{\hbar v} \int_{-\infty}^x V(x') \varphi(x') dx' - \frac{i}{\hbar v} \int_x^{\infty} e^{2ik(x-x')} V(x') \varphi(x') dx'. \end{aligned} \quad (3.37)$$

$$(3.38)$$

We have split the integral over x' into $x' < x$ and $x' > x$. The second integral can be neglected because the exponential oscillates rapidly while $\varphi(x)$ and $V(x)$ vary slowly over a projectile wavelength. Keeping only the first integral, we finally need to solve the integral equation

$$\varphi(x) = 1 - \frac{i}{\hbar v} \int_{-\infty}^x V(x') \varphi(x') dx'. \quad (3.39)$$

The solution is easily found by first differentiating to obtain

$$\frac{d\varphi(x)}{dx} = -\frac{i}{\hbar v} V(x) \varphi(x), \quad (3.40)$$

and then together with the boundary condition

$$\lim_{x \rightarrow -\infty} \varphi(x) = 1, \quad (3.41)$$

we find the same solution for φ as in (3.33). The solution for ψ is finally

$$\psi(x) = \exp\left(ikx - \frac{i}{\hbar v} \int_{-\infty}^x V(x') dx'\right). \quad (3.42)$$

One assumption in the derivation was that $V(x)$ varies slowly over one wavelength of the particle, which can be expressed in the form of $ka \gg 1$. The other assumption

was that $\varphi(x)$ also varies slowly over one wavelength. Referring back to (3.33) and setting $V(x')$ to some average value V , we see that this assumption is just $k \gg V/\hbar v$ or, as before, $V/E \ll 1$.

These two conditions for the high energy approximation can be compared to the one of the Born approximation. Multiplying (3.26) and (3.27), we obtain

$$ka \frac{V}{E} = 2 \frac{Va}{\hbar v}, \quad (3.43)$$

which can be of arbitrary size, while for the Born approximation to converge rapidly we had the requirement that $Va/\hbar v \ll 1$.

3.3.2 The eikonal approximation in three dimensions

To derive an expression for the wave function of the projectile after the scattering in a three dimensional problem, we proceed in a similar manner as in the second case in one dimension. Starting with the Lippmann-Schwinger equation (3.7), we introduce a linearized Green's function to solve for the wave function. The Green's function (3.6) can be rewritten as

$$G(\mathbf{r} - \mathbf{r}') = -\frac{2m}{(2\pi)^3 \hbar^2} \int \frac{e^{i\mathbf{p} \cdot (\mathbf{r} - \mathbf{r}')}}{p^2 - k^2 - i\varepsilon} d^3p, \quad \varepsilon \rightarrow 0^+. \quad (3.44)$$

Again, we require that $ka \gg 1$ and $V/E \ll 1$. But this means that the projectile will only be scattered by small angles from its original direction which is given by \mathbf{k} . Therefore, one can expand the momentum \mathbf{p} in the integral of (3.44) in terms of the original momentum \mathbf{k} and a small correction \mathbf{q} , i.e.

$$\mathbf{p} = \mathbf{k} + \mathbf{q}, \quad d^3p = d^3q. \quad (3.45)$$

Inserting (3.45) into (3.44) and neglecting a term quadratic in q in the denominator yields

$$G(\mathbf{r} - \mathbf{r}') = -\frac{2m}{(2\pi)^3 \hbar^3} e^{i\mathbf{k} \cdot (\mathbf{r} - \mathbf{r}')} \int \frac{e^{i\mathbf{q} \cdot (\mathbf{r} - \mathbf{r}')}}{2\mathbf{k} \cdot \mathbf{q} - i\varepsilon} d^3q \quad (3.46)$$

$$= -\frac{i}{\hbar v} e^{i\mathbf{k} \cdot \mathbf{r}} \delta^2(\mathbf{b} - \mathbf{b}') \Theta(z - z'), \quad (3.47)$$

If we make a similar ansatz to the one made in the one dimensional case,

$$\psi(\mathbf{r}) = e^{i\mathbf{k} \cdot \mathbf{r}} \varphi(\mathbf{r}) \quad (3.48)$$

where $\varphi(\mathbf{r})$ varies slowly over the wavelength of the projectile, we can proceed in the same way as before and get

$$\psi_{\mathbf{k}}(\mathbf{r}) = \exp \left(i\mathbf{k} \cdot \mathbf{r} - \frac{i}{\hbar v} \int_{-\infty}^z V(\mathbf{b} + \hat{\mathbf{k}}z') dz' \right). \quad (3.49)$$

We have introduced in (3.47) cylindrical coordinates of the form $\mathbf{r} = \mathbf{b} + \hat{\mathbf{k}}z$, where $\mathbf{b} \perp \mathbf{k}$.

3.3.3 The eikonal scattering amplitude

We may now insert the wave function found in the previous section into the expression for the scattering amplitude

$$f^E(\mathbf{k}_f, \mathbf{k}_i) = -\frac{2m}{4\pi\hbar^2} \int e^{-i\mathbf{k}_f \cdot \mathbf{r}} V(\mathbf{r}) e^{i\mathbf{k}_i \cdot \mathbf{r} - \frac{i}{\hbar v} \int_{-\infty}^z V(\mathbf{b} + \hat{\mathbf{k}}_i z') dz'} dz d^2b \quad (3.50)$$

$$= -\frac{2m}{4\pi\hbar^2} \int e^{i\Delta \cdot \mathbf{r}} V(\mathbf{b} + \hat{\mathbf{n}}z) e^{-\frac{i}{\hbar v} \int_{-\infty}^z V(\mathbf{b} + \hat{\mathbf{n}}z') dz'} dz d^2b, \quad (3.51)$$

where $\Delta = \mathbf{k}_i - \mathbf{k}_f$. We choose the coordinate system such that $\mathbf{r} = \mathbf{b} + \hat{\mathbf{n}}z$, with $\hat{\mathbf{n}} \perp \Delta$. Then we also have

$$e^{i\Delta \cdot \mathbf{r}} = e^{i\Delta \cdot \mathbf{b}}. \quad (3.52)$$

Integrating over the z -coordinate, one obtains

$$f^E(\mathbf{k}_f, \mathbf{k}_i) = -\frac{2m}{4\pi\hbar^2} \int e^{i\Delta \cdot \mathbf{b}} \left(\int V(\mathbf{b} + \hat{\mathbf{n}}z) e^{-\frac{i}{\hbar v} \int_{-\infty}^z V(\mathbf{b} + \hat{\mathbf{n}}z') dz'} dz \right) d^2b \quad (3.53)$$

$$= \frac{k_i}{2\pi i} \int e^{i\Delta \cdot \mathbf{b}} (e^{i\chi(\mathbf{b})} - 1) d^2b, \quad (3.54)$$

with the eikonal phase shift function

$$\chi(\mathbf{b}) = -\frac{1}{\hbar v} \int_{-\infty}^{\infty} V(\mathbf{b} + \hat{\mathbf{n}}z') dz'. \quad (3.55)$$

We also introduce the quantity

$$\Gamma(\mathbf{b}) = 1 - e^{i\chi(\mathbf{b})}, \quad (3.56)$$

which will be useful when we consider multi-particle scattering in terms of the Glauber approximation.

The eikonal scattering amplitude $f^E(\mathbf{k}_f, \mathbf{k}_i)$ is expanded in a similar fashion to the Born series by writing the exponential containing the eikonal function in a Taylor series:

$$f^E(\mathbf{k}_f, \mathbf{k}_i) = \sum_{n=1}^{\infty} \bar{f}_n^E(\mathbf{k}_f, \mathbf{k}_i), \quad (3.57)$$

where

$$\bar{f}_n^E(\mathbf{k}_f, \mathbf{k}_i) = \frac{k}{2\pi} \frac{i^{n-1}}{n!} \int e^{i\Delta \cdot \mathbf{b}} [\chi(\mathbf{b})]^n d^2b. \quad (3.58)$$

If we insert $\chi(\mathbf{b})$ into the expression for $\bar{f}_1^E(\mathbf{k}_f, \mathbf{k}_i)$, we obtain the same result as for $\bar{f}_1^B(\mathbf{k}_f, \mathbf{k}_i)$. This fact is used in chapter 5 to numerically calculate the Glauber approximation.

3.4 The Glauber approximation

While the eikonal approximation is well suited to problems concerning the scattering of two particles, an extension is required for a more general case of a composite target. This extension was first proposed by Glauber [32, 35, 36] and now carries his name. The main ideas of the Glauber approximation are best illustrated by first examining the problem of scattering off a bound particle and then the general case of a many-body target.

3.4.1 Scattering by a bound particle

As it was done in the case of the eikonal approximation, we start by developing the theory in one dimension and extend it to the full three dimensions.

Before the collision, the target is in an eigenstate $|u_i\rangle$ of its Hamiltonian $H(q)$, with an eigenvalue E_i and a position coordinate q . The projectile is described by a coordinate x and the time-dependent Schrödinger equation for the combined system which is represented by the state vector $|\Omega(t)\rangle$ as

$$\left(-\frac{\hbar^2}{2m}\frac{\partial^2}{\partial x^2} + V(x-q) + H(q)\right) |\Omega(t)\rangle = i\hbar\frac{\partial}{\partial t} |\Omega(t)\rangle. \quad (3.59)$$

We remove the dependence on the Hamiltonian $H(q)$ governing the dynamics of the bound target particle by writing

$$|\Omega(t)\rangle = e^{-iH(q)t/\hbar} |\psi\rangle. \quad (3.60)$$

Inserting this into the Schrödinger equation immediately leads to

$$\left(-\frac{\hbar^2}{2m}\frac{\partial^2}{\partial x^2} + e^{iH(q)t/\hbar} V(x-q) e^{-iH(q)t/\hbar}\right) |\psi\rangle = i\hbar\frac{\partial}{\partial t} |\psi\rangle. \quad (3.61)$$

But the time-dependent coordinate operator in the Heisenberg picture is

$$q(t) = e^{iH(q)t/\hbar} q e^{-iH(q)t/\hbar}, \quad (3.62)$$

and since x and q commute, we finally write the Schrödinger equation as

$$\left(\frac{\hbar^2}{2m}\frac{\partial^2}{\partial x^2} + i\hbar\frac{\partial}{\partial t}\right) |\psi\rangle = V(x-q(t)) |\psi\rangle. \quad (3.63)$$

To solve this time-dependent version of (3.28) we make a similar ansatz as in (3.29)

$$|\psi\rangle = e^{i(kx-\omega t)} \varphi(x, t) |u_i\rangle. \quad (3.64)$$

Here, $\varphi(x, t)$ is an operator that implicitly depends on q , and $\omega = E/\hbar = \hbar k^2/2m$. The main assumption again is, that φ varies slowly as a function of x . Therefore,

upon inserting (3.64) into (3.63) we drop the term containing second partial derivative with respect to x and obtain

$$\left(\frac{\partial}{\partial x} + \frac{1}{v} \frac{\partial}{\partial t} \right) \varphi(x, t) = -\frac{i}{\hbar v} V(x - q(t)) \varphi(x, t). \quad (3.65)$$

To solve this equation, we cannot simply write φ as an exponential as it was done before, but we can still write it as a power series. Considering a simpler example, the solution of the equation

$$\frac{d\varphi(x)}{dx} = -\frac{i}{\hbar v} V(x) \varphi(x), \quad (3.66)$$

where $V(x)$ is an operator is given by

$$\varphi(x) = 1 - \frac{i}{\hbar v} \int_{-\infty}^x dx'' V(x'') + \left(\frac{i}{\hbar v} \right)^2 \int_{-\infty}^x dx' \int_{-\infty}^{x'} dx'' V(x'') V(x') + \dots \quad (3.67)$$

If $V(x)$ commutes for any values of x the right-hand side is simply the exponential

$$\exp \left(-\frac{i}{\hbar v} \int_{-\infty}^x V(x') dx' \right)$$

as before. If the operators do not commute, it is convenient to abbreviate the power series by defining

$$\varphi(x) = \left\{ \exp \left(-\frac{i}{\hbar v} \int_{-\infty}^x V(x') dx' \right) \right\}_+, \quad (3.68)$$

where the brackets $\{ \}_+$ indicate that the terms in the series expansion are ordered in the correct way as in (3.67).

With this definition it is now straightforward to solve for the operator $\varphi(x, t)$

$$\varphi(x, t) = \left\{ \exp \left(-\frac{i}{\hbar c} \int_{-\infty}^x V \left(x' - q \left(t - \frac{x - x'}{v} \right) \right) dx' \right) \right\}_+. \quad (3.69)$$

Before we finally evaluate the scattering amplitude, we first introduce the actual approximation method by considering the amplitude for the projectile to be at point x at time t and the target particle to be in a state $|u_f\rangle$ at the same time. This is just the scalar product

$$\langle u_f | \psi(x, t) \rangle = e^{i(kx - \omega t)} \langle u_f | \left\{ e^{-\frac{i}{\hbar v} \int_{-\infty}^x V(x' - q(t - \frac{x - x'}{v})) dx'} \right\}_+ | u_i \rangle. \quad (3.70)$$

Since $|u_i\rangle$ and $|u_f\rangle$ are eigenstates of the Hamiltonian $H(q)$ with the energies E_i and E_f , respectively, this expression is simplified by removing the time-dependence from q using

$$q \left(t - \frac{x - x'}{v} \right) = e^{i\frac{H(q)}{\hbar}(t - \frac{x}{v})} q \left(\frac{x'}{v} \right) e^{-i\frac{H(q)}{\hbar}(t - \frac{x}{v})}. \quad (3.71)$$

Using (3.71) we remove the t - and x -dependence from the integral in the exponent of (3.70) and find

$$\begin{aligned} \langle u_f | \psi(x, t) \rangle &= e^{i(kx - \omega t)} \langle u_f | e^{i\frac{H(q)}{\hbar} (t - \frac{x}{v})} \left\{ e^{-\frac{i}{\hbar v} \int_{-\infty}^x V(x' - q(\frac{x'}{v}))} \right\}_+ e^{-i\frac{H(q)}{\hbar} (t - \frac{x}{v})} u_i \rangle \\ &= e^{i \left[\left(k + \frac{E_i - E_f}{\hbar v} \right) x - \left(\omega + \frac{E_i - E_f}{\hbar} \right) t \right]} \langle u_f | \left\{ e^{-\frac{i}{\hbar v} \int_{-\infty}^x V(x' - q(\frac{x'}{v}))} \right\}_+ u_i \rangle. \end{aligned} \quad (3.72)$$

This expression accounts for energy and momentum conservation. However, momentum conservation is only correct for small changes of the bound particle's energy ($|E_i - E_f|/E \ll 1$). To eliminate the ordering of the operator in (3.72), $H(q)$ in the original Schrödinger equation (3.63) needs to be much less than the energy E of the incident particle, not only for the initial and final state of the target, but for all intermediate states as well. This assumption is similar to that of the eikonal approximation that the momentum transfer must be small. Furthermore, the removal of the time-dependence of $q(t)$ is related to the retardation effect, i.e., q should be evaluated at a time at which the projectile is at x' and will reach x at t . This retardation can be safely neglected, if the velocity of the projectile is much larger than the velocity of the bound target.

So, assuming $|E_i - E_f|/E \ll 1$ and that the ratio of target and projectile velocities is also much less than one, we finally simplify (3.72) to

$$\langle u_f | \psi(x, t) \rangle = e^{i(kx - \omega t)} \langle u_f | e^{-\frac{i}{\hbar v} \int_{-\infty}^x V(x' - q) dx'} u_i \rangle. \quad (3.73)$$

One can now generalize the above to three dimensions for a time-independent wave function as

$$\psi_{\mathbf{k}, i}(\mathbf{r}, \mathbf{q}) = \exp \left(i\mathbf{k} \cdot \mathbf{r} - \frac{i}{\hbar v} \int_{-\infty}^z V(\mathbf{b} + \hat{\mathbf{k}}z' - \mathbf{q}) dz' \right) |u_i(\mathbf{q})\rangle. \quad (3.74)$$

Given the wave-function above, one can now analogously proceed to the derivation of (3.11) to find the scattering amplitude. The amplitude will now depend on the initial and final wave vectors of the projectile \mathbf{k}_i and \mathbf{k}_f as well as on the initial and final state of the target u_i and u_f . One finds

$$f_{fi}^G(\mathbf{k}_f, \mathbf{k}_i) = -\frac{2m}{4\pi\hbar^2} \int e^{-i\mathbf{k}_f \cdot \mathbf{r}} u_f^*(\mathbf{q}) V(\mathbf{r} - \mathbf{q}) \psi_{\mathbf{k}_i, i} d^3r d^3q. \quad (3.75)$$

By choosing the z -axis perpendicular to the momentum transfer, one can perform the z integration as in (3.53)–(3.54) to obtain

$$f_{fi}(\mathbf{k}_f, \mathbf{k}_i) = \frac{k_i}{2\pi i} \int e^{i(\mathbf{k}_i - \mathbf{k}_f) \cdot \mathbf{b}} \int u_f^*(\mathbf{q}) [e^{i\chi(\mathbf{b} - \mathbf{s})} - 1] u_i(\mathbf{q}) d^3q d^2b. \quad (3.76)$$

The vector \mathbf{s} stands for the components of \mathbf{q} that are perpendicular to the momentum transfer (and lies therefore in the same plane as \mathbf{b}),

$$\mathbf{s} = \mathbf{q} - (\hat{\mathbf{n}} \cdot \mathbf{q}) \hat{\mathbf{n}}. \quad (3.77)$$

The phase shift χ is given by

$$\chi(\mathbf{b} - \mathbf{s}) = -\frac{1}{\hbar v} \int_{-\infty}^{\infty} V(\mathbf{b} - \mathbf{s} + \hat{\mathbf{n}}z) dz . \quad (3.78)$$

This expression for the phase shift is the same as (3.55) except that the impact parameter is replaced by the impact parameter relative to the coordinate \mathbf{s} of the target. There is no dependence on the z component of the target coordinate because of the infinite range of the integral.

3.4.2 Many-body scattering

It is straightforward to extend the model of the scattering of a single bound particle with a projectile to the scattering of a many-body system. One only has to replace the single-particle wave functions u_i and u_f by multi-particle wave functions and the phase-shift χ by a total phase-shift χ_{tot} in (3.76). Since χ is only an integral over the scattering potential and the total potential is the sum of the individual ones, χ_{tot} is also only the sum of the phase shifts from each target particle, i.e.

$$\chi_{\text{tot}}(\mathbf{b}, \mathbf{s}_1, \dots, \mathbf{s}_N) = \sum_{j=1}^N \chi_j(\mathbf{b} - \mathbf{s}_j) \quad (3.79)$$

for N target particles. The scattering amplitude for many-body scattering in the Glauber approximation is then

$$\begin{aligned} f_{fi}^G(\mathbf{k}_f, \mathbf{k}_i) &= \frac{k_i}{2\pi i} \int e^{i(\mathbf{k}_i - \mathbf{k}_f) \cdot \mathbf{b}} \int u_f^*(\mathbf{q}_1, \dots, \mathbf{q}_N) [e^{i\chi_{\text{tot}}(\mathbf{b}, \mathbf{s}_1, \dots, \mathbf{s}_N)} - 1] \\ &\quad \times u_i(\mathbf{q}_1, \dots, \mathbf{q}_N) d^3q_1 \dots d^3q_N d^2b . \end{aligned} \quad (3.80)$$

As for single-particle scattering in the eikonal approximation, one can define the quantity

$$\Gamma_{\text{tot}}(\mathbf{b}, \mathbf{s}_1, \dots, \mathbf{s}_N) = 1 - e^{i\chi_{\text{tot}}(\mathbf{b}, \mathbf{s}_1, \dots, \mathbf{s}_N)} . \quad (3.81)$$

This leads to the expression

$$\begin{aligned} f_{fi}^G(\mathbf{k}_f, \mathbf{k}_i) &= \frac{k_i i}{2\pi} \int e^{i(\mathbf{k}_i - \mathbf{k}_f) \cdot \mathbf{b}} \int u_f^*(\mathbf{q}_1, \dots, \mathbf{q}_N) \Gamma_{\text{tot}}(\mathbf{b}, \mathbf{s}_1, \dots, \mathbf{s}_N) \\ &\quad \times u_i(\mathbf{q}_1, \dots, \mathbf{q}_N) d^3q_1 \dots d^3q_N d^2b \end{aligned} \quad (3.82)$$

for the scattering amplitude. If one furthermore introduces

$$\Gamma_j(\mathbf{b} - \mathbf{s}_j) = 1 - e^{i\chi_j(\mathbf{b}, \mathbf{s}_j)} , \quad (3.83)$$

one obtains

$$\Gamma_{\text{tot}}(\mathbf{b}, \mathbf{s}_1, \dots, \mathbf{s}_N) = 1 - \prod_{j=1}^N [1 - \Gamma_j(\mathbf{b} - \mathbf{s}_j)] \quad (3.84)$$

$$= \sum_{j=1}^N \Gamma_j - \sum_{j \neq l} \Gamma_j \Gamma_l + \dots + (-1)^{N-1} \prod_{j=1}^N \Gamma_j. \quad (3.85)$$

If one now inserts the last equation into (3.82) one obtains a multiple-scattering expansion. The first term in (3.85) describes the single interaction between the projectile and each of the target constituents, the next terms describe double, triple, etc, scattering corrections. The maximal number of scattering events between projectile and target constituents can only be N . This a consequence of the approximation which assumes scattering mainly into the forward direction.

3.4.3 Cross sections in the Glauber approximation

For the calculation of the excitation of pionium in the following chapters, we are mainly interested in the cross sections for a transition from an initial state u_i to a final state u_f of the pionium atom but not in the projectile. The cross section for such a transition is

$$\sigma_{fi}^G = \int \frac{k_f}{k_i} |F_{fi}^G(\mathbf{k}_f, \mathbf{k}_i)|^2 d\Omega_{k_f}. \quad (3.86)$$

Since the energy change of the projectile is neglected, the ratio k_f/k_i is unity. The angular integration over the sphere with radius k_f can be replaced by an integration over the tangent plane in the forward direction (i.e. in direction of \mathbf{k}_f)

$$d\Omega_{k_f} \rightarrow \frac{d^2 k_f}{k^2}. \quad (3.87)$$

Inserting (3.76) and (3.87) into the expression for the cross section, one obtains

$$\begin{aligned} \sigma_{fi}^G &= \left(\frac{k}{2\pi}\right)^2 \int \frac{d^2 k_f}{k^2} \iint d^2 b d^2 b' e^{i(\mathbf{k}_i - \mathbf{k}_f) \cdot (\mathbf{b} - \mathbf{b}')} \iint d^3 q' d^3 q u_i^*(\mathbf{q}') u_f(\mathbf{q}') \\ &\quad \times \left[e^{-i\chi^*(\mathbf{b}' - \mathbf{s}')} - 1 \right] \left[e^{i\chi(\mathbf{b} - \mathbf{s})} - 1 \right] u_f^*(\mathbf{q}) u_i(\mathbf{q}) \end{aligned} \quad (3.88)$$

$$\begin{aligned} &= \int d^2 b \iint d^3 q' d^3 q u_i^*(\mathbf{q}') u_f(\mathbf{q}') \left[e^{-i\chi^*(\mathbf{b}' - \mathbf{s}')} - 1 \right] \\ &\quad \times \left[e^{i\chi(\mathbf{b} - \mathbf{s})} - 1 \right] u_f^*(\mathbf{q}) u_i(\mathbf{q}), \end{aligned} \quad (3.89)$$

where the representation

$$\int d^2 k_f e^{i(\mathbf{k}_i - \mathbf{k}_f) \cdot (\mathbf{b} - \mathbf{b}')} = (2\pi)^2 \delta^2(\mathbf{b} - \mathbf{b}') \quad (3.90)$$

of the delta-function was used.

Using the completeness relation of the states u_f

$$\sum_f u_f(\mathbf{q}') u_f^*(\mathbf{q}) = \delta^3(\mathbf{q}' - \mathbf{q}), \quad (3.91)$$

the the total cross section for a target starting in an initial state u_i simplifies to

$$\sigma_{\text{tot}}^G = \sum_f \sigma_{fi}^G = \int d^2b \int d^3q |u_i(\mathbf{q})|^2 |e^{i\chi(\mathbf{b}-\mathbf{s})} - 1|. \quad (3.92)$$

Later on, we will also use the transition amplitude to calculate the excitation cross section. One can rewrite (3.89) as

$$\sigma_{fi}^G = \int d^2b \left| \int d^3q u_f^*(\mathbf{q}) [e^{i\chi(\mathbf{b}-\mathbf{s})} - 1] u_i(\mathbf{q}) \right|^2. \quad (3.93)$$

If the excitation cross section is written in this form, it is easy to read off the transition amplitude for an excitation of the target from a state u_i to a state u_f as

$$a_{fi}^G(\mathbf{b}) = \int d^3q u_f^*(\mathbf{q}) [e^{i\chi(\mathbf{b}-\mathbf{s})} - 1] u_i(\mathbf{q}), \quad (3.94)$$

consistent with what one would expect.

4 Calculations in the first order Born approximation

In this chapter I will review some of the work that has been done on calculating the electro-magnetic interaction pionium–target-nucleus in the first order Born approximation. Besides the leading term in first order, the interaction due to the scalar part of the potential, corrections due to excitation of the target (incoherent scattering), corrections due to the vector potential, and relativistic corrections have so far been calculated. The calculation of the first order Born approximation of the scalar part of the target-nucleus potential is also the basis for the work in the following chapter on the Glauber approximation. This will be the topic of section 4.1. Section 4.2 will deal mainly with the incoherent effects, and also introduce a gauge invariant treatment of the problem. In section 4.3, finally, we will discuss the corrections to the first order Born approximation due to the vector potential in the Hamiltonian and relativistic effects. I will follow closely the published work by Halabuka *et al* [13] for the first section, and Heim *et al* [14, 15] for sections two and three.

4.1 The leading term: the scalar potential

4.1.1 Theory

After discussing the general scattering problem in the previous chapter, we now come to the specific case of a $\pi^+\pi^-$ -atom interacting with the screened Coulomb potential of the target nucleus. Since the pionium is moving at relativistic energies, we can treat the problem semi-classically, i.e., in the rest-frame of the $\pi^+\pi^-$ -atom the heavy target nucleus can be described as a classical particle on a straight-line trajectory, $\mathbf{R}(t) = \{b, 0, vt\}$, at nearly the speed of light, while the $\pi^+\pi^-$ -atom is treated quantum mechanically. The coordinate system is specified in figure 4.1. If we neglect the short-range strong interactions, the Hamiltonian for the pionium can be written as

$$H(t) = H_0 + H_{\text{int}}(t), \quad (4.1)$$

where

$$H_0 = \frac{\mathbf{p}_1^2}{2m} + \frac{\mathbf{p}_2^2}{2m} - \frac{e^2}{|\mathbf{r}_1 - \mathbf{r}_2|} \quad (4.2)$$

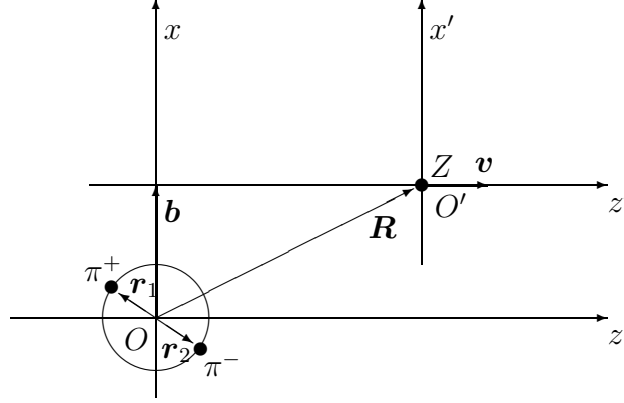


Figure 4.1: A relativistic heavy nucleus with charge Z is moving past a pionium atom. The relevant impact parameter values b are of the order of the pionium's dimensions while the electron cloud of the heavy atom extends over a much larger region ($a_\pi = a_0/136.566$). (Reproduced from [13].)

describes the two interacting pions with mass m , and

$$\begin{aligned}
 H_{\text{int}}(t) = & e(\Phi(\mathbf{r}_1, t) - \Phi(\mathbf{r}_2, t)) - \frac{e}{2mc} (\mathbf{p}_1 \cdot \mathbf{A}(\mathbf{r}_1, t) + \mathbf{A}(\mathbf{r}_1, t) \cdot \mathbf{p}_1) \\
 & + \frac{e}{2mc} (\mathbf{p}_2 \cdot \mathbf{A}(\mathbf{r}_2, t) + \mathbf{A}(\mathbf{r}_2, t) \cdot \mathbf{p}_2) + \frac{e^2}{2mc^2} (\mathbf{A}^2(\mathbf{r}_1, t) + \mathbf{A}^2(\mathbf{r}_2, t))
 \end{aligned} \tag{4.3}$$

describes the interaction with the time-dependent field of the relativistic nucleus. Since the velocities of the pions in the bound and free states are of the order $v_\pi/c \approx \alpha$ or smaller, the non-relativistic approximation for $H(t)$ is reasonable.

The scalar and vector potentials, $\Phi(\mathbf{r}_i, t)$ and $\mathbf{A}(\mathbf{r}_i, t)$, respectively, are given by the screened Coulomb potential of the nucleus. In its rest frame they are

$$\begin{cases} \Phi'(\mathbf{r}') = \frac{Ze}{r} \sum_{k=1}^3 A_k \exp(-\alpha_k r'), \\ \mathbf{A}'(\mathbf{r}') = 0, \end{cases} \tag{4.4}$$

where any magnetic moment of the target nucleus is neglected. For $r' \rightarrow 0$, (4.4) becomes the Coulomb potential for the bare nucleus with charge Z if $\sum_{k=1}^3 A_k = 1$. The parameters A_k and α_k are obtained from a six-parameter fit and are available for $Z = 1$ to $Z = 92$ [37]. With these parameters, the sum of exponentials in (4.4) accurately approximates the Dirac-Hartree-Fock-Slater (DHFS) screening function of a neutral atom in its ground states. The approximation is best for small values of r' , which is well suited for the application to the pionium excitation calculation since the dimension of the $\pi^+\pi^-$ -atom is much smaller than that of the target atom. The parameters A_k and α_k are found by requiring that the six momenta $\langle r^n \rangle$, $n =$

$-1, \dots, 4$, calculated using the analytical charge distribution, coincide with those of the full DHFS calculation.

In this section, incoherent scattering off the target atom is neglected. It will be investigated in detail in section 4.2. For low Z targets, scattering off the target electrons will be a relatively large contribution to the cross section since the incoherent cross section scales with Z , while the coherent cross section scales with Z^2 .

After boosting the target-atom to the rest-frame of the pionium, the scalar and vector potential become

$$\begin{cases} \Phi(\mathbf{r}, t) = \frac{Ze}{2\pi^2} \sum_{k=1}^3 A_k \int \frac{\exp[\mathbf{i}\mathbf{s} \cdot (\mathbf{r} - \mathbf{R}(t))]}{s^2 + \alpha_k^2 - (\beta s_z)^2} d^3s, \\ \mathbf{A}(\mathbf{r}, t) = \beta \Phi(\mathbf{r}, t) \hat{\mathbf{z}}, \end{cases} \quad (4.5)$$

with $\beta = v/c$. If we insert the scalar and vector potentials of (4.5) into the expression for $H_{\text{int}}(t)$ (4.3), we see that the terms containing the vector potential linearly, are smaller than the scalar part by at least $v_\pi/(2c) \approx \alpha/2$, and the term containing \mathbf{A}^2 is smaller by at least α^2 . For now, these terms are neglected, but they will be treated in detail in section 4.3.

The transition amplitude from a state i to a state f , due to the scalar potential of the nucleus, can be written in first order Born approximation as

$$a_{fi}^B(b) = \frac{e}{i\hbar} \int_{-\infty}^{\infty} dt e^{i\omega t} \int d^3r \psi_f^*(\mathbf{r}) \left[\Phi\left(\frac{\mathbf{r}}{2}, t\right) - \Phi\left(-\frac{\mathbf{r}}{2}, t\right) \right] \psi_i(\mathbf{r}), \quad (4.6)$$

where $\omega = (E_f - E_i)/\hbar$ and $\mathbf{r} = \mathbf{r}_1 - \mathbf{r}_2$. One can insert $\Phi(\mathbf{r}, t)$ from (4.5) and expand the exponentials in spherical harmonics

$$e^{\pm i\mathbf{s} \cdot \mathbf{r}/2} = 4\pi \sum_{l,m} (\pm 1)^{l+m} j_l(sr/2) Y_{lm}^*(\hat{\mathbf{s}}) Y_{lm}(\hat{\mathbf{r}}) \quad (4.7)$$

where j_l are spherical Bessel functions and Y_{lm} spherical harmonics. The pionium wave functions are split into angular and radial parts

$$\psi_i(\mathbf{r}) = Y_{l_i m_i}(\hat{\mathbf{r}}) R_{n_i l_i}(r), \quad (4.8)$$

and similarly for ψ_f . The integral over $\hat{\mathbf{r}}$ can then be performed by noting that the integral over three spherical harmonics is

$$\int d^2\hat{r} Y_{l_f m_f}^*(\hat{\mathbf{r}}) Y_{l m}(\hat{\mathbf{r}}) Y_{l_i m_i}(\hat{\mathbf{r}}) = \frac{(-1)^{m_f}}{\sqrt{4\pi}} \hat{l}_f \hat{l}_i \begin{pmatrix} l_f & l & l_i \\ 0 & 0 & 0 \end{pmatrix} \begin{pmatrix} l_f & l & l_i \\ -m_f & 0 & m_i \end{pmatrix} \quad (4.9)$$

with $\hat{l} = \sqrt{2l+1}$. The integration over r is absorbed into the radial form factor of pionium, defined as

$$F_{fi}^l(k) = \int_0^\infty dr r^2 R_f(r) j_l(kr) R_i(r). \quad (4.10)$$

The integral over ϕ_s is just an integral expression of the Bessel function J_m

$$J_m(x) = \frac{i^{-m}}{2\pi} \int_0^{2\pi} e^{iz \cos \phi} e^{im\phi} d\phi. \quad (4.11)$$

Finally, one introduces the straight-line trajectory factor [38]

$$B_{lm}(b, q_0, s) = \Theta(s - q_0) Y_{lm} \left(\cos^{-1} \left(\frac{q_0}{s} \right), 0 \right) J_m \left(b\sqrt{s^2 - q_0^2} \right), \quad (4.12)$$

which results from the time-integration. $\Theta(x)$ denotes the step function and $q_0 = \omega/v$.

The result for the transition amplitude in first order Born approximation is

$$\begin{aligned} a_{fi}^B(b) &= \frac{2Z\alpha}{i\beta} \sqrt{4\pi(2l_f + 1)(2l_i + 1)} (-1)^{m_f} \sum_{lm} i^{l-m} \sqrt{2l+1} \begin{pmatrix} l_f & l & l_i \\ 0 & 0 & 0 \end{pmatrix} \\ &\times [1 - (-1)^l] \begin{pmatrix} l_f & l & l_i \\ -m_f & m & m_i \end{pmatrix} \sum_{k=1}^3 A_k \int_0^\infty s ds \frac{B_{lm}(b, q_0, s) F_{fi}^l \left(\frac{s}{2} \right)}{s^2 + \alpha_k^2 - (q_0\beta)^2}. \end{aligned} \quad (4.13)$$

The probability for a transition from a state i to a state f , summed over the unobserved magnetic quantum numbers m_f and averaged over m_i , as a function of the impact parameter b , is given by

$$\begin{aligned} P_{fi}^B(b) &= \frac{1}{2l_i + 1} \sum_{m_f, m_i} |a_{fi}^B(b)|^2 = 32\pi \left(\frac{Z\alpha}{\beta} \right)^2 (2l_f + 1) \sum_{l, m} [1 - (-1)^l] \\ &\times \begin{pmatrix} l_f & l & l_i \\ 0 & 0 & 0 \end{pmatrix}^2 \left[\int_0^\infty s ds \sum_{k=1}^3 \frac{A_k B_{lm}(b, q_0, s) F_{fi}^l \left(\frac{s}{2} \right)}{s^2 + \alpha_k^2 - (\beta q_0)^2} \right]^2, \end{aligned} \quad (4.14)$$

The excitation cross section is therefore

$$\begin{aligned} \sigma_{fi}^B &= 2\pi \int_0^\infty b db P_{fi}^B(b) \\ &= 16\pi \left(\frac{Z\alpha}{\beta} \right)^2 (2l_f + 1) \int_{q_0}^\infty s ds \left[\sum_{k=1}^3 \frac{A_k}{s^2 + \alpha_k^2 - (\beta q_0)^2} \right]^2 \\ &\times \sum_l (2l + 1) [1 - (-1)^l] \begin{pmatrix} l_f & l & l_i \\ 0 & 0 & 0 \end{pmatrix}^2 \left[F_{fi}^l \left(\frac{s}{2} \right) \right]^2. \end{aligned} \quad (4.15)$$

Using the completeness of the set of all final states f one can write the total cross section for excitation and breakup of pionium as

$$\begin{aligned} \sigma_{\text{tot}, i}^B &= \sum_f \sigma_{fi}^B \\ &= 16\pi \left(\frac{Z\alpha}{\beta} \right)^2 \int_{q_0}^\infty s ds \left[\sum_{k=1}^3 \frac{A_k}{s^2 + \alpha_k^2 - (\beta q_0)^2} \right]^2 [1 - F_{ii}^0(s)]^2. \end{aligned} \quad (4.16)$$

This result is only approximately true, since we neglected the dependence of $q_0 = \omega/v$ by setting q_0 instead to an appropriate constant value, e.g., the pionium ground state binding energy.

4.1.2 Radial form factors

The accurate evaluation of the radial form factors (4.10) is crucial for the calculation of the cross sections. First we discuss the bound-bound form factors and later on the bound-free form factors.

4.1.2.1 Bound-bound form factors

The radial part of the wave function of a bound state is given by the spherical Coulomb wave function

$$R_i(r) \equiv R_{n_i l_i}(r) = N_i (\zeta_i r)^{l_i} e^{-\zeta_i r} {}_1F_1(-n_r^i, 2l_i + 2, 2\zeta_i r), \quad (4.17)$$

with the radial quantum number $n_r^i = n_i - l_i - 1$ and $\zeta_i = Z/(a_\pi n_i)$. a_π is the Bohr radius of pionium in its ground state, it is smaller by a factor $m_\pi/(2m_e)$ than the Bohr radius of a hydrogen atom, $a_\pi \approx 387.5$ fm. The ground state binding energy is larger by the same factor than the ground state binding energy of hydrogen, $E_0 \approx 1.856$ keV.

The normalization constant N_i is defined as

$$N_i = \frac{2^{l_i+1} \zeta_i^2}{(2l_i + 1)!} \left[\frac{(n_i + l_i)!}{\zeta_i n_r^i! n_i} \right]^{1/2}. \quad (4.18)$$

Writing the confluent hypergeometric function ${}_1F_1$ as a Kummer series, one gets

$$R_{n_i l_i}(r) = N_i (\zeta_i r)^{l_i} e^{-\zeta_i r} \sum_{k_i=0}^{n_r^i} c_{k_i}^i (\zeta_i r)^{k_i}, \quad (4.19)$$

with the constant coefficients

$$c_{k_i}^i = \frac{(-n_r^i)_{k_i} 2^{k_i}}{(2l_i + 2)_{k_i} k_i!}, \quad (4.20)$$

where $(a)_{k_i}$ denotes the Pochhammer symbol [39].

To evaluate the bound-bound form factor, we insert the expression (4.19) for the radial wave function of the initial state and the same wave function with the subscript i replaced by f into (4.10). First, we define new dimensionless variables

$$x = (\zeta_i + \zeta_f)r, \quad \tilde{s} = \frac{s}{\zeta_i + \zeta_f}. \quad (4.21)$$

Then one obtains

$$F_{fi}^l(s) = N_{if} \sum_{k=0}^{n_r^i + n_r^f} d_{if,k} g_l^{l_i + l_f + 2 + k}(\tilde{s}), \quad (4.22)$$

with

$$N_{if} = \frac{N_i N_f}{(\zeta_i + \zeta_f)^{3 + l_i + l_f}} \zeta_i^{l_i} \zeta_f^{l_f} \quad (4.23)$$

and the spherical Hankel transforms

$$g_l^\gamma(\tilde{s}) = \int_0^\infty x^\gamma e^{-x} j_l(\tilde{s}x) dx. \quad (4.24)$$

These transforms can be calculated by using a stable recurrence relation in l and γ [40]. The coefficients $d_{if,k}$, finally, are given by

$$d_{if,k} = \sum_{k_f = \max(0, k - n_r^i)}^{\min(k, n_r^f)} c_{k-k_f}^i \zeta_i^{k-k_f} c_{k_f}^f \zeta_f^{k_f}. \quad (4.25)$$

4.1.2.2 Bound-free form factors

To calculate the bound-free form factors, we first need to write down the continuum wave function. The radial part is given by

$$R_{\epsilon_f l_f} = N'_f (qr)^{l_f} \exp(-iqr) {}_1F_1(l_f + 1 + i\eta, 2l_f + 2; 2iqr), \quad (4.26)$$

where ϵ_f and q are the asymptotic kinetic energy and relative momentum, respectively. The Coulomb parameter is defined by $\eta = \mu Z e^2 / (\hbar^2 q)$, where $\mu = m/2$ is the reduce mass. The normalization constant is [39]

$$N'_f = \frac{2^{l_f} \exp(\pi\eta/2) |\Gamma(l_f + 1 + i\eta)|}{(2l_f + 1)!}. \quad (4.27)$$

We introduce new dimensionless variables

$$x = \zeta_i r, \quad \tilde{q} = \frac{q}{\zeta_i}, \quad \tilde{s} = \frac{s}{\zeta_i}. \quad (4.28)$$

For small relative momenta in the continuum state, $\tilde{q} < 1$, the power series expansion of the Coulomb wave function [39]

$$R_{\epsilon_f l_f} = N'_f \sum_{k_f = l_f + 1}^{\infty} A_{k_f}^{l_f} (\tilde{q}x)^{k_f - 1} \quad (4.29)$$

with the coefficients satisfying

$$\begin{aligned} A_{l_f + 1}^{l_f} &= 1; & A_{l_f + 2}^{l_f} &= -\frac{\eta}{l_f + 1}; \\ (k + l_f)(k - l_f - 1)A_{k_f}^{l_f} + 2\eta A_{k_f - 1}^{l_f} + A_{k_f - 2}^{l_f} &= 0 & \text{for } k_f > l_f + 2, \end{aligned} \quad (4.30)$$

converges rapidly. The resulting form factor

$$F_{fi}^l = \frac{N_i N_f'}{\zeta_i^3} \sum_{k_i=0}^{n_r^i} c_{k_i}^i \sum_{k_f=l_f+1}^{\infty} A_{k_f}^{l_f} \tilde{q}^{k_f-1} g_l^{l_i+k_i+k_f+1}(\tilde{s}) \quad (4.31)$$

again contains the Hankel transforms (4.24).

For $\tilde{q} \geq 1$, the infinite series in (4.31) converges poorly. Inserting the Coulomb wave function (4.26) into the expression for the form factor (4.10) yields

$$F_{fi}^l(s) = N_i N_f' \frac{\tilde{q}^{l_f}}{\zeta_i^3} \sum_{k_i=0}^{n_r^i} c_{k_i}^i I_{fi,k_i}^l, \quad (4.32)$$

where the integrals are given by

$$I_{fi,k_i}^l(s) = \int_0^{\infty} x^{l_{if}+k_i} \exp[-(1+i\tilde{q})x] j_l(\tilde{s}x) {}_1F_1(l_f+1+i\eta, 2l_f+2; 2i\tilde{q}x) dx, \quad (4.33)$$

with $l_{if} = l_i + l_f + 2$. Using the trigonometric expansion of the spherical Bessel function [39], one gets the finite sum

$$I_{fi,k_i}^l = \sum_{n=0}^l \frac{(l+n)!}{n!(l-n)!} \int_0^{\infty} x^{l_{if}+k_i} \frac{1}{(2\tilde{s}x)^{n+1}} {}_1F_1(l_f+1+i\eta, 2l_f+2; 2i\tilde{q}x) \times \exp[-(1+i\tilde{q})x] (i^{n-l-1} \exp(i\tilde{s}x) + i^{l+1-n} \exp(-i\tilde{s}x)) dx. \quad (4.34)$$

After performing the Kummer transformation [39] one obtains

$$I_{fi,k_i}^l = \frac{1}{\tilde{s}} \Re \sum_{n=0}^l \frac{(l+n)!}{n!(l-n)!} \frac{i^{l+1-n}}{(2\tilde{s})^n} \int_0^{\infty} x^{l_{if}+k_i-n-1} \times \exp[-(1+i(\tilde{q}+\tilde{s}))x] {}_1F_1(l_f+1+i\eta, 2l_f+2; 2i\tilde{q}x) dx. \quad (4.35)$$

The resulting integrals can be expressed as hypergeometric functions ${}_2F_1$ [40, 41], and the integrals I_{fi,k_i}^l become

$$I_{fi,k_i}^l = \frac{1}{\tilde{s}} \Re \sum_{n=0}^l \frac{(l+n)!}{n!(l-n)!} \frac{i^{l+1-n}}{(2\tilde{s})^n} \frac{(l_{if}+k_i-n-1)!}{(1+i(\tilde{q}+\tilde{s}))^{l_{if}+k_i-n}} \times {}_2F_1\left(l_{if}+k_i-n, l_f+1+i\eta, 2l_f+2; \frac{2i\tilde{q}}{1+i(\tilde{q}+\tilde{s})}\right). \quad (4.36)$$

Because $n \leq l \leq l_i + l_f$, the Kummer series of the hypergeometric function above

does not terminate. However, by applying formula 15.3.9 from [39], one gets

$$\begin{aligned}
& {}_2F_1 \left(l_{if} + k_i - n, l_f + 1 + i\eta, 2l_f + 2; \frac{2i\tilde{q}}{1 + i(\tilde{q} + \tilde{s})} \right) \\
&= (2l_f + 1)! \left[\frac{\Gamma(n - 1 - l_i - k_i - i\eta)}{(l_f - l_i - k_i + n - 1)! \Gamma(l_f + 1 - i\eta)} \left(\frac{2i\tilde{q}}{1 + i(\tilde{q} + \tilde{s})} \right)^{n - k_i - l_{if}} \right. \\
&\quad \times {}_2F_1 \left(l_{if} + k_i - n, l_i - l_f + k_i - n + 1, l_i + k_i - n + 2 + i\eta; \frac{i(\tilde{q} - \tilde{s}) - 1}{2i\tilde{q}} \right) \\
&\quad + \frac{\Gamma(l_i + k_i - n + 1 + i\eta)}{(l_i + l_f + k_i - n + 1)! \Gamma(l_f + 1 + i\eta)} \left(\frac{2i\tilde{q}}{1 + i(\tilde{q} + \tilde{s})} \right)^{l_i - l_f + k_i - n} \\
&\quad \times \left(\frac{1 + i(\tilde{s} - \tilde{q})}{1 + i(\tilde{s} + \tilde{q})} \right)^{n - 1 - l_i - k_i - i\eta} \\
&\quad \left. \times {}_2F_1 \left(l_f - l_i + n - k_i, n - l_i - l_f - 1 - k_i, n - l_i - k_i - i\eta; \frac{i(\tilde{q} - \tilde{s}) - 1}{2i\tilde{q}} \right) \right]. \tag{4.37}
\end{aligned}$$

In this form, the hypergeometric functions can now be written as a sum of polynomials. The first term is a polynomial in $[i(\tilde{q} - \tilde{s}) - 1]/(2i\tilde{q})$ of order $l_f - l_i - k_i + n - 1$ or zero, and the second term is at most of order $l_i + l_f + k_i - n + 1$.

4.1.3 Results

In this section we show the main results from [13]. In figure 4.2 the excitation probability $P_{fi}^B(b)$ as a function of the impact parameter b , is shown for various initial and final states. The expression (4.14) was evaluated for a Titanium target ($Z = 22$) at a projectile energy of 4.7 GeV. One observes, that the excitation probability peaks near the Bohr radius of the $\pi^+\pi^-$ -atom for transitions with the ground state as the initial state, and at slightly larger values of the impact parameter for other ground states. This is in contrast to the size of the charge distribution of the target atoms, shown in figure 4.3, which is also plotted in terms of the ponium Bohr radius, but on a logarithmic scale. One sees that most of the atom's electron cloud lies outside the relevant range of impact parameters set by the ponium, but the deviation from a bare Coulomb potential is already noticeable at much smaller scales, around $r \leq 5a_\pi$. The screening has, therefore, a large effect on the results, but solid state effects can be ignored.

To calculate the cross section, one could in principle integrate over $bP_{fi}^B(b)$, but as can be seen in figure 4.2, this integral converges very slowly. In first order Born approximation it is therefore much more precise and faster to calculate the excitation and total cross sections from (4.15) and (4.16), respectively.

Figure 4.4 verifies that the SCA approach is suitable for the energy range we are interested in. The factor $1/\beta^2$ in the total cross section (4.16) has been factored out. The remaining energy dependence originates from the term $(\beta q_0)^2$ in the denomina-

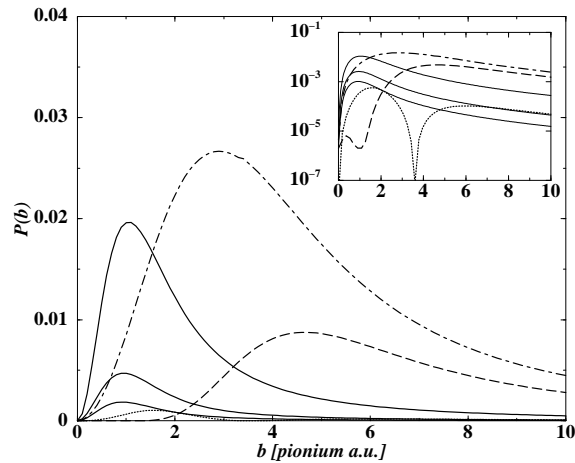


Figure 4.2: The excitation probability P_{fi}^B as a function of the impact parameter b (in pionium Bohr radii a_π), for transitions from the ground state to $2p$, $3p$, $4p$ (solid curves, top to bottom, respectively), and $2s \rightarrow 3p$ (broken curve), $2p \rightarrow 3s$ (dotted line), $2p \rightarrow 3d$ (chain curve). The insert shows the same diagram with a logarithmic scale for the ordinate. The calculations are for a Ti target and 4.7 GeV projectile energy. (Reproduced from [13].)

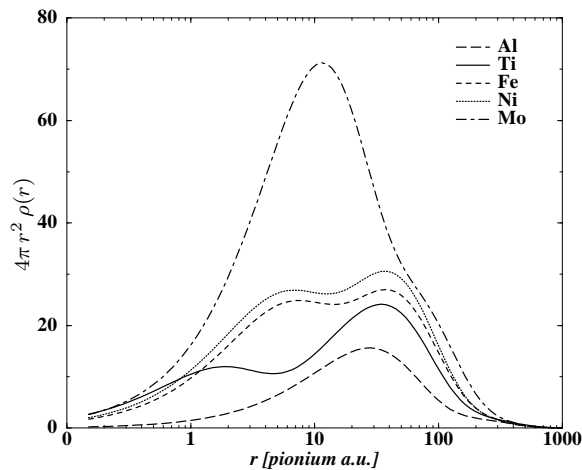


Figure 4.3: The charge distribution determined from the analytical fit to the Dirac-Hartree-Fock-Slater ground state wave functions for different target materials, as a function of the radial variable (in pionium's a_π). (Reproduced from [13].)

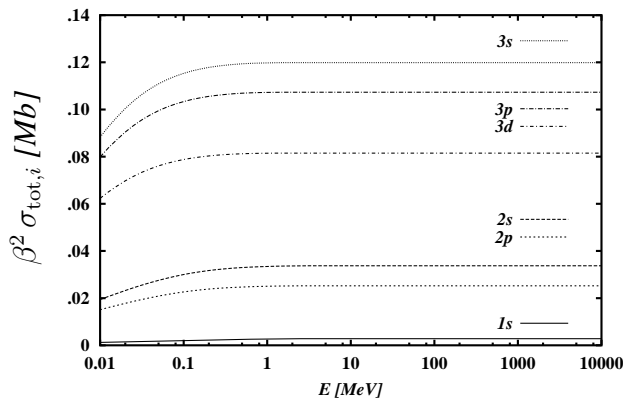


Figure 4.4: The total inelastic cross section from different initial states i (as indicated in the figure), multiplied with β^2 , over a wide range of projectile energies (from 10 keV to 10 GeV). The calculations are for a Ti target. (Reproduced from [13].)

tor of the screening function. As is seen in figure 4.4, $\beta^2\sigma_{\text{tot},i}$ is essentially constant in the energy range of interest to the DIRAC experiment, i.e., 2–10 GeV.

4.2 Coherent and incoherent atomic scattering

In the previous section, only transitions between different states of the pionium system were taken into account, while the target atom was only providing the Coulomb potential. The real situation is of course much more complicated as the target atom can also enter an excited state. In that case the electrons of the target are affected individually, so that the form-factor for a target-inelastic process takes the form of an incoherent sum over all electrons, in contrast to the coherent action of the electrons and nucleus of the target-elastic process. From this argument it is clear that the target-incoherent cross section is proportional to Z while the target-elastic cross section is proportional to Z^2 . Since the scattering of the target-electrons increases the cross section, this effect is also referred to as anti-screening [42, 43]. At large momentum transfer the anti-screening correction can be estimated by multiplying the coherent cross section by a factor $(1 + 1/Z)$ [44, 45, 46]. This section closely follows the work of Heim *et al* [14].

4.2.1 Formalism

In this section a new formalism to the pionium–atom scattering is introduced. It is more closely related to standard electron scattering formalism as for example in [47, 48, 49].

The Feynman diagram showing the general form of the pionium–atom scattering is shown in figure 4.5. The cross section for this process is given by

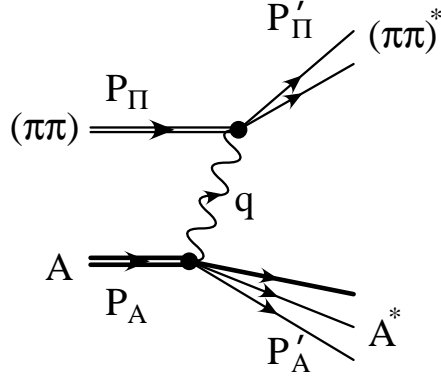


Figure 4.5: The lowest order Feynman diagram for the simultaneous excitation of projectile (pionium) and target (atom). The atomic momenta are P_A and P'_A before and after the collision, those of the pionium P_Π and P'_Π . The momentum of the exchanged photon is $q = P'_\Pi - P_\Pi = -(P'_A - P_A)$. (Reproduced from [14].)

$$\sigma = \frac{1}{4I} \frac{1}{(2\pi)^2} 2M_A 2M_\Pi \int d^4q \frac{(4\pi e^2)^2 W_A^{\mu\nu} W_{\mu\nu\Pi}}{(q^2)^2} \quad (4.38)$$

where I is the incoming flux, $W_A^{\mu\nu}$ and $W_\Pi^{\mu\nu}$ are the electromagnetic tensors describing the electromagnetic interaction of the atom and pionium with the photon, respectively. As we are not interested in the final state of the atom, we can average over all initial spin states and sum over all final states and directions for a specific final state momentum P' . The tensor for the atom is therefore

$$W_A^{\mu\nu} = \frac{1}{4\pi M_A} \sum_X \langle 0, P_A | J^{\mu\dagger} | X, P'_A \rangle \langle X, P'_A | J^\nu | 0, P_A \rangle (2\pi)^4 \delta^4(P_A - q - P'_A) \quad (4.39)$$

and similarly for the pionium if its final state is not resolved either.

It is well known that gauge invariance or current conservation requires that the electromagnetic tensor can be written in terms of two scalar functions W_1 and W_2 that are functions of q and Pq ,

$$W^{\mu\nu} = \left(-g^{\mu\nu} + \frac{q^\mu q^\nu}{q^2} \right) W_1(q^2, Pq) + \left(P^\mu - \frac{Pq q^\mu}{q^2} \right) \left(P^\nu - \frac{Pq q^\nu}{q^2} \right) \frac{W_2(q^2, Pq)}{M^2}. \quad (4.40)$$

The product of the two tensors in the cross section can be written in terms of W_1 and W_2 ,

$$\begin{aligned} W_A^{\mu\nu} W_{\mu\nu\Pi} = & 3W_{1,\Pi} W_{1,A} + \left(-1 + \frac{\Delta^2}{q^2} \right) W_{1,\Pi} W_{2,A} + \left(-1 + \frac{\omega^2}{q^2} \right) W_{2,\Pi} W_{1,A} \\ & + \left(\gamma + \frac{\omega\Delta}{q^2} \right)^2 W_{2,\Pi} W_{2,A} \end{aligned} \quad (4.41)$$

where γ is the (relative) Lorentz factor between the atom and pionium. The energy of the photon in the respective rest frame of the atom ($-\Delta$) and pionium (ω) is

$$\Delta = -\frac{P_A q}{M_A}, \quad \omega = \frac{P_\Pi q}{M_\Pi}. \quad (4.42)$$

It was argued in section 4.1.1 that the cross section is dominated by the charge operator (there referred to as scalar interaction). Therefore, we neglect the terms containing W_1 and only keep the last term of the previous expression

$$W_A^{\mu\nu} W_{\mu\nu\Pi} \approx \gamma^2 W_{2,\Pi} W_{2,A}. \quad (4.43)$$

This estimate is valid to better than 0.5%, even though the argument needs to be made more carefully (refer to [14]).

In the application to pionium–atom scattering, the masses M_A and M_Π are much larger than the momentum transfer q of the photon. One can therefore neglect recoil and identify Δ and ω with the excitation energy of the atom and pionium in their respective rest frames. This fixes q_0 and q_z . The spatial parts of the photon momentum in the pionium rest frame will be denoted by s and in the atom's rest frame by k . In the rest frame of the atom we have

$$\begin{aligned} q_{0,A} &= -\Delta \\ q_{z,A} &= k_z = -\frac{\Delta}{\beta} - \frac{\omega}{\gamma\beta} \end{aligned} \quad (4.44)$$

and in the rest frame of pionium

$$\begin{aligned} q_{0,\Pi} &= \omega \\ q_{z,\Pi} &= s_z = -\frac{\Delta}{\gamma\beta} - \frac{\omega}{\beta} \end{aligned} \quad (4.45)$$

We can write

$$q^2 = -\left(\frac{\Delta^2}{\beta^2\gamma^2} + \frac{\omega^2}{\beta^2\gamma^2} + \frac{2\omega\Delta}{\beta^2\gamma} + q_\perp^2 \right) =: -(q_\parallel^2 + q_\perp^2). \quad (4.46)$$

Inserting the above into (4.38) and replacing the integration over $d^4q = \frac{1}{\gamma\beta} d\omega d\Delta d^2q_\perp$, one obtains

$$\sigma = \int d\omega d\Delta d^2q_\perp \frac{4\alpha^2}{\beta^2} \frac{W_{2,\Pi}(\omega, q^2) W_{2,A}(\Delta, q^2)}{(q_\parallel^2 + q_\perp^2)^2}. \quad (4.47)$$

Since the W_2 are scalar functions they can be evaluated in the respective rest frames. Assuming that the charge operator is the dominant contribution, W_2 is related to W_A^{00} in the rest frame of the atom by

$$W_{2,A} = \frac{q^4}{k^4} W_{\text{rf},A}^{00} \quad (4.48)$$

with $k^2 = \mathbf{k}^2 = \Delta^2 - q^2$ [50]. From (4.39) we get

$$W_A^{00} = \frac{1}{4\pi M_A} \sum_X \langle 0 | J^{0\dagger}(q) | X, P'_A \rangle \langle X, P'_A | J^0(q) | 0 \rangle (2\pi)^4 \delta^4(P_A - q - P'_A) . \quad (4.49)$$

This expression can be rewritten in terms of the (non-relativistic) density operator

$$W_A^{00} = \sum_X \langle 0 | \rho(\mathbf{q}) | X, E_X \rangle \langle X, E_X | \rho(\mathbf{q}) | 0 \rangle \delta(E_{0,A} + \Delta - E_X) \quad (4.50)$$

$$= \sum_X |F_{X0,A}(\mathbf{q})|^2 \delta(E_{0,A} + \Delta - E_X) . \quad (4.51)$$

One can proceed similarly for the pionium in its rest frame and finally obtain

$$\begin{aligned} \sigma = \int d\omega d\Delta d^2q_\perp \frac{4\alpha^2}{\beta^2} \frac{q^4}{s^4 k^4} & \left[\sum_X |F_{X0,A}(\mathbf{k})|^2 \delta(E_{0,A} + \Delta - E_X) \right] \\ & \times \left[\sum_{X'} |F_{X'0,\Pi}(\mathbf{s})|^2 \delta(E_{0,\Pi} + \omega - E_{X'}) \right] . \end{aligned} \quad (4.52)$$

To simplify the summation over the final states in (4.52), we let ω and Δ take some average value ω_0 and Δ_0 . This removes the dependence on those variables from the sums. We can therefore use the closure relation for the final states, to obtain

$$\sigma = \int d^2q_\perp \frac{4\alpha^2}{\beta^2} \frac{q^4}{s^4 k^4} S_{\text{inc},A}(\mathbf{k}) S_{\text{inc},\Pi}(\mathbf{s}) \quad (4.53)$$

where q^2 , s^2 and k^2 now use these average values ω_0 and Δ_0 , and

$$S_{\text{inc},A}(\mathbf{k}) = \sum_X |F_{X0,A}(\mathbf{k})|^2 \quad (4.54)$$

$$S_{\text{inc},\Pi}(\mathbf{s}) = \sum_{X'} |F_{X'0,A}(\mathbf{s})|^2 \quad (4.55)$$

4.2.2 Atomic form factors

The pionic form factors have been discussed in section 4.1, therefore, only the atomic form factors remain to be calculated.

4.2.2.1 Atomic ground state elastic form factors

In the Dirac-Hartree-Fock-Slater theory, the ground state atomic wave function Ψ_0 is given by a Slater determinant constructed from the independent particle orbitals,

$$\Psi_0 = \frac{1}{\sqrt{Z!}} \sum_p \text{sign}(p) \Phi_{p(1)}(\mathbf{r}_1) \cdots \Phi_{p(Z)}(\mathbf{r}_Z) , \quad (4.56)$$

where Z is the number of electrons, p denotes the permutations of the indices and Φ_j are single-particle orbitals. The elastic form factor can now be written as

$$F_{00}(\mathbf{k}) = \langle \Psi_0 | \sum_{j=1}^Z \exp(i\mathbf{k} \cdot \mathbf{r}_j) | \Psi_0 \rangle . \quad (4.57)$$

Due to the orthogonality of the orbitals, this reduces to

$$F_{00}(\mathbf{k}) = \sum_{j=1}^Z \langle \Phi_j(\mathbf{r}_j) | \exp(i\mathbf{k} \cdot \mathbf{r}_j) | \Phi_j(\mathbf{r}_j) \rangle . \quad (4.58)$$

Expanding the exponential in spherical harmonics and inserting the orbital wave functions, one obtains

$$\begin{aligned} F_{00}(\mathbf{k}) &= \sum_{j=1}^Z (2l_j + 1) \delta_{\chi_j, \chi'_j} \sum_{\lambda, \mu} i^\lambda \sqrt{4\pi} Y_{\lambda\mu}^*(\hat{\mathbf{k}}) \sqrt{2\lambda + 1} \begin{pmatrix} l_j & l_j & \lambda \\ 0 & 0 & 0 \end{pmatrix} \\ &\times (-1)^{m'_j} \begin{pmatrix} l_j & l_j & \lambda \\ m_j & -m_j & \mu \end{pmatrix} \mathcal{R}_{jj}^\lambda(k) \end{aligned} \quad (4.59)$$

with the spin orbitals χ_j and χ'_j . The radial form factor is defined as

$$\mathcal{R}_{ij}^\lambda(k) = \int_0^\infty dr r^2 R_{n_i l_i}(r) j_\lambda(kr) R_{n_j l_j}(r), \quad (4.60)$$

where $R_{nl}(r)$ denote the radial wave functions for the orbitals.

Averaging $|F_{00}(\mathbf{k})|^2$ over all directions $\hat{\mathbf{q}}$ and using the orthogonality relation of the spherical harmonics yields

$$\begin{aligned} |F_{00}(k)|^2 &= \frac{1}{4\pi} \int d^2\hat{k} |F_{00}(\mathbf{k})|^2 \\ &= \sum_{\lambda, \mu} (2\lambda + 1) \left\{ \sum_{j=1}^Z (-1)^{m'_j} (2l_j + 1) \delta_{\chi_j, \chi'_j} \begin{pmatrix} l_j & l_j & \lambda \\ 0 & 0 & 0 \end{pmatrix} \right. \\ &\quad \left. \times \begin{pmatrix} l_j & l_j & \lambda \\ m_j & -m'_j & \mu \end{pmatrix} \mathcal{R}_{jj}^\lambda(k) \right\}^2 . \end{aligned} \quad (4.61)$$

Obviously all electrons contribute coherently to the form factor, as expected. Due to the first $3j$ -symbol, only even multipoles contribute to the sum.

The form factor $F_{00}(k)$ only describes the contribution by the electrons. To obtain the complete elastic form factor one needs to add the charge of the nucleus, i.e.,

$$F_{\text{atom}}(k) = Z - F_{00}(k) . \quad (4.62)$$

4.2.2.2 Atomic inelastic scattering functions

The inelastic atomic form factor can be written as

$$F_{X0}(\mathbf{k}) = \langle \Psi_X | \sum_{j=1}^Z \exp(i\mathbf{k} \cdot \mathbf{r}_j) | \Psi_0 \rangle . \quad (4.63)$$

The total inelastic scattering function is the incoherent sum over all states X , other than the ground state

$$\begin{aligned} S_{\text{inc}}(\mathbf{k}) &= \sum_{X \neq 0} |F_{X0}(\mathbf{k})|^2 \\ &= \sum_{\text{all } X} |F_{X0}(\mathbf{k})|^2 - |F_{00}(\mathbf{k})|^2 \\ &= Z + \sum_{i=1}^Z \sum_{j \neq i}^Z \langle \Psi_0 | \exp(i\mathbf{k} \cdot [\mathbf{r}_j - \mathbf{r}_i]) | \Psi_0 \rangle - |F_{00}(\mathbf{k})|^2 . \end{aligned} \quad (4.64)$$

In terms of the single-electron orbitals, we can write

$$S_{\text{inc}}(\mathbf{k}) = Z - \sum_{i=1}^Z \sum_{j=1}^Z |\langle \Phi_j | \exp(i\mathbf{k} \cdot \mathbf{r}) | \Phi_j \rangle|^2 . \quad (4.65)$$

To evaluate S_{inc} we still need the matrix elements

$$\begin{aligned} \langle \Phi_j | \exp(i\mathbf{k} \cdot \mathbf{r}) | \Phi_j \rangle &= \delta_{\chi_i \chi_j} (-1)^{m_i} \sqrt{4\pi(2l_i + 1)(2l_j + 1)} \sum_{\lambda, \mu} i^\lambda Y_{\lambda\mu}^*(\hat{\mathbf{k}}) \sqrt{2\lambda + 1} \\ &\quad \times \begin{pmatrix} l_i & l_j & \lambda \\ 0 & 0 & 0 \end{pmatrix} \begin{pmatrix} l_i & l_j & \lambda \\ -m_i & m_j & \mu \end{pmatrix} \mathcal{R}_{ij}^\lambda(k) . \end{aligned} \quad (4.66)$$

Averaging over the direction $\hat{\mathbf{k}}$ yields

$$\begin{aligned} S_{\text{inc}}(k) &= \frac{1}{4\pi} \int d^2\hat{k} S_{\text{inc}}(\mathbf{k}) \\ &= Z - \sum_{i=1}^Z \sum_{j=1}^Z \delta_{\chi_i \chi_j} (2l_i + 1)(2l_j + 1) \sum_{\lambda} (2\lambda + 1) \begin{pmatrix} l_i & l_j & \lambda \\ 0 & 0 & 0 \end{pmatrix}^2 \\ &\quad \times \begin{pmatrix} l_i & l_j & \lambda \\ m_i & -m_j & m_j - m_i \end{pmatrix}^2 [\mathcal{R}_{ij}^\lambda(k)]^2 . \end{aligned} \quad (4.67)$$

4.2.2.3 Comparison with other models

Other ways to model the atomic structure are detailed in [14]. They include the Thomas-Fermi model using the well-known Molière parameterization [51] for the

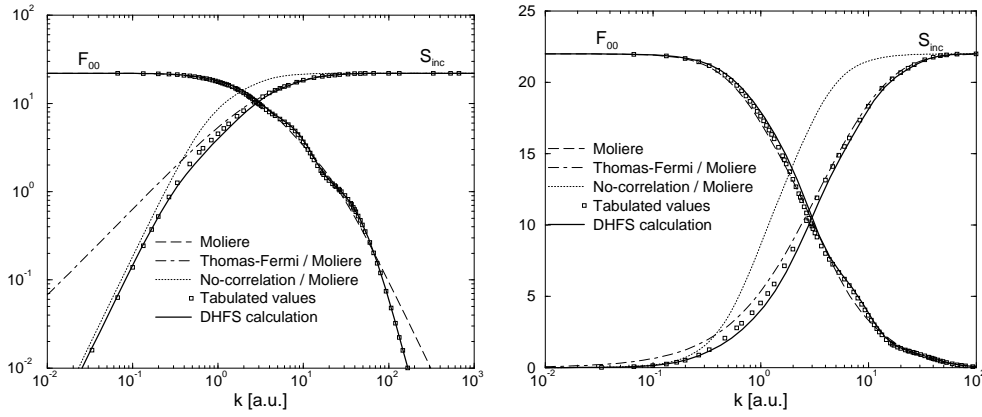


Figure 4.6: Electronic part F_{00} of the coherent atomic form factor and incoherent scattering function S_{inc} for Ti ($Z = 22$). The asymptotic behavior is more easily seen from the log-log diagram on the left. The range of relevance for the cross section calculations is $0.1 \leq k \leq 100$ a.u. For an explanation of the different models, see text. (Reproduced from [14].)

screening function

$$\chi(r) = \sum_{i=1}^3 B_i \exp(-\beta_i r/b) \quad (4.68)$$

with the parameters

$$B_1 = 0.1 \quad B_2 = 0.55 \quad B_3 = 0.35 \quad (4.69)$$

$$\beta_1 = 6.0 \quad \beta_2 = 1.2 \quad \beta_3 = 0.3 \quad (4.70)$$

and $b = a_{\text{Bohr}}(9\pi^2/128)^{1/8} Z^{-1/3}$. The coherent form factor then becomes

$$F_{00}(k) = Z \sum_{i=1}^3 \frac{B_i}{1 + (bk/\beta_i)^2} \quad (4.71)$$

for the electrons, and $F_{\text{atom}}(k) = Z - F_{00}(k)$, as before.

For the inelastic form factors one finds in the non-correlation limit [14]

$$S_{\text{inc}}(\mathbf{k}) = Z - |F_{00}(\mathbf{k})|^2/Z. \quad (4.72)$$

In figure 4.6, the electronic part of the coherent form factor $F_{00,A}$ and the incoherent scattering function $S_{\text{inc},A}$ for different models are compared to tabulated values [52, 53]. One can see that the DHFS calculation outlined in the previous section does very well. The simplified Thomas-Fermi-Molière model and the non-correlation limits on the other hand either miss features in the central region of the relevant values of k or show a wrong asymptotic behavior for either large or small values of k .

4.2.3 Numerical method and results

The radial form factors for the pionium are calculated as was described in section 4.1.2. For the atom, starting from a simple analytical charge distribution as given, e.g., by Salvat *et al* [37] or Molière [51], one solves the Schrödinger or Dirac equation for each occupied orbital. The resulting charge distribution is iteratively refined to obtain improved orbitals until self-consistency is reached. Using these orbitals one can then evaluate the integrals in (4.61) and in (4.67).

It is interesting to first check the relevant range of q_{\perp} for the cross sections as given by (4.47) and (4.52). The differential cross section can be seen to consist of three parts

$$\frac{d\sigma}{dq_{\perp}} = 2\pi q_{\perp} \frac{4\alpha^2}{\beta} (\text{photon}) \times (\text{atom}) \times (\text{pionium}), \quad (4.73)$$

where the photon, atom and pionium parts are given by

$$(\text{photon}) = \frac{1}{q^4} = \frac{1}{(q_l^2 + q_{\perp}^2)^2} \quad (4.74)$$

$$(\text{atom}) = W_{2,A} = \begin{cases} |F_{00,A}(q)|^2 & \text{for coherent scattering} \\ (q^4/k^4)S_{\text{inc},A}(k) & \text{for incoherent scattering} \end{cases} \quad (4.75)$$

$$(\text{pionium}) = W_{2,\Pi} = (q^4/s^4)S_{\text{inc},\Pi}(s). \quad (4.76)$$

Figure 4.7 shows each contribution and the differential cross section. The full curves refer to the total cross section for target-elastic scattering off a Ni ($Z = 28$) target for pionium in its ground state. The broken curves correspond to target-inelastic scattering.

The arrows indicate the relevant momentum scales: q_l for the photon, $k_{TF} = Z^{1/3}/a_{\text{Bohr}}$ for the atom, and k_{Π} for the pionium. The product of the three factors shows that the main contribution to the cross section comes from the range of q_{\perp} between k_{TF} and k_{Π} .

Figure 4.8 shows $d\sigma_{\text{inc}}/d \ln q_{\perp}$ for a ground state pionium scattering incoherently off Ti ($Z = 22$) at 5 GeV projectile energy. The full curve shows the integrand of (4.52) calculated using the incoherent form factor (4.61). The simple estimation of scaling the coherent cross section by a factor $1/Z$ clearly underestimates the correct result. On the other hand the no-correlation limit using the coherent form factor (4.61) overestimates the correct result by an even larger amount. Using the simple $1/Z$ scaling would introduce a considerable error into the inclusive cross sections. The ratio

$$\frac{\sigma_{\text{coh}}(1 + 1/Z)}{\sigma_{\text{coh}} + \sigma_{\text{inc}}}$$

amounts to 0.795 (Li), 0.958 (Al), 0.978 (Ti), 0.987 (Ni), 0.991 (Mo), and 0.996 (Pt). Thus only for the heavy targets the required accuracy of 1% can be attained with such a crude approximation for the incoherent part.

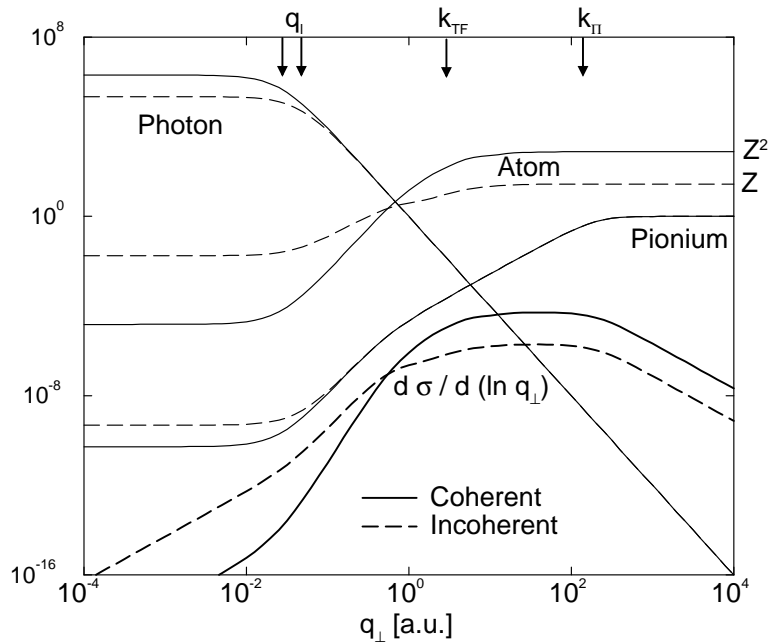


Figure 4.7: Various contributions to the integrand for the cross section vs. q_{\perp} , on a log-log scale. To compensate for the logarithmic q_{\perp} -axis, the integrand is represented as $d\sigma/d \ln q_{\perp}$. The individual curves are labelled in the figure. The cross sections correspond to target-elastic (solid lines) and target-inelastic (dashed lines) pionium scattering off Ni ($Z = 28$) at a projectile energy $E = 5$ GeV, summed over all final states of the pionium. The arrows at the upper edge indicate the relevant momentum scales. See text for details. (Reproduced from [14].)

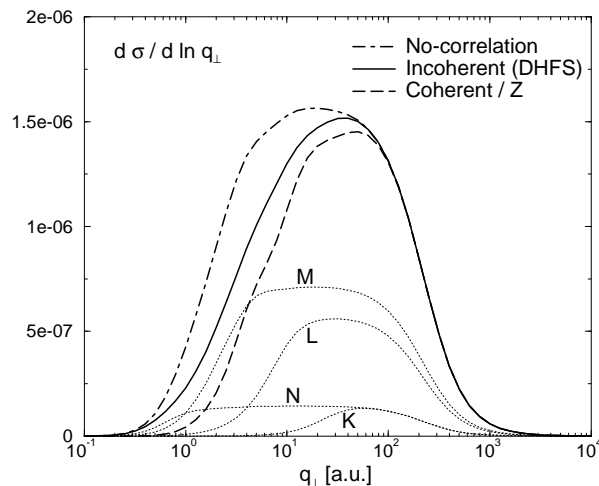


Figure 4.8: Integrand for incoherent (target-inelastic) cross section of ground state pionium scattering off Ti at energy 5 GeV, versus q_{\perp} (on a log-scale). The areas under the curves yield the respective cross sections. Calculations with $\omega_0 = 1.858$ keV and $\Delta_0 = 0$. The contributions from the individual shells (dotted lines) are labelled in the figure. (Reproduced from [14].)

4.3 Corrections due to the magnetic terms

4.3.1 Corrections from the non-relativistic Hamiltonian

To complete the calculation in first order Born approximation, the evaluation of the “magnetic” parts of the Hamilton (4.3) is still required. It was shown in (4.5) that the vector potential is just given by $\mathbf{A} = \beta\Phi\hat{z}$ for pionium moving past the target atom at the relativistic velocity $v = \beta c$ in the z -direction. The first-order transition amplitude from a pionium state $|i\rangle$ to a state $|f\rangle$ due to the part of the Hamiltonian containing one factor \mathbf{A} is given by

$$a_{fi}^{B,\text{magn}} = \frac{1}{i\hbar} \int_{-\infty}^{\infty} dt e^{i\omega t} \left(-\frac{e\beta}{2m_{\pi}c} \right) \left\{ 2\langle f | [\Phi(\mathbf{r}/2) + \Phi(-\mathbf{r}/2)] (-i\hbar) \frac{\partial}{\partial z} |i\rangle + \langle f | (-i\hbar) \left(\frac{\partial}{\partial z} [\Phi(\mathbf{r}/2) + \Phi(-\mathbf{r}/2)] \right) |i\rangle \right\}. \quad (4.77)$$

The derivative only acts on the initial state $|i\rangle$ on the right. This is accomplished by using $\mathbf{p} \cdot \mathbf{A}|i\rangle = \mathbf{A} \cdot \mathbf{p}|i\rangle + (\mathbf{p} \cdot \mathbf{A})|i\rangle$.

The atomic potential can again be written in momentum space representation and be boosted to the rest frame of the pionium (cf. (4.5)). Then one obtains

$$\Phi(\mathbf{r}/2) + \Phi(-\mathbf{r}/2) = \frac{2}{2\pi^2} \int d^3s \frac{F_A \left(\sqrt{s^2 - (\beta s_z)^2} \right)}{s^2} e^{-i\mathbf{s} \cdot \mathbf{R}} \left(e^{i\mathbf{s} \cdot \mathbf{r}/2} + e^{-i\mathbf{s} \cdot \mathbf{r}/2} \right) \quad (4.78)$$

with the atomic (elastic or inelastic) form factor F_A given in the previous section and in [14]. Inserting $\mathbf{R}(t) = \mathbf{b} + vt\hat{z}$ for the straight-line trajectory one can evaluate the time-integral

$$\int_{-\infty}^{\infty} dt e^{i(\omega t - \mathbf{s} \cdot \mathbf{R}(t))} = e^{-i\mathbf{q}_{\perp} \cdot \mathbf{b}} \frac{2\pi}{v} \delta(s_z - \omega/v). \quad (4.79)$$

In the second term of (4.77) the z -derivative is applied to $[\exp(i\mathbf{s} \cdot \mathbf{r}/2) + \exp(-i\mathbf{s} \cdot \mathbf{r}/2)]$. The derivative thus yields a factor $(is_z/2)$ and changes the sign between the two exponentials. The second term, therefore, becomes proportional to the well-known first-order transition amplitude due to the scalar potential (4.13). The result is just $(-\hbar\omega/4m_{\pi}c^2)a_{fi}^B$. Because $\hbar\omega$ is the difference in binding energies of the initial and final pionium states, this term will be of order of α^2 compared to the scalar part.

The remaining z -derivative is applied to the initial (bound) state of the pionium wave function. In spherical coordinates, the z -component of the gradient is given by [54,

Eq. (A37)]

$$\begin{aligned} \frac{\partial}{\partial z} [g(r)Y_{lm}(\theta, \phi)] &= \sqrt{\frac{l^2 - m^2}{(2l+1)(2l-1)}} Y_{l-1,m}(\theta, \phi) \left\{ \frac{dg}{dr} + \frac{l+1}{r}g \right\} \\ &+ \sqrt{\frac{(l+1)^2 - m^2}{(2l+1)(2l+3)}} Y_{l+1,m}(\theta, \phi) \left\{ \frac{dg}{dr} - \frac{l}{r}g \right\}. \end{aligned} \quad (4.80)$$

We can write the hydrogenic wave function of pionium with a Laguerre polynomial in the radial part. The derivatives applied to the radial part can then be expressed with the help of the recurrence relations satisfied by the Laguerre polynomials [41] and one obtains

$$\begin{aligned} \frac{\partial}{\partial z} [R_{nl}(r)Y_{lm}(\theta, \phi)] &= \frac{Z}{la_\pi} \sqrt{\frac{l^2 - m^2}{(2l+1)(2l-1)}} Y_{l-1,m}(\theta, \phi) \\ &\quad \times \left\{ R_{nl}(r) + \sqrt{1 - (l/n)^2} R_{n,l-1}(r) \right\} \\ &- \frac{Z}{(l+1)a_\pi} \sqrt{\frac{(l+1)^2 - m^2}{(2l+1)(2l+3)}} Y_{l+1,m}(\theta, \phi) \\ &\quad \times \left\{ R_{nl}(r) + \sqrt{1 - [(l+1)/n]^2} R_{n,l+1}(r) \right\}. \end{aligned} \quad (4.81)$$

One can see that this term, combined with the prefactor from (4.77) scales as

$$\frac{\beta\hbar}{m_\pi c a_\pi} = \frac{1}{2}\alpha\beta \quad (4.82)$$

compared to the amplitude of the scalar term. It therefore dominates the contribution of the vector-potential to the Hamilton.

Writing the excitation cross section as the integral over \mathbf{q}_\perp of (4.73), we obtain

$$\sigma_{fi} = 4 \left(\frac{\alpha}{\beta} \right)^2 \int d^2q_\perp \frac{|F_A(\mathbf{k})|^2}{q^4} |F_{\text{II}}(\mathbf{s})|^2, \quad (4.83)$$

where F_A denotes the form factor of the target atom (given in (4.62) for target-elastic scattering and in (4.67) for target-inelastic scattering) and F_{II} the form factors for pionium. The form factor for the interaction with the scalar part of the interaction can be written as

$$\begin{aligned} F_{\text{II}}^{\text{scalar}}(\mathbf{s}) &= (-1)^{m_f} \sqrt{(2l_f+1)(2l_i+1)} \sum_{l,m} (2l+1) \sqrt{\frac{(l-|m|)!}{(l+|m|)!}} P_l^{|m|} \left(\frac{\omega}{vs} \right) e^{-im\phi_s} \\ &\quad \times [1 - (-1)^l] (-1)^{\frac{l-1}{2}} \begin{pmatrix} l_f & l & l_i \\ 0 & 0 & 0 \end{pmatrix} \begin{pmatrix} l_f & l & l_i \\ -m_f & m & m_i \end{pmatrix} F_{E_f l_f, n_i l_i}^l \left(\frac{s}{2} \right), \end{aligned} \quad (4.84)$$

with the radial form factor F_{fi}^l for bound-bound or bound-free transitions as (4.10).

For the terms of the Hamiltonian containing one factor \mathbf{A} the pionic form factor with the use of (4.81) can now be written as

$$\begin{aligned}
F_{\Pi}^{B,\text{magn}}(\mathbf{s}) &= (-1)^{m_f} \sqrt{(2l_f + 1)(2l_i + 1)} \sum_{l,m} (2l + 1) \sqrt{\frac{(l - |m|)!}{(l + |m|)!}} P_l^{|m|} \left(\frac{\omega}{vS} \right) e^{-im\phi_s} \\
&\times \left\{ \frac{\hbar\beta}{m_\pi c a_\pi} [1 + (-1)^l] (-1)^{l/2} \frac{1}{2l_i + 1} [W_{fi}^-(l, m) \mathcal{R}_{fi}^-(l, s/2) \right. \\
&\quad \left. - W_{fi}^+(l, m) \mathcal{R}_{fi}^+(l, s/2)] - \frac{\hbar\omega}{4m_\pi c^2} [1 - (-1)^l] (-1)^{\frac{l-1}{2}} \right. \\
&\quad \left. \times \begin{pmatrix} l_f & l & l_i \\ 0 & 0 & 0 \end{pmatrix} \begin{pmatrix} l_f & l & l_i \\ -m_f & m & m_i \end{pmatrix} F_{E_f l_f, n_i l_i}^l(s/2) \right\} \quad (4.85)
\end{aligned}$$

where

$$W_{fi}^\pm(l, m) = \sqrt{1 - \left(\frac{m_i}{l_i^\pm} \right)^2} \begin{pmatrix} l_f & l & l_i \pm 1 \\ 0 & 0 & 0 \end{pmatrix} \begin{pmatrix} l_f & l & l_i \pm 1 \\ -m_f & m & m_i \end{pmatrix}, \quad (4.86)$$

$$\mathcal{R}_{fi}^\pm(l, s/2) = F_{E_f l_f, n_i l_i}^l(s/2) + \sqrt{1 - \left(\frac{l_i^\pm}{n_i} \right)^2} F_{E_f l_f, n_i l_i \pm 1}^l(s/2), \quad (4.87)$$

with $l_i^\pm = \max(l_i, l_i \pm 1)$ were introduced.

The second term in (4.85) has the same form as the scalar form factor (including the same selection rules), but is suppressed by the prefactor $\hbar\omega/4m_\pi c^2$. The first term satisfies different selection rules. From the $3j$ -symbols and the term $[1 + (-1)^l]$, one can see that $l_f - l_i$ must be odd, but due to the Legendre polynomial, transitions with $m_f - m_i$ even will be favored. This means that this term changes the z -parity $(-1)^{l+m}$ of the pionium. It turns out that the small z -parity changing amplitude in the scalar part interferes destructively with this term, making the total amplitude for the z -parity changing transitions even smaller.

4.4 Conclusions

Pionium interacting with the Coulomb field of a target-atom is fully understood in first order Born approximation. All transition cross-sections can be calculated for bound-bound and bound-free transitions as well as the total and ionization cross sections. The evaluation of the cross sections has reached (at least in first order perturbation theory) the accuracy of much better than 1%.

The main contribution stems from the interaction with the scalar part of the target-atoms Coulomb potential. Significant corrections are due to the excitation of the target atom due to incoherent scattering off the target-electrons (of the order of $1/Z$). The corrections due to the magnetic term linear in the external field amount to less than 1%.

The remaining contributions due to relativistic corrections to the ponium Hamiltonian and due to the diamagnetic term (\mathbf{A}^2), as well as a ‘seagull’ contribution, are so small (contributions of the order 10^{-10}) that we refer to [15] for details.

5 Excitation cross sections in Glauber approximation

5.1 Introduction

The leading order terms of these cross sections are well known and have been calculated using different parameterizations of the screened potential of the atom [13, 14, 15, 18]. Since the $\pi^+\pi^-$ -atoms are highly relativistic, it seems to be a reasonable approach to neglect multiple photon exchange processes, but it has been found recently that the total cross section calculated in the eikonal approximation (Glauber-theory) is smaller than the one calculated in the Born approximation by between 2% (for small nuclear charge number Z) and 14% (for large Z) [16]. In this chapter we evaluate the partial cross sections in Glauber theory for arbitrary initial and final bound states of the ponium.

We would like to point out that even though the methods developed in this paper are motivated by an experiment in high energy physics, they are also of general interest for the atomic physics community. Similar problems, e.g. projectile electron excitation and loss in fast collisions with neutral target atoms, have been tackled recently by Voitkiv *et al* [55, 56].

The work in this chapter has been published in [17]. It is therefore self-contained and might repeat some of the information that was already given in the previous chapters.

5.2 The Coulomb interaction between ponium and the target atoms

In order to describe the excitation of the ponium atoms through the electromagnetic interaction with the target atoms, we use the semi-classical approximation (SCA). In the rest-frame of the ponium, the much heavier target atoms move past with almost the speed of light on a straight-line trajectory, $\mathbf{R} = \{b, 0, vt\}$, and are treated classically, while the ponium atom is located at the origin of the coordinate system and is treated quantum-mechanically (Fig. 5.1).

The non-relativistic Hamiltonian describing the $\pi^+\pi^-$ -system is

$$H = H_0 + H_{\text{int}} . \tag{5.1}$$

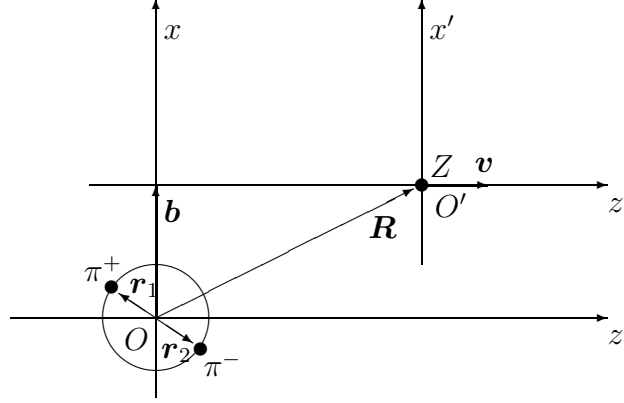


Figure 5.1: An atom is moving past a pionium atom at relativistic speed $v \approx c$.

The first part, H_0 , describes the $\pi^+\pi^-$ pair,

$$H_0 = \frac{\mathbf{p}^2}{2\mu} - \frac{e^2}{r}, \quad (5.2)$$

where we have introduced the reduced mass $\mu = m_\pi/2$ and the relative coordinate and momentum, $\mathbf{r} = \mathbf{r}_1 - \mathbf{r}_2$ and $\mathbf{p} = \mu\dot{\mathbf{r}} = (\mathbf{p}_1 - \mathbf{p}_2)/2$, respectively. The second term in (5.1), H_{int} , describes the interaction between the pionium and the target atom, which can be split into three terms

$$H_{\text{int}} = H_\Phi + H_{1,A} + H_{2,A}, \quad (5.3)$$

where

$$H_\Phi = e [\Phi(\mathbf{r}/2) - \Phi(-\mathbf{r}/2)], \quad (5.4)$$

$$H_{1,A} = -\frac{e}{2m_\pi c} \{ \mathbf{p} \cdot [\mathbf{A}(\mathbf{r}/2) + \mathbf{A}(-\mathbf{r}/2)] \\ + [\mathbf{A}(\mathbf{r}/2) + \mathbf{A}(-\mathbf{r}/2)] \cdot \mathbf{p} \}, \quad (5.5)$$

$$H_{2,A} = \frac{e^2}{2m_\pi c^2} [\mathbf{A}^2(\mathbf{r}/2) + \mathbf{A}^2(-\mathbf{r}/2)]. \quad (5.6)$$

In the following we will only consider H_Φ which yields the main contribution to the cross-section. The corrections due to the magnetic terms contained in $H_{1,A}$ and $H_{2,A}$ (and due to the correct relativistic treatment of H_{int}) have been found to be much less than 1% [15] (refer also to section 4.3). We also do not consider the case of target excitations, also referred to as incoherent scattering or anti-screening. This is expected to contribute of the order of $1/Z$ to the coherent scattering, i.e., without target excitation. The exact contributions have been calculated by Heim *et al* [14] in first order Born approximation (see also section 4.2). While they are relatively large for small Z , higher order corrections are most significant for large Z .

5.2.1 Born approximation

The transition amplitude $a_{fi}(b)$ from an initial state $i = \{n_i, l_i, m_i\}$ to a final state $f = \{n_f, l_f, m_f\}$, where n , l , and m denote the principal, angular, and magnetic quantum numbers respectively, is given in first order perturbation theory as

$$a_{fi}^B = \frac{1}{i\hbar} \int_{-\infty}^{\infty} dt \exp(i\omega t) \int d^3r \psi_f^*(\mathbf{r}) H_{\text{int}} \psi_i(\mathbf{r}), \quad (5.7)$$

where $\omega = (E_f - E_i)/\hbar$. For H_{int} we use only the scalar interaction (5.4) and for the potential Φ we assume a Moliere-type screened potential with the parameters tabulated by Salvat *et al* [37],

$$\Phi(r) = \frac{Ze}{r} \sum_{k=1}^3 A_k e^{-\alpha_k r}. \quad (5.8)$$

These parameters have been found by an analytical fitting procedure to Dirac-Hartree-Fock-Slater (DHFS) data. The excitation cross-section is then calculated by integrating over the impact parameter

$$\sigma_{fi} = \int d^2b |a_{fi}(\mathbf{b})|^2. \quad (5.9)$$

Following the derivation of Halabuka *et al* [13] (see also section 4.1), we arrive at the following expression for the cross section (in the Lorentz gauge) summed over the final and averaged over the initial magnetic quantum numbers.

$$\begin{aligned} \sigma_{fi}^B = & 16\pi \left(\frac{Z\alpha}{\beta} \right)^2 (2l_f + 1) \int_{q_0}^{\infty} q dq \left(\sum_k \frac{A_k}{q^2 + \alpha_k^2 - (\beta q_0)^2} \right)^2 \\ & \times \sum_l (2l + 1) [1 - (-1)^l] \begin{pmatrix} l_f & l & l_i \\ 0 & 0 & 0 \end{pmatrix}^2 (F_{fi}^l(q/2))^2, \end{aligned} \quad (5.10)$$

The radial form-factors

$$F_{fi}^l(q) = \int_0^{\infty} r^2 dr R_{n_f l_f}(r) j_l(qr) R_{n_i l_i}(r) \quad (5.11)$$

can be evaluated efficiently with the recursion relations derived in [40]. Here, $R_{nl}(r)$ is the radial part of a hydrogen-like wave-function and j_l denotes the spherical Bessel function. We have furthermore introduced $q_0 = \omega/v$ in (5.10).

The total cross section can be found via the closure approximation. For completeness we just quote the result from Ref. [13].

$$\sigma_{\text{tot}}^B = 16\pi \left(\frac{Z\alpha}{\beta} \right)^2 \int_{q_0}^{\infty} q dq \left(\sum_k \frac{A_k}{q^2 + \alpha_k^2 - (\beta q_0)^2} \right)^2 (1 - F_{ii}^0(q)). \quad (5.12)$$

5.2.2 Glauber approximation

In the Glauber approximation [32, 33], the transition amplitude is given by (refer to section 3.4.3)

$$a_{fi}^G(b) = \int d^3r \psi_f^*(\mathbf{r}) [1 - \exp(i\chi(b, \mathbf{r}))] \psi_i(\mathbf{r}), \quad (5.13)$$

with the eikonal function

$$\chi(b, \mathbf{r}) = -\frac{1}{\hbar} \int_{-\infty}^{\infty} dt H_{\text{int}}(b, \mathbf{r}, t). \quad (5.14)$$

We may rewrite the eikonal function as $\chi(b, \mathbf{r}) = \chi^+(b, \mathbf{r}) - \chi^-(b, \mathbf{r})$, where

$$\begin{aligned} \chi^\pm(b, \mathbf{r}) &= -\frac{e}{\hbar} \int_{-\infty}^{\infty} dt \Phi(\pm \mathbf{r}/2, t) \\ &= -\frac{Ze^2}{\hbar} \sum_{k=1}^3 A_k \int_{-\infty}^{\infty} dt \frac{\exp(-\alpha_k |\mathbf{r}/2 \mp \mathbf{R}(t)|)}{|\mathbf{r}/2 \mp \mathbf{R}(t)|} \\ &= -\frac{2Z\alpha}{\beta} \sum_{k=1}^3 A_k K_0 \left(\alpha_k \sqrt{\left(\frac{x}{2} \mp b\right)^2 + \left(\frac{y}{2}\right)^2} \right). \end{aligned} \quad (5.15)$$

K_0 denotes the McDonald function [39, Section 9.6]. The Glauber cross section σ_{fi}^G is then found by inserting $a_{fi}^G(b)$ into (5.9).

One can easily check that the expansion of the Glauber cross section to first order in χ yields the first-order cross-section (5.10) with $q_0 = 0$ which will be denoted in the following by

$$\sigma_{n_f l_f, n_i l_i}^{(1)} = \sigma_{n_f l_f, n_i l_i}^B \Big|_{q_0=0}. \quad (5.16)$$

As $q_0 \sim (E_f - E_i)$, this just means that we neglect the energy difference between the final and initial state, which is, in fact, one of the approximations made in Glauber theory (sudden approximation). We will show in section 5.3.2 that this approximation is valid here.

Unfortunately, it is not possible to simplify the Glauber cross section further for arbitrary cases of i and f . For certain transitions, e.g., the 1s–2p transition, and a bare Coulomb field one can reduce the integration further [57]. We are, however, interested in reliably calculating the partial cross sections for arbitrary initial and final states. This problem does not arise in the case of the total cross section, either, where one can use closure and reduce the problem to a one-dimensional integral [16], which can be written as

$$\sigma_{\text{tot}}^G = 4\pi \int_0^\infty q dq |f(q)|^2 (1 - F_{ii}^0(q)), \quad (5.17)$$

where

$$f(q) = \int d^3r [1 - \exp(i\chi(b, \mathbf{r}))] \exp(i\mathbf{q} \cdot \mathbf{r}). \quad (5.18)$$

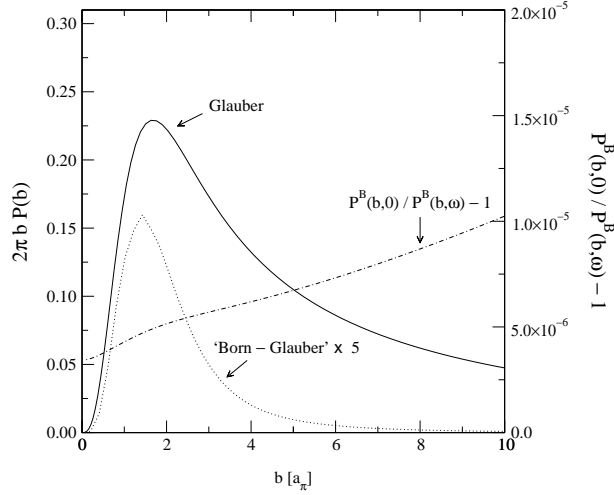


Figure 5.2: Comparison of the transition probabilities for the transition $1s-2p$ of the ponium due to the Coulomb interaction with a Ni ($Z = 28$) atom. The slow convergence of $2\pi b |a_{fi}^G(b)|^2$ (solid line) is clearly visible, whereas the higher order terms (difference between first order (Born) and Glauber approximation, dotted line) are limited to small b . The convergence of the higher order terms is therefore much faster as can be seen from the dotted curve which is scaled with a factor 5. Also shown is the relative difference of the probabilities in first order with or without a finite ω (dash-dotted line). While this difference increases slightly with b , the higher order terms are only appreciable for small b , and their relative contribution remains small compared to the required accuracy.

A further difficulty stems from the fact that the convergence of the b -integration in (5.9) is very slow, as can be seen in figure 5.2. In first order, one avoids this by Fourier-transforming the transition amplitudes and performing the b -integration analytically [13]. The main contribution of the higher order effects are found at small values of b due to the screening effect; impact parameters b larger than $10 a_\pi$ (the Bohr radius of ponium), contribute very little. Therefore, instead of evaluating σ_{fi}^G directly, we calculate only the difference between the Born- and Glauber-approximation

$$\Delta_{fi} = 2\pi \int_0^\infty b db \left(|a_{fi}^{(1)}|^2 - |a_{fi}^G|^2 \right). \quad (5.19)$$

Figure 5.2 displays the integrand of (5.19) as well as the integrand for the full Glauber cross section for the $1s-2p$ transition due to interaction with a Ni target atom. We can calculate Δ_{fi} numerically and combine it with the accurate results for $\sigma_{fi}^{(1)}$ from Halabuka *et al* [13] (with $q_0 = 0$) to finally obtain the full Glauber cross section

$$\sigma_{fi}^G = \sigma_{fi}^{(1)} - \Delta_{fi}. \quad (5.20)$$

Since we are mainly interested in the magnitude of the corrections due to multi-

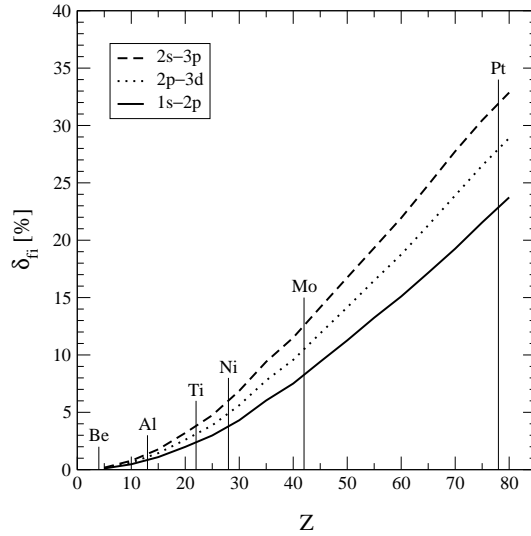


Figure 5.3: The Z -dependence of the relative correction δ_{fi} (defined in (5.21)) to the excitation cross sections for the three transitions $1s-2p$, $2p-3d$, and $2s-3p$.

photon processes we define relative correction as

$$\delta_{fi} = \Delta_{fi}/\sigma_{fi}^{(1)}, \quad (5.21)$$

which is the difference between first order and Glauber cross section normalized to the first order cross section.

5.3 Results

5.3.1 Relative differences between Glauber and Born approximation

As was expected from the results for the total cross sections [16], where the difference between Born and Glauber approximation ranges from 2% to 14%, we found large relative differences between the Born and Glauber approximation for the excitation cross sections. In figure 5.3, one can see that, for example, for the excitation of the pionium from the $1s$ to the $2p$ -state, δ_{fi} (5.21) increases from around 2% for Ti up to 23% for Pt and similarly for other initial and final states.

At first sight, it might seem that up to 30% relative difference in the excitation cross sections for heavy target materials is inconsistent with the relative difference for the total cross sections. However, one has to take into account that multi-photon exchange allows for additional transitions that are strongly suppressed in Born approximation and even strictly forbidden in first order sudden approximation. Table 5.1

shows a comparison of the relative differences. We define

$$\sigma_{\text{ex}}(n_i, l_i) = \frac{1}{2l_i + 1} \sum_{m_i} \sum_{(n_f, l_f, m_f)}^{(n_f, l_f, m_f)_{\text{max}}} \sigma_{(n_f, l_f, m_f), (n_i, l_i, m_i)} \quad (5.22)$$

as the sum of the bound-bound excitation cross section over all available final states ($n_{\text{max}} = 8$, currently) and averaging over the initial magnetic quantum number m_i . By $\sigma_{\text{ex}}(\text{B})$ we denote the sum (5.22) restricted to include only final states that can be reached in the Born approximation. Those final states are determined by the selection rule evident in (5.10) that demands $(l_i + l_f)$ to be odd. Table 5.1 shows that the relative differences for the sums over the states available in first order transitions (column three) are consistent with the values for $Z = 28$ in figure 5.3. This is expected, as the relative differences for excitations from the same initial state are of the same order of magnitude. However, they deviate significantly from the relative differences of the total cross sections shown in the fifth column. This discrepancy vanishes if one compares the relative differences of the sums over all available channels (column four) with the results for the total cross sections. This is possible because the Glauber cross sections are smaller than the first order ones. The agreement is best for $n_i > 2$. For $n_i \leq 2$ the last column of table 5.1 indicates that a considerable part of the total cross sections stems from transitions into the continuum. This suggests that if we were able to take into account the ionization cross sections as well, we would see the same consistency as for $n_i > 2$ where the ionization is only a minor contribution to the total cross section.

Another way to attempt a systematic evaluation of the excitation cross sections is to evaluate the terms of the Glauber series up to the required accuracy. However, figure 5.4 shows that the two-photon corrections already reach the 1% level at around $Z = 10$. For Z up to 30, one can estimate the multi-photon corrections to the cross section by taking into account only two-photon interactions (dotted curve). But for larger values of Z the corrections due to three-photon interactions reach the 1% level (dashed line). For Z larger than 60 even higher order terms need to be calculated as can be seen from the comparison of the solid (Glauber approximation) and the dash-dotted (all corrections up to order $(Z\alpha)^6$) curves.

This clearly illustrates that calculations using the Born approximation and even including the first few higher order Born terms are not sufficiently accurate for targets with large Z . Since we try to establish a consistent method of calculating the excitation cross sections for a large variety of targets from Be ($Z = 4$) to Pt ($Z = 78$) it seems best to use the Glauber approximation for all of them.

Table 5.1: Comparison of the relative differences of the accumulated excitation cross sections for initial states with principal and angular quantum numbers n_i and l_i , respectively. The terms σ_{ex} and $\sigma_{\text{ex}}(\text{B})$ are defined in (5.22) and the following text, the superscripts ‘G’ and ‘(1)’ indicate the full Glauber calculation or only the first order contribution. The total cross sections $\sigma_{\text{tot}}^{(1)}$ and $\sigma_{\text{tot}}^{\text{G}}$ are defined in (5.12) taking into account (5.16), and (5.17), respectively. The relative difference of the sums over excitations allowed in first order (third column) are much larger than the corresponding values from the total cross sections (fifth column), while the fourth column, taking into account all transitions, agrees well with the relative difference of the total cross sections. The last column indicates the ratio of total bound-bound excitation cross sections to the total cross sections. The values given in the table are for a Ni ($Z = 28$) target.

n_i	l_i	$1 - \sigma_{\text{ex}}^{\text{G}}(\text{B})/\sigma_{\text{ex}}^{(1)}$	$1 - \sigma_{\text{ex}}^{\text{G}}/\sigma_{\text{ex}}^{(1)}$	$1 - \sigma_{\text{tot}}^{\text{G}}/\sigma_{\text{tot}}^{(1)}$	$\sigma_{\text{ex}}^{\text{G}}/\sigma_{\text{tot}}^{\text{G}}$
1	0	3.7%	2.0%	1.3%	62.1%
2	0	5.2%	1.6%	1.8%	88.9%
2	1	5.0%	2.2%	1.7%	87.3%
3	0	6.6%	2.1%	2.2%	94.1%
3	1	6.5%	2.0%	2.1%	93.0%
3	2	6.0%	2.3%	2.0%	92.3%
4	0	7.6%	2.4%	2.4%	95.6%
4	1	7.4%	2.3%	2.4%	94.7%
4	2	7.3%	2.3%	2.4%	93.9%
4	3	6.8%	2.5%	2.3%	93.5%

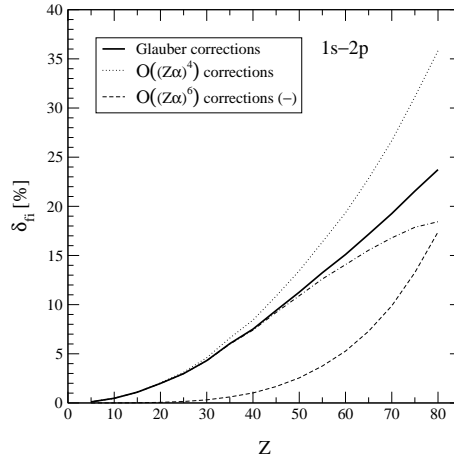


Figure 5.4: Comparison of the contributions of two- and three-photon exchange processes to the relative correction to the excitation cross section for a $1s-2p$ transition in Glauber theory. The solid line shows the correction due to the Glauber approximation. The dotted line shows corrections to the first order due to terms of order $\mathcal{O}((Z\alpha)^4)$, the dashed line shows corrections due to terms of order $\mathcal{O}((Z\alpha)^6)$. The dash-dotted curve shows corrections due to all terms up to $\mathcal{O}((Z\alpha)^6)$. It clearly differs from the Glauber approximation for $Z > 60$.

5.3.2 Estimation of the accuracy of the Glauber approximation

To check the validity of the sudden approximation we go back to the definition of the S -matrix [58, Eq. II.3.17]

$$S = \mathcal{T} \exp \left(-\frac{i}{\hbar} \int dt \tilde{H}_{\text{int}}(t) \right), \quad (5.23)$$

where \tilde{H}_{int} in the interaction picture replaces H_{int} (as defined in (5.3)), i.e.,

$$\tilde{H}_{\text{int}} = e^{iH_0 t/\hbar} H_{\text{int}} e^{-iH_0 t/\hbar}. \quad (5.24)$$

In the sudden approximation the exponentials in (5.24) become 1 since it is assumed that $H_0 t \ll 1$. To get an estimate on the accuracy of the sudden limit, we proceed similarly to the Born approximation [13] and replace the non-interacting Hamilton operators by some average energy difference between the initial and final state $\omega_0 = vq_0$, i.e.,

$$e^{iH_0 t/\hbar} H_{\text{int}} e^{-iH_0 t/\hbar} \simeq e^{i\omega_0 t} H_{\text{int}}. \quad (5.25)$$

Using this approximation, the S -matrix can again be summed to all orders and the transition amplitude is of the form (5.13) with a modified eikonal function

$$\chi'(b, \mathbf{r}) = -\frac{1}{\hbar} \int_{-\infty}^{\infty} dt e^{i\omega_0 t} H_{\text{int}}(b, \mathbf{r}, t). \quad (5.26)$$

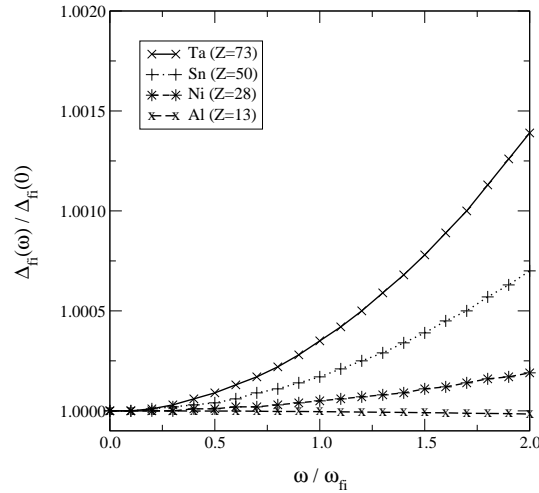


Figure 5.5: The higher order corrections to the excitation cross-section $\Delta_{fi}(\omega)$ normalized to $\omega = 0$ (sudden limit). Shown are the curves for the 1s–2p transition due to interaction with the Ta, Sn, Ni and Al atoms.

Similarly to (5.15) we get

$$\chi'^{\pm}(b, \mathbf{r}) = -\frac{2Z\alpha}{\beta} \sum_{k=1}^3 A_k e^{\pm iq_0 z/2} K_0 \left(\alpha'_k \sqrt{\left(\frac{x}{2} \mp b\right)^2 + \left(\frac{y}{2}\right)^2} \right), \quad (5.27)$$

with

$$\alpha'_k = \sqrt{\alpha_k^2 + (q_0/\gamma)^2}. \quad (5.28)$$

The advantage of this approximation is that the expansion of the excitation cross section with respect to χ' exactly yields the Born cross section (5.10) as the first term.

As the replacement of (5.25) is only an approximation, we let ω_0 vary between 0 and $2\omega_{fi}$. Figure 5.5 shows that the higher order contributions to the cross section calculated with this ω_0 and in the sudden approximation, only differ by less than 0.1% in the case of a Ni target and less than 0.15% in the worst case of Ta. It has already been shown by Heim *et al* [14] that the cross sections to first order also differ by less than 1%. In figure 5.2 the dash-dotted line shows the relative difference of the first order transition probabilities for $\omega_0 = 0$ and a finite ω_0 as a function of the impact parameter b . One can see that while the difference increases with b , it is very small and it should not have a great influence on the higher order corrections as they are limited to small b . It is therefore expected that the sudden limit should have even less effect on those corrections than on the first order terms.

5.4 Conclusion

For the success of the DIRAC experiment it is essential that the excitation and ionization cross-sections of the ponium are known to 1% or better. So far, only calcu-

lations to first order have been available. The results by Afanasyev *et al* [16] showed that higher order effects need to be taken into account for an accurate calculation of the total cross sections of pionium interacting with matter. We have systematically calculated the bound-bound excitation cross sections for the target elements Be, Al, Ti, Ni, Mo, Ta, and Pt for all initial and final quantum numbers limited by $n \leq 8$. We have investigated the dependence of the size of the corrections on the charge number Z of the nucleus of the target material. We have found that only using the full Glauber cross section one will be able to reach the desired 1% level in accuracy for $Z > 60$. For smaller Z one could possibly evaluate systematically higher order terms of the Born series, but already for $Z > 10$ the first order is not sufficiently accurate.

The accuracy of the Glauber approximation itself can only be estimated. We have shown that the sudden approximation, i.e., neglecting the excitation energy compared to the kinetic energy, is valid and using an average ω_0 changes the results very little. To ultimately check the contributions due to higher order processes, a coupled channel calculation could be attempted. One should note, however, that since the higher order contributions are of the order of 10% of the first order result, they need only be calculated to about 10% to reach an overall accuracy of 1%.

6 Coupled channel calculation

We would like to use a coupled channel calculation to verify the results of the last chapter. It was shown that the higher order corrections (multi-photon-exchange) calculated in the Glauber approximation reduce the excitation cross sections for pionium interacting with the Coulomb field of a target atom by as much as 30%. Since we want to verify the Glauber approximation, we only use the scalar part of the interaction Hamiltonian (5.4).

6.1 Theory

The coupled channel approach is a way to solve the Schrödinger equation of pionium interacting with the target atom in a limited space of basis functions.

We write the wavefunction of an atom in terms of eigenstates (bound or free) $\psi_k(\mathbf{r}, t)$ of the free Hamiltonian H_0 (5.2), i.e.,

$$\psi(\mathbf{r}, t) = \sum_k a_k(t) \psi_k(\mathbf{r}, t), \quad (6.1)$$

where $a_k(t)$ are the amplitudes and

$$\psi_k(\mathbf{r}, t) = \varphi_k(\mathbf{r}) e^{-iE_k t/\hbar} \quad (6.2)$$

are the mutual orthogonal eigenstates.

Inserting (6.1) into the Schrödinger equation

$$\left(-\frac{\hbar^2 \nabla^2}{2m} + V(r) \right) \psi(\mathbf{r}, t) = i\hbar \frac{\partial}{\partial t} \psi(\mathbf{r}, t) \quad (6.3)$$

we immediately find the coupled channel equation for the amplitudes a_k

$$\dot{a}_k = -\frac{i}{\hbar} \sum_j V_{kj} a_j. \quad (6.4)$$

In order to solve the coupled channel equations, one needs to specify initial conditions. We assume that the pionium is initially in a state i , then

$$\begin{aligned} a_i(t \rightarrow -\infty) &= 1, \\ a_{j \neq i}(t \rightarrow -\infty) &= 0. \end{aligned} \quad (6.5)$$

Because the expansion of the wave function is in terms of mutual orthogonal eigenstates, the amplitudes a_k can be interpreted as occupation amplitudes in the limit $t \rightarrow \pm\infty$.

The probability for an excitation from an initial state i to any of the final states k , taken into account in the calculation, is

$$P_k(b) = |a_k(t \rightarrow \infty)|^2. \quad (6.6)$$

The cross section is then the integral over the impact parameter b

$$\sigma_k = 2\pi \int_0^\infty P_k(b) b db. \quad (6.7)$$

But, as is well known from section 4.1.3, the integral over the impact parameter converges very poorly. Since we only want to check the validity of the Glauber approximation, we will instead compare values of $P_k(b)$ at certain b with the results from the Born and Glauber approximations.

6.2 Matrix element V_{kj} for bound-bound transitions

The main numerical problem is the efficient evaluation of the matrix element V_{kj} given by the integral

$$V_{kj} = \int d^3r \varphi_k^*(\mathbf{r}) [\Phi(\mathbf{r}/2) - \Phi(-\mathbf{r}/2)] \varphi_j(\mathbf{r}) e^{i\omega_{kj}t}, \quad (6.8)$$

where $\omega_{kj} = (E_k - E_j)/\hbar$. The potential Φ is a screened Coulomb potential of the target nucleus with parameters A_k and α_k taken from [37]. Written in Fourier space (refer to section 4.1.1), the potential becomes

$$\Phi(\mathbf{r}, t) = \frac{Ze^2}{2\pi^2} \sum_k A_k \int d^3s \frac{e^{i\mathbf{s}\cdot(\mathbf{r}-\mathbf{R}(t))}}{s^2 + \alpha_k^2 - (\beta s_z)^2}, \quad (6.9)$$

where $\mathbf{R}(t) = (b, 0, vt)$ describes the straight-line trajectory.

We can rewrite (6.8) as

$$\begin{aligned} V_{kj} &= \frac{Ze^2}{2\pi^2} e^{i\omega_{kj}t} \sum_i A_i \int d^3s \frac{e^{-i\mathbf{s}\cdot\mathbf{R}(t)}}{s^2 + \alpha_i^2 - (\beta s_z)^2} \\ &\quad \times \int d^3r \varphi_k^*(\mathbf{r}) [e^{i\mathbf{s}\cdot\mathbf{r}/2} - e^{-i\mathbf{s}\cdot\mathbf{r}/2}] \varphi_j(\mathbf{r}). \end{aligned} \quad (6.10)$$

Now we apply the multipole expansion to the exponentials in the second line of (6.10):

$$\begin{aligned} e^{i\mathbf{s}\cdot\mathbf{r}/2} - e^{-i\mathbf{s}\cdot\mathbf{r}/2} &= 4\pi \sum_{lm} i^l [1 - (-1)^l] j_l(rs/2) \\ &\quad \times Y_{lm}^*(\hat{\mathbf{s}}) Y_{lm}(\hat{\mathbf{r}}). \end{aligned} \quad (6.11)$$

The wave functions φ_k can be split up into radial and angular parts

$$\varphi_k(\mathbf{r}) = R_{n_k l_k}(r) Y_{l_k m_k}(\hat{\mathbf{r}}), \quad (6.12)$$

where $R_{n_k l_k}(r)$ are the hydrogen-like bound or free wave functions.

If we insert (6.11) and (6.12) into (6.10) we obtain

$$\begin{aligned} V_{kj} &= \frac{2Ze^2}{\pi} e^{i\omega_{kj}t} \sum_i A_i \int d^3s \frac{e^{-i\mathbf{s}\cdot\mathbf{R}(t)}}{s^2 + \alpha_i^2 - (\beta s_z)^2} \sum_{lm} i^l [1 - (-1)^l] Y_{lm}^*(\hat{\mathbf{s}}) \\ &\times \int dr r^2 R_k(r) j_l(rs/2) R_j(r) \int d^2\hat{r} Y_{l_k m_k}^*(\hat{\mathbf{r}}) Y_{lm}(\hat{\mathbf{r}}) Y_{l_j m_j}(\hat{\mathbf{r}}). \end{aligned} \quad (6.13)$$

The integral over r in (6.13) is the radial form factor

$$F_{kj}^l(s) = \int dr r^2 R_k(r) j_l(rs) R_j(r), \quad (6.14)$$

which can be evaluated efficiently for bound-bound transitions by a recursion relation given in [40]. For bound-free transitions a method is outlined by Halabuka et al. [13] (see section 4.1.2).

The angular integral in (6.13) can be evaluated in terms of $3j$ -symbols

$$\int d\hat{r} Y_{l_k m_k}^*(\hat{\mathbf{r}}) Y_{lm}(\hat{\mathbf{r}}) Y_{l_j m_j}(\hat{\mathbf{r}}) = (-1)^{m_j} \frac{\hat{l}_k \hat{l}_j}{\sqrt{4\pi}} \begin{pmatrix} l_k & l & l_j \\ 0 & 0 & 0 \end{pmatrix} \begin{pmatrix} l_k & l & l_j \\ -m_k & m & m_j \end{pmatrix}, \quad (6.15)$$

with $\hat{l} = \sqrt{2l+1}$.

Now we can insert (6.14) and (6.15) into (6.13) and we obtain

$$\begin{aligned} V_{kj} &= \frac{Ze^2}{\pi^{3/2}} \hat{l}_k \hat{l}_j (-1)^{m_k} e^{i\omega_{kj}t} \sum_i A_i \int d^3s \frac{e^{-i\mathbf{s}\cdot\mathbf{R}(t)}}{s^2 + \alpha_i^2 - (\beta s_z)^2} \\ &\times \sum_{lm} i^l [1 - (-1)^l] \hat{l} \begin{pmatrix} l_k & l & l_j \\ 0 & 0 & 0 \end{pmatrix} \begin{pmatrix} l_k & l & l_j \\ -m_k & m & m_j \end{pmatrix} Y_{lm}^*(\hat{\mathbf{s}}) F_{kj}^l(s/2). \end{aligned} \quad (6.16)$$

We proceed by evaluating the angular part of the integral over \mathbf{s} as far as possible,

$$I_{lm}^i(s) = A_i \int d\hat{\mathbf{s}} \frac{Y_{lm}^*(\hat{\mathbf{s}}) e^{-i\mathbf{s}\cdot\mathbf{R}(t)}}{s^2 + \alpha_i^2 - (\beta s_z)^2}. \quad (6.17)$$

Firstly, we separate the spherical harmonics into ϑ_s and φ_s dependent components

$$Y_{lm}^*(\hat{\mathbf{s}}) = Y_{lm}(\vartheta_s, 0) e^{-im\varphi_s}. \quad (6.18)$$

Then we write the components of \mathbf{s} in terms of the spherical coordinates

$$s_x = s \sin \vartheta_s \cos \varphi_s, \quad (6.19a)$$

$$s_y = s \sin \vartheta_s \sin \varphi_s, \quad (6.19b)$$

$$s_z = s \cos \vartheta_s. \quad (6.19c)$$

Thus the scalar product becomes

$$\mathbf{s} \cdot \mathbf{R}(t) = bs \sin \vartheta_s \cos \varphi_s + vts \cos \vartheta_s. \quad (6.20)$$

Inserting (6.18) and (6.20) into (6.17) we obtain

$$\begin{aligned} I_{lm}^i(s) = & A_i \int_0^\pi d\vartheta_s \sin \vartheta_s \frac{Y_{lm}(\vartheta_s, 0) e^{-ivts \cos \vartheta_s}}{s^2(1 - \beta^2 \cos^2 \vartheta_s) + \alpha_i^2} \\ & \times \int_0^{2\pi} d\varphi_s e^{-i(m\varphi_s + bs \sin \vartheta_s \cos \varphi_s)}, \end{aligned} \quad (6.21)$$

where the φ_s -integral is an integral representation of the Bessel function J_m [39]

$$J_m(x) = \frac{i^m}{2\pi} \int_0^{2\pi} d\varphi_s \exp[-i(m\varphi + x \cos \varphi_s)]. \quad (6.22)$$

We can write

$$I_{lm}^i(s) = \frac{2\pi A_i}{i^m} \int_0^\pi d\vartheta_s \sin \vartheta_s J_m(bs \sin \vartheta_s) \frac{Y_{lm}(\vartheta_s, 0) e^{-ivts \cos \vartheta_s}}{s^2(1 - \beta^2 \cos^2 \vartheta_s) + \alpha_i^2} \quad (6.23a)$$

$$= \frac{2\pi A_i}{i^m} \int_{-1}^1 dx J_m(bs \sqrt{1-x^2}) \frac{Y_{lm}(\cos^{-1} x, 0) e^{-ivts x}}{s^2(1 - (\beta x)^2) + \alpha_i^2}, \quad (6.23b)$$

where we set $x = \cos \vartheta_s$.

To prepare the result for easier numerical implementation, we replace the spherical harmonics by the associated Legendre polynomials (which are more readily provided by numerical computation libraries)

$$Y_{lm}(\vartheta, 0) = \sqrt{\frac{2l+1}{4\pi}} \sqrt{\frac{(l-m)!}{(l+m)!}} P_l^m(\cos \theta), \quad (6.24)$$

to obtain

$$I_{lm}^i(s) = \frac{\sqrt{\pi} \hat{l} A_i}{i^m} \sqrt{\frac{(l-m)!}{(l+m)!}} \int_{-1}^1 dx \frac{P_l^m(x) J_m(bs \sqrt{1-x^2}) e^{-ivts x}}{s^2(1 - \beta^2 x^2) + \alpha_i^2}. \quad (6.25)$$

Looking back to (6.16), we see from the term $[1 - (-1)^l]$ that l must be odd. We now rewrite the integral over x in two ways for m odd or m even. We use the symmetry relation

$$P_l^m(-x) = (-1)^{l+m} P_l^m(x), \quad (6.26)$$

and because l is odd we have

$$P_l^m(-x) = (-1)^{m+1} P_l^m(x) \quad \text{for } l \text{ odd.} \quad (6.27)$$

We change the integration over x over the interval $[-1, 1]$ to an interval from $[0, 1]$ using the symmetry or anti-symmetry of the Legendre polynomials

$$\begin{aligned} \int_{-1}^1 dx \frac{P_l^m(x) J_m(bs\sqrt{1-x^2}) e^{-ivtsx}}{s^2(1-\beta^2x^2) + \alpha_i^2} &= \int_{-1}^0 + \int_0^1 \\ &= \int_0^1 dx \frac{(-1)^{m+1} P_l^m(x) J_m(bs\sqrt{1-x^2}) e^{ivtsx}}{s^2(1-\beta^2x^2) + \alpha_i^2} \\ &\quad + \int_0^1 dx \frac{P_l^m(x) J_m(bs\sqrt{1-x^2}) e^{-ivtsx}}{s^2(1-\beta^2x^2) + \alpha_i^2} \end{aligned} \quad (6.28a)$$

$$= \int_0^1 dx \frac{P_l^m(x) J_m(bs\sqrt{1-x^2})}{s^2(1-\beta^2x^2) + \alpha_i^2} [(-1)^{m+1} e^{ivtsx} + e^{-ivtsx}] . \quad (6.28b)$$

The last term in (6.28b) can be evaluated for the two cases (m odd or even)

$$[(-1)^{m+1} e^{ivtsx} + e^{-ivtsx}] = \begin{cases} 2 \cos(vtsx) & \text{if } m \text{ is odd,} \\ -2i \sin(vtsx) & \text{if } m \text{ is even.} \end{cases} \quad (6.29)$$

So finally, by combining (6.25), (6.28b), and (6.29) we obtain

$$I_{lm}^i(s) = \frac{2\sqrt{\pi} \hat{l}A_i}{i^m} \sqrt{\frac{(l-m)!}{(l+m)!}} \int_0^1 dx \frac{P_l^m(x) J_m(bs\sqrt{1-x^2}) \cos(vtsx)}{s^2(1-\beta^2x^2) + \alpha_i^2} \quad (6.30)$$

for m odd and

$$I_{lm}^i(s) = -\frac{2\sqrt{\pi} \hat{l}A_i}{i^{m-1}} \sqrt{\frac{(l-m)!}{(l+m)!}} \int_0^1 dx \frac{P_l^m(x) J_m(bs\sqrt{1-x^2}) \sin(vtsx)}{s^2(1-\beta^2x^2) + \alpha_i^2} \quad (6.31)$$

for m even.

One can see that the potential V_{kj} as written in (6.16) except for the phase $\exp i\omega_{kj}t$ (which vanishes in the sudden limit) is always real-valued as we have

$$i^{l-m} = (-1)^{(l-m)/2} \quad \text{for } m \text{ odd,} \quad (6.32)$$

$$i^{l-m+1} = (-1)^{(l-m+1)/2} \quad \text{for } m \text{ even.} \quad (6.33)$$

The integral I_{lm}^i can be readily evaluated using methods for oscillatory functions. For example the routine `gsl_integration_qawo` from the GNU scientific library can be used to perform the numerical integration.

V_{kj} finally becomes

$$\begin{aligned}
V_{kj}(b, t) &= \frac{2Ze^2}{\pi} \hat{l}_k \hat{l}_j (-1)^{m_k} e^{i\omega_{kj}t} \int ds s^2 \sum_l (-1)^{(l-m)/2} [1 - (-1)^l] \hat{l}^2 \\
&\quad \times \begin{pmatrix} l_k & l & l_j \\ 0 & 0 & 0 \end{pmatrix} \begin{pmatrix} l_k & l & l_j \\ -m_k & m & m_j \end{pmatrix} \sqrt{\frac{(l-m)!}{(l+m)!}} F_{kj}^l(s/2) \\
&\quad \times \int_0^1 dx \sum_i A_i \frac{P_l^m(x) J_m(bs\sqrt{1-x^2}) \cos(vtsx)}{s^2(1-\beta^2x^2) + \alpha_i^2} \quad \text{for } m \text{ odd,}
\end{aligned} \tag{6.34}$$

$$\begin{aligned}
V_{kj}(b, t) &= -\frac{2Ze^2}{\pi} \hat{l}_k \hat{l}_j (-1)^{m_k} e^{i\omega_{kj}t} \int ds s^2 \sum_l (-1)^{(l-m+1)/2} [1 - (-1)^l] \hat{l}^2 \\
&\quad \times \begin{pmatrix} l_k & l & l_j \\ 0 & 0 & 0 \end{pmatrix} \begin{pmatrix} l_k & l & l_j \\ -m_k & m & m_j \end{pmatrix} \sqrt{\frac{(l-m)!}{(l+m)!}} F_{kj}^l(s/2) \\
&\quad \times \int_0^1 dx \sum_i A_i \frac{P_l^m(x) J_m(bs\sqrt{1-x^2}) \sin(vtsx)}{s^2(1-\beta^2x^2) + \alpha_i^2} \quad \text{for } m \text{ even.}
\end{aligned} \tag{6.35}$$

In this form, the matrix elements $V_{kj}(b, t)$ can now be evaluated numerically.

6.3 Solving the coupled channel equation

If one only includes bound states, one can evaluate the matrix elements and solve the system of differential equation (6.4) using, for example, Gear's method [59, 60]. By using tabulated matrix elements for a given impact parameter b with small enough time-steps, it is possible to solve the system of equations for $n \leq 6$ in a few minutes. (The tabulation of course takes much longer. The advantage is that one can in this way, rerun the calculation of the evolution with different initial states or step-sizes.)

Figures 6.1 and 6.2 show the evolution of the occupation probabilities ($|a_k|^2$) for the lowest states with $n \leq 3$. The target is a Pt-atom ($Z = 78$) and the system of base-states is chosen as all bound states with $n \leq 6$. One can see that the occupation probability for states other than the initial state, increases rapidly at close distances to the target atom and then approaches a constant value.

To confirm that the matrix elements are correct and that the numerical methods work correctly, we simultaneously solve the set of differential equations

$$\dot{a}_k^{(1)} = -\frac{i}{\hbar} \sum_j V_{kj} \delta_{ji} \tag{6.36}$$

which results in the Born approximation. By plotting both the results of the direct calculation of the occupation probability in the Born approximation (4.14) and the

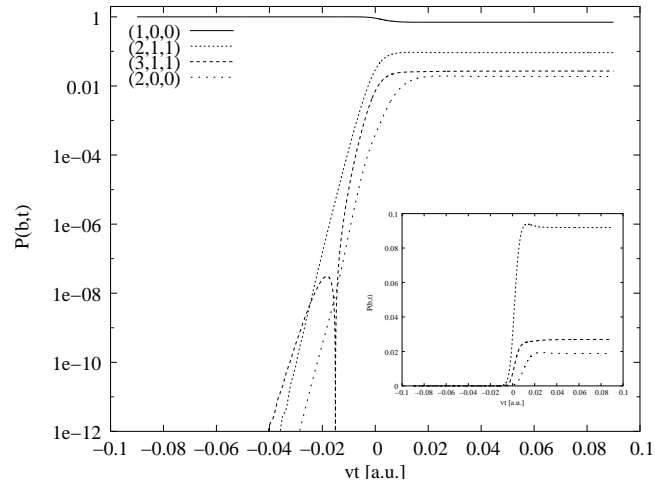


Figure 6.1: Time evolution of the occupation probabilities of pionium states in the interaction with Pt at impact parameter $b = 1 a_\pi$. The insert shows the same plot on a linear scale without the initial state (1,0,0).

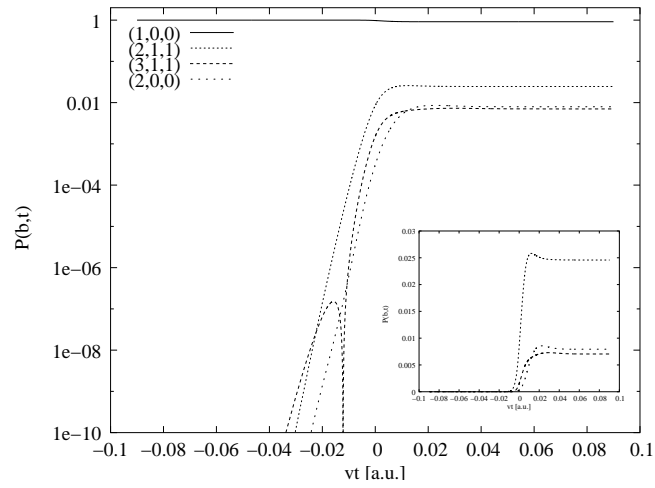


Figure 6.2: Time evolution of the occupation probabilities of pionium states in the interaction with Pt at impact parameter $b = 3 a_\pi$. The insert shows the same plot on a linear scale without the initial state (1,0,0).

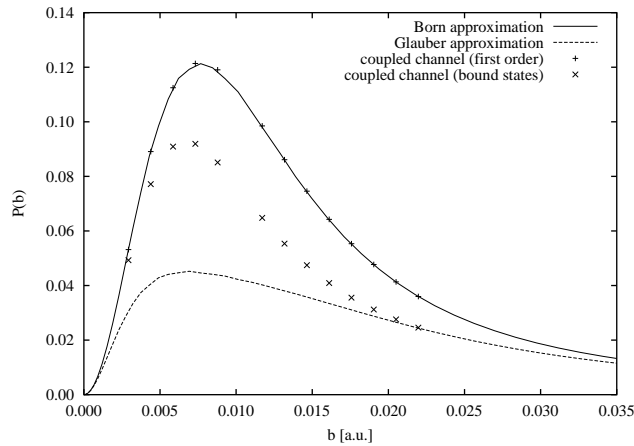


Figure 6.3: Comparison of coupled channel calculation for bound states only with the results from the Born and Glauber approximation. Plotted is the transition probability from a pionic 1s to a 2p state. The target is Pt ($Z = 78$).

asymptotic values of the solution to (6.36) one can compare the results. Figure 6.3 shows the transition probability from a 1s state to a 2p state due to the interaction with the Coulomb field of a Pt target atom. One can see that the Born approximation and the direct numerical evaluation of the time-integral agree quite well. The numerical procedure appears to work. However, the Glauber approximation and the full coupled channel calculation do not agree at all. For a Ni target (figure 6.4), the situation is similar, even though the difference between the results are not as large. For transitions to states with $n > 2$, shown in figures 6.5 and 6.6, the difference between the coupled channel and the Glauber results is even more pronounced.

6.4 Continuum states

One can argue that the discrepancy between the coupled channel calculation with bound states only and the Glauber calculation arises from not taking into account any continuum states for the pionic system. It was noted in chapter 5, table 5.1, (also refer to [13]), that for initial states with $n \leq 2$ ionization contributes a large part to the total cross section (up to 30%). Including at least some continuum states into the calculation should therefore lower the resulting transition probability for the bound states.

However, the coupling to the continuum is usually the main difficulty in a coupled channel calculation. Since the calculation of matrix elements for continuum-continuum transitions are numerically hard to do, we will neglect those transitions.

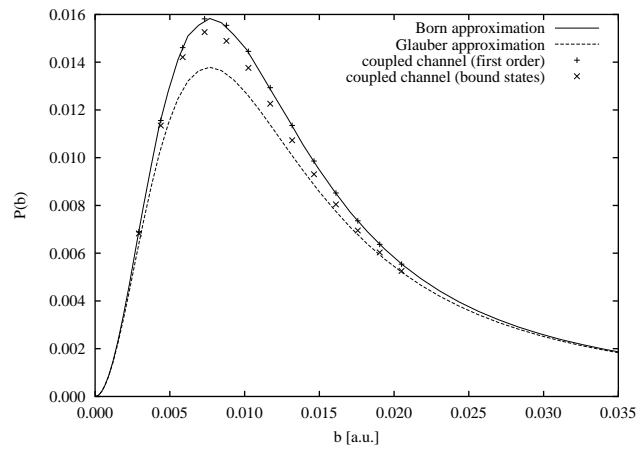


Figure 6.4: Comparison of a coupled channel calculation for bound states only, with the results from the Born and Glauber approximation. Plotted is the transition probability from a pionium $1s$ to a $2p$ state. The target is Ni ($Z = 28$).

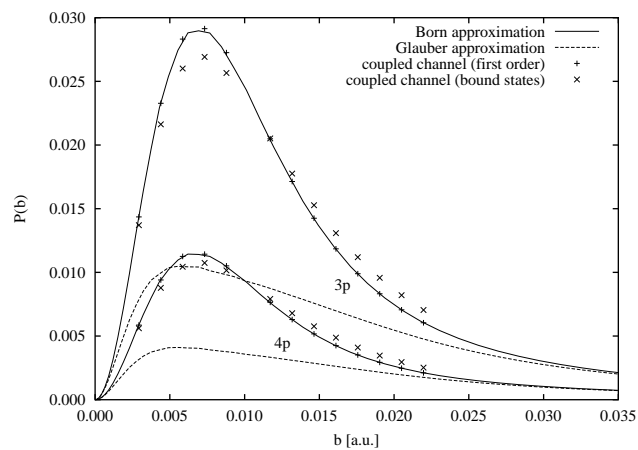


Figure 6.5: Comparison of a coupled channel calculation for bound states only, with the results from the Born and Glauber approximation. Plotted is the transition probability from a pionium $1s$ to $3p$ and $4p$ states. The target is Pt ($Z = 78$).

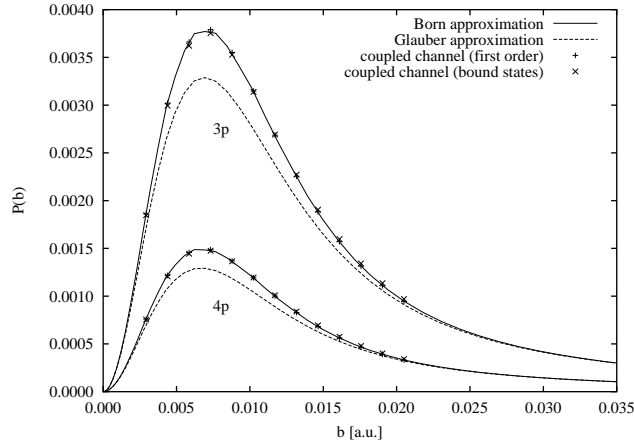


Figure 6.6: Comparison of a coupled channel calculation for bound states only, with the results from the Born and Glauber approximation. Plotted is the transition probability from a ponium 1s to 3p and 4p states. The target is Ni ($Z = 28$).

6.4.1 Rescaling of the amplitudes

One very simple way to couple the ponium moving through the Coulomb field of the target atom, is not to track the transitions into continuum states at every time-step, but to simulate such a transition as happening only once at a certain time t_0 . This avoids us having to calculate the transition matrix for every bound-continuum transition at arbitrary times. Instead, we use the ionization probability $P_k^{\text{ion}}(b)$ that was calculated in first Born approximation and rescale all $a_k(b, t)$ at time t_0 via

$$a_k(b, t_0) \Leftarrow \sqrt{1 - P_k^{\text{ion}}(b)} a_k(b, t_0) . \quad (6.37)$$

One can justify this approach, because the ionization probability is usually largest for small distances to the target-nucleus. Figure 6.7 shows how the transition probabilities for transitions to the 2p, 3p, and 4p state from the ponium ground state vary with the time t_0 when the transition to the continuum is applied. One can compare the result with the ones shown in figures 6.3 and 6.5 at $b = 1 a_\pi$, in atomic units $b \approx 0.007$ a.u. The rescaling, if applied before the ponium passes the atom, does lower the transition probability and the transition probability comes closer to the result of the Glauber approximation. This is shown in figure 6.8 for a Pt target and in figure 6.9 for a Ni target. Unfortunately, even though there is a qualitative agreement for a 1s–2p transition, for 1s–3p and 1s–4p transitions (not plotted here), the results do not look convincing. This is not surprising, since the approximation is very crude. The transition probabilities, however, are suppressed by the right order of magnitude.

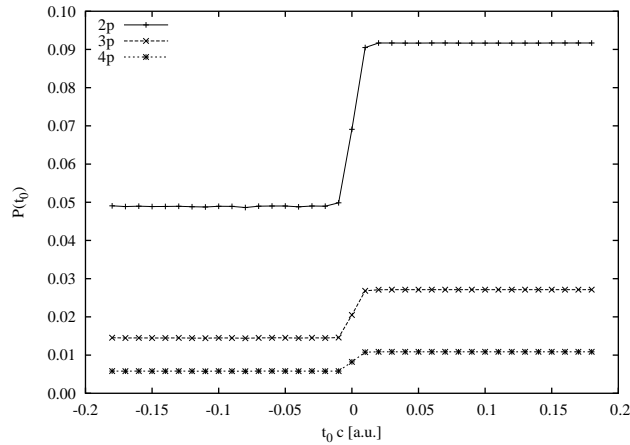


Figure 6.7: The transition probabilities for pionium interacting with a Pt target as a function of t_0 , the time when a rescaling due to ionization is applied. The impact parameter $b = 1 a_\pi$.

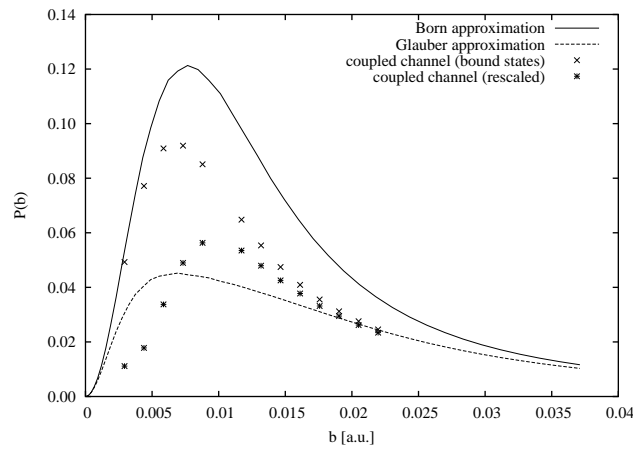


Figure 6.8: The transition probability from a $1s$ to a $2p$ state for pionium interacting with a Pt target, as a function of the impact parameter b . We show the Born and Glauber approximation as solid and dashed lines. The \times indicates the result from the coupled channel calculation only taking into account bound states as the basis set, the $*$ indicates the results of a coupled channel calculation with the rescaling as defined in (6.37) applied at $ct_0 = 0.02$.

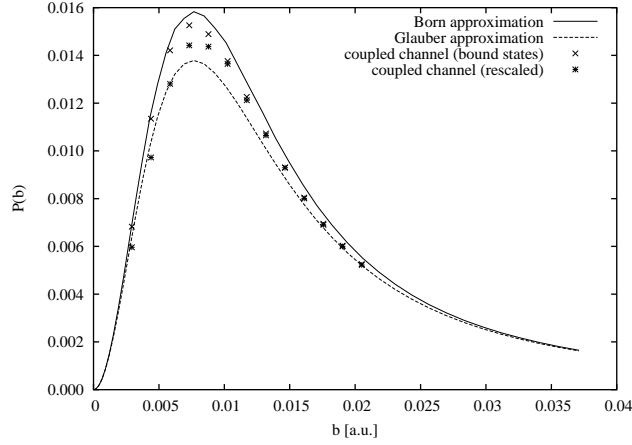


Figure 6.9: The transition probability from a 1s to a 2p state for pionium interacting with a Ni target, as a function of the impact parameter b . We show the Born and Glauber approximation as solid and dashed lines. The \times indicates the result from the coupled channel calculation only taking into account bound states as the basis set, the $*$ indicates the results of a coupled channel calculation with the rescaling as defined in (6.37) applied at $ct_0 = 0.02$.

6.4.2 Weyl wave packets

A more sophisticated method to describe continuum states of pionium is the use of Weyl wave packets. One needs to split a certain energy range into finite intervals centered around E_k with a width ΔE_k . If one integrates the exact continuum wave function $\phi_E \exp(-iEt/\hbar)$ over the energy interval, one obtains the Weyl wave packets

$$\Psi_{E_k}(\mathbf{r}, t) = \frac{1}{\sqrt{\Delta E_k}} \int_{E_k - \Delta E_k/2}^{E_k + \Delta E_k/2} \phi_E(\mathbf{r}) e^{-i(E-E_k)t/\hbar} dE. \quad (6.38)$$

Since the continuum wave functions are normalized on the energy and the energy intervals do not overlap, the Weyl wave packets are orthonormal. One can also use stationary wave packets, $\Psi_{E_k}(\mathbf{r}, t) = \phi_{E_k}(\mathbf{r}) \exp(-iE_k t/\hbar)$, which have the advantage that the integration over the energy interval does not contain the oscillating exponential

$$\phi_{E_k}(\mathbf{r}) = \frac{1}{\sqrt{\Delta E_k}} \int_{E_k - \Delta E_k/2}^{E_k + \Delta E_k/2} \phi_E(\mathbf{r}) dE. \quad (6.39)$$

One can insert the wave packet into (6.8) and separate the continuum wave function into angular and radial parts as before. The calculation of the matrix element is then analogous to section 6.2, except that one keeps the integral over the energy and replaces the radial form factor with the bound-free radial form factor discussed in section 4.1.2.

We have again tabulated the resulting matrix elements, but since the extra energy integral makes the numerical calculation very time-consuming, only data for a few

values of b are currently available ($b = 1.0, 1.2, 3.0 a_\pi$). The effect of the coupling to the continuum in this way turns out to be very small. At $b = 1.0$, e.g., the difference between the coupled channel calculation using only bound states and the one using the Weyl wave packets as well, amounts to 0.26%, at $b = 3.0$ it is 0.14%. We checked that the new matrix elements do have some effect on the solution of the coupled channel equations by scaling them with a factor larger than 1. This does indeed lower the final transition probability and changes in the final result are quite dramatic for even small changes in the scaling factor. This shows that a very fine balance is required to get a numerically stable result.

6.5 Conclusion

We have applied the coupled channel formalism to the problem of calculating the transition probability between two states of the pionium interacting with a target atom. We would have liked to show unambiguously that the Glauber calculation gives the correct results for the excitation cross sections. Since the calculations are very computer intensive, we only evaluate the transition probabilities as a function of the impact parameter, instead of the cross section.

The matrix elements for transitions between bound states have been tabulated and were verified by comparing the result of the numerical time-integration to the Born approximation. The coupled channel equations were solved using Gear's method. Taking into account a basis of bound-states up to $n = 6$, the resulting transition probabilities are lower than in Born approximation, as expected, but still much larger than the Glauber approximation.

Since ionization makes a large contribution to the total cross sections for low lying states, one can assume that including such effects in the coupled channel calculation will bring the results closer to the Glauber approximation. Using a simple model to include ionization effects by rescaling the occupation probability at a time when the pionium just about passes the target atom, gives a fairly reasonable result, close to the Glauber approximation.

A more sophisticated way of dealing with transitions into the continuum is to use pseudo states, for example the Weyl wave packets. The matrix elements between bound and continuum states take considerably more time to evaluate since another integral (over the energy E) is involved. The results using a limited set of continuum states do not improve compared to the ones using only bound states.

The coupled channel approach presented here, should in principle lead to a conclusive result to determine whether the large difference between Glauber and Born approximation (especially for heavy targets) is correct. To keep computation time reasonable, only limited sets of basis states can be included. So far, we can only verify, that the first order Born approximation does overestimate the true transition probability, but not whether the Glauber approximation gives a better estimate.

7 Monte Carlo simulation of the evolution of pionium

The DIRAC experiment aims to measure the lifetime of pionium. But, as was shown in chapter 2, it does not detect the decay products of the annihilation, but instead counts the number of pion pairs resulting from the breakup (ionization) of the $\pi^+\pi^-$ -atom. Taken together with the pionium production rate (2.8) this leads to an experimental value for the breakup probability. To translate this breakup probability into a value for the lifetime of pionium, a relationship between the two values needs to be found. We can arrive at a dependency (depending on the target materials) of the breakup probability on τ_0 , by simulating the evolution of pionium in the target using Monte Carlo methods. As input we use the cross sections calculated with the methods of chapter 4 (Born approximation) and chapter 5 (Glauber approximation for higher orders combined with first order Born approximation), as well as the results in first order sudden approximation of Afanasyev and Santamarina [61]. In this chapter, these cross section sets will be labeled *Born2*, *Glauber*, and *Born1*, respectively (ref. to section 7.3).

7.1 The simulation

The simulation of pionium starts with its creation according to the production cross section (2.8) and terminates when the $\pi^+\pi^-$ -atom has been annihilated, broken-up, or left the target in a bound state. In between we simulate the interaction of the $\pi^+\pi^-$ -atoms with the target atoms using the cross sections calculated in the previous chapters.

7.1.1 Pionium production

As it has been shown in section 2.3, pionium is created due to final state Coulomb interaction of two oppositely charged pions from the decay of short lived hadrons. Since the cross section describing the creation of pionium is proportional to the square of the hydrogen-like wavefunction at the origin, i.e. $\sim |\psi_{nlm}(0)|^2$, it is clear that pionium is produced in an S -wave state, since

$$|\psi_{nlm}(0)|^2 = \begin{cases} \frac{(\alpha M_\pi/2)^3}{\pi n^3} & \text{if } l = m = 0, \\ 0 & \text{if } l \neq 0. \end{cases} \quad (7.1)$$

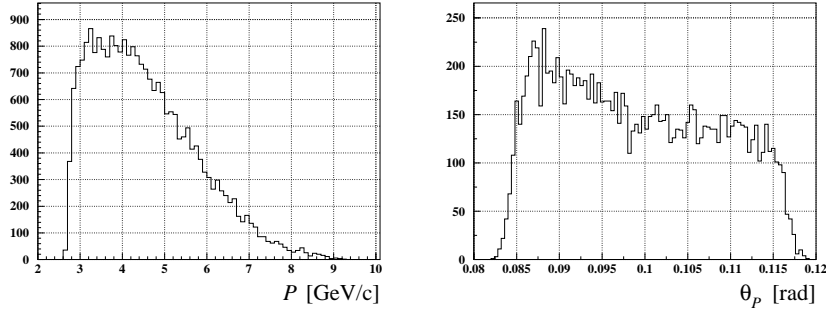


Figure 7.1: Laboratory momentum magnitude and angular distribution of low relative momentum $\pi^+\pi^-$ -atoms.

We can therefore set the initial quantum numbers of the $\pi^+\pi^-$ -atoms by drawing n from a $1/n^3$ distribution and letting $l = m = 0$.

The distribution of the initial momentum (magnitude and angular) is somewhat more complicated to do accurately and depends on experimental data (figure 7.1) Where available, this information has been used to specify the initial distribution of the laboratory momentum of the $\pi^+\pi^-$ -atoms, but using simplified initial conditions ($P = P_{\text{avg}}$, $\theta = 0$) made very little difference to the final result and made the simulation much easier to implement.

The final parameter to be specified before starting the simulation is the position of the ponium production. Since the target width was chosen such that the nuclear interaction length is much larger than the width, $\pi^+\pi^-$ -atoms are generated uniformly throughout the target. Furthermore, the transverse coordinates are unimportant, as the atoms travel very close to the beam direction (compare right-hand graph of figure 7.1) and will therefore only leave through the sides perpendicular to the proton beam.

7.1.2 Ponium annihilation

Once an atom has been created in its initial state, specified by \mathbf{P} , n , l , and m , its dynamics are those of a free system that can either be annihilated, mainly via the $\pi^+\pi^- \rightarrow \pi^0\pi^0$ channel [21], or be electromagnetically scattered by one of the target atoms.

The annihilation probability is inversely proportional to the lifetime of the atomic bound state. The strong interaction decay to two neutral pions dominates the lifetime and is related to the $a_0^0 - a_0^2$ scattering lengths difference and to the wave function at the origin by

$$\frac{1}{\tau_{nlm}} = \frac{16\pi}{9} \frac{\sqrt{M_\pi^2 - M_{\pi^0}^2 - \frac{1}{4}M_\pi^2 \alpha^2}}{M_\pi} (a_0^0 - a_0^2)^2 (1 + \delta_\Gamma) |\psi_{nlm}(0)|^2, \quad (7.2)$$

where M_π and M_{π^0} are the masses of the charged and the neutral pion, respectively, and δ_Γ is a correction to next-to-leading order ($\delta_\Gamma = 0.058$) [62]. Using Chiral Per-

turbation Theory, Colangelo *et al* [22] have been able to calculate the most precise value for the scattering lengths difference to date ($a_0^0 - a_0^2 = 0.265 \pm 0.004$). Employing this value in (7.2) yields

$$\tau_{100} = (2.9 \pm 0.1) \cdot 10^{-15} \text{ s}. \quad (7.3)$$

Note, however, that due to (7.1), pionium may only decay from S states. Moreover, the lifetime of any S state is related to the lifetime of the ground state, by

$$\tau_{n00} = n^3 \tau. \quad (7.4)$$

For the purpose of simulating pionium in the target, we shall from now on refer to τ as the *pionium lifetime*.

Hence, the probability for a $\pi^+\pi^-$ -atom to be annihilated per unit length, after the Lorentz transformation to the laboratory system, is given by

$$p_{nlm}^{\text{anh}} = \frac{1}{\lambda_{nlm}^{\text{anh}}} = \begin{cases} \frac{2M_\pi}{Pn^3\tau} & \text{if } l = m = 0, \\ 0 & \text{other cases,} \end{cases} \quad (7.5)$$

where $\lambda_{nlm}^{\text{anh}}$ is the annihilation mean free path.

7.1.3 Electromagnetic interaction of pionium with the target

The electromagnetic pionium–target scattering of a pionic atom in an initial nlm bound state can induce a transition to another $n'l'm'$ bound state. The probability of such an interaction per unit length is given by

$$p_{nlm}^{n'l'm'} = \frac{\rho N_0}{A} \sigma_{nlm}^{n'l'm'}, \quad (7.6)$$

where ρ is the target density, A its atomic weight, N_0 is the Avogadro number, and $\sigma_{nlm}^{n'l'm'}$ are the discrete (bound–bound) transition cross sections.

The breakup mechanism is analogous to the discrete one; the breakup probability per unit length of an atomic bound state nlm is given by

$$p_{nlm}^{\text{br}} = \frac{1}{\lambda_{nlm}^{\text{br}}} = \frac{\rho N_0}{A} \sigma_{nlm}^{\text{br}}, \quad (7.7)$$

where σ_{nlm}^{br} is the breakup (ionization) cross section.

Finally, the total cross section gives the probability of an atom to undergo an electromagnetic interaction and of course fulfills

$$\sigma_{nlm}^{\text{em}} = \sum_{n'l'm'} \sigma_{nlm}^{n'l'm'} + \sigma_{nlm}^{\text{br}}. \quad (7.8)$$

The total probability for a pionic atom to suffer an electromagnetic collision per unit length is then given by

$$p_{nlm}^{\text{em}} = \frac{1}{\lambda_{nlm}^{\text{em}}} = \frac{\rho N_0}{A} \sigma_{nlm}^{\text{em}}, \quad (7.9)$$

where $\lambda_{nlm}^{\text{em}}$ is the mean free path before an electromagnetic interaction takes place. Exploiting the completeness of the eigenstates of the Coulomb Hamiltonian the total electromagnetic cross sections can be calculated directly and not just via (7.8). In the previous chapters, the total cross section was usually indicated as σ^{tot} , it was calculated in the Born approximation in section 4 and in the Glauber approximation in section 5 equation (5.17).

The electromagnetic cross sections have been obtained with different approaches in [13, 14, 15, 17, 18] (refer also to chapters 4 and 5). We will devote section 7.4 to discussing the different breakup probabilities they lead to.

To get an insight into the magnitude of these interaction probabilities, we show in figure 7.2 the average values of the annihilation, ionization, de-excitation, and excitation probabilities per unit length. The average is taken over the even z -parity states (i.e., $l - m$ even) for fixed n . The atoms are created in even z -parity states ($l = m = 0$) and the transitions to odd z -parity states are strongly suppressed. The figure shows the probabilities using the coherent (interaction with the atom as a whole) contribution of the *Born2* set of cross sections. Any other choice among the cross section sets described in section 7.3, would lead to very similar results. The averages are defined as

$$\bar{p}_n^{\text{anh}} = \frac{1}{n(n+1)/2} \sum_{lm} p_{nlm}^{\text{anh}}, \quad (7.10)$$

$$\bar{p}_n^{\text{br}} = \frac{1}{n(n+1)/2} \sum_{lm} p_{nlm}^{\text{br}}, \quad (7.11)$$

$$\bar{p}_n^{n' < n} = \frac{1}{n(n+1)/2} \sum_{lm} \sum_{n' < n, l' m'} p_{nlm}^{n' l' m'}, \quad (7.12)$$

$$\bar{p}_n^{n' > n} = \frac{1}{n(n+1)/2} \sum_{lm} \left(p_{nlm}^{\text{em}} - p_{nlm}^{\text{br}} - \sum_{n' \leq n, l' m'} p_{nlm}^{n' l' m'} \right), \quad (7.13)$$

where $n(n+1)/2$ is the number of even z -parity states for a given n .

7.1.4 Pionium evolution in the target

To simulate the evolution of a pionic atom we use, in principle, the following algorithm:

1. We generate a laboratory momentum \mathbf{P} , an initial set of quantum numbers, and an initial position \mathbf{R} for the atom as described in subsection 7.1.1.

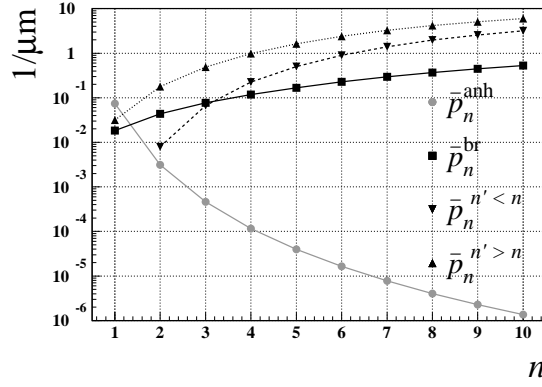


Figure 7.2: Annihilation, ionization, de-excitation and excitation probabilities per unit length according to equations (7.10), (7.11), (7.12), and (7.13).

2. We generate a free path according to:

$$p(x) dx = \frac{1}{\lambda_{nlm}} e^{-x/\lambda_{nlm}} dx \quad (7.14)$$

where $\lambda_{nlm} = \lambda_{nlm}^{\text{em}} \lambda_{nlm}^{\text{anh}} / (\lambda_{nlm}^{\text{em}} + \lambda_{nlm}^{\text{anh}})$ is the mean free path before either an interaction or the annihilation takes place.

3. We displace the atom by the distance x :

$$\mathbf{R}' = x \frac{\mathbf{P}}{P} + \mathbf{R}. \quad (7.15)$$

4. We determine whether the atom has been annihilated, excited (or de-excited) in a discrete collision, or broken up. The relative weights of the respective branches of the evolution are given by the probabilities of equations (7.5), (7.6), and (7.7).
5. If the atom has been scattered and suffered a discrete transition, we return to step 2 using the new quantum numbers n' , l' and m' and the new position \mathbf{R}' as the initial values.

7.2 Breakup probability calculation

In principle, the breakup probability calculation of ponium should be straightforward once we have established the Monte Carlo model. The rest would be a matter of generating an atom sample and computing how many of them break up in the target. However, two main difficulties arise when trying to implement the algorithm.

The first difficulty is due to the presence of an infinite number of atomic bound states in the calculations. Clearly, only a finite number of states can be taken into account in the simulation of the evolution of ponium. In our calculations we have

imposed a cut on the states with $n \leq n_{\max}$. This would not pose a serious problem if the atoms, being created mainly in very low n states, could not get highly excited. Unfortunately, excitation to ever higher lying bound states constitutes a major branch in the evolution of ponium. As a consequence we cannot directly calculate the breakup probability as outlined in the previous paragraph.

The second difficulty arises from the fact that we have not calculated the ionization cross section σ_{nlm}^{br} needed in (7.11) for all cross section sets. These cross sections are only available in first order Born approximation [13, 14, 15]. We therefore need an indirect way to compute the breakup probability without referring to the breakup probability per unit length.

We have discussed in the previous section that ponium terminates its evolution in the target by being either annihilated or broken up. However, the atom can also leave the target in a bound state. This would happen if one of the generated free paths in the Monte Carlo procedure carries it to a position outside the target. The breakup probability (P_{br}), the annihilation probability (P_{anh}), and the probability to leave the target in a discrete state (P_{dsc}) are related by:

$$1 = P_{\text{br}} + P_{\text{anh}} + P_{\text{dsc}} . \quad (7.16)$$

This equation allows us to compute the breakup probability indirectly.

7.2.1 Computational difficulties due to physical characteristics of the problem

The probability to generate an atom in a specific shell decreases as $1/n^3$. This means that the number of atoms created with $n \geq 4$ is very small. If the atoms could not get excited to states with large n , we could safely solve the evolution system by setting $n_{\max} > 4$. However, as we saw in figure 7.2, the atoms have a tendency to be excited, as n increases, rather than being annihilated or ionized.

Hence we expect a significant fraction of atoms excited into $n > n_{\max}$ shells, even for large values of n_{\max} . The probability of an atom in a nlm state to be excited into a state beyond the cut, i.e. with $n > n_{\max}$, is given by

$$p_{nlm}^{n' > n_{\max}} = p_{nlm}^{\text{em}} - p_{nlm}^{\text{br}} - \sum_{n' \leq n_{\max}, l' m'} p_{nlm}^{n' l' m'} \quad (7.17)$$

where we have used (7.6), (7.7) and (7.9). However, once the atom jumps into one of these states we lose control over it and we have to stop its evolution.

To analyze the change of the Monte Carlo results with n_{\max} we have modeled the evolution of a sample of atoms by changing n_{\max} from 7 to 9. We observed three main effects:

- The fraction of annihilated atoms ($P_{\text{anh}}(n \leq n_{\max})$) does not change significantly.

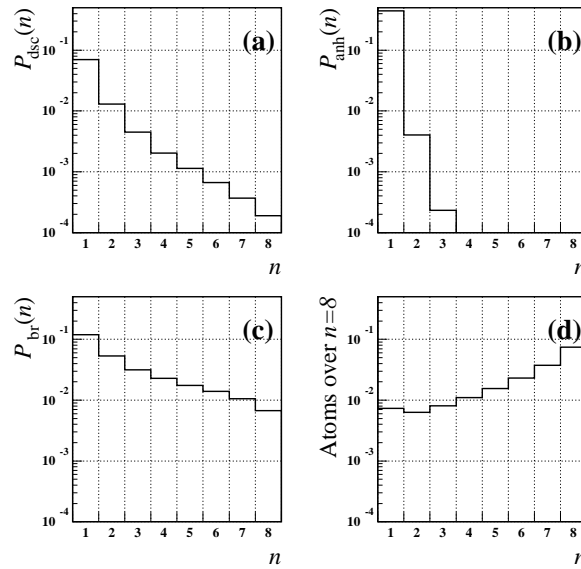


Figure 7.3: Probabilities of finishing the evolution in a discrete state (a), by annihilation (b), or by ionization (c) as a function of the parent state’s principal quantum number. In (d) we show the probability for an atom in a state n to be excited into a non-controlled state with $n > 8$. The results are for ponium in a $95 \mu\text{m}$ Ni target and the lifetime is assumed to be $3 \cdot 10^{-15}$ s.

- The portion of atoms leaving the target in discrete states ($P_{\text{dsc}}(n \leq n_{\text{max}})$) changes only slightly.
- The fraction of dissociated atoms ($P_{\text{br}}(n \leq n_{\text{max}})$) changes significantly.

This effect can be understood by checking the dependence of the annihilation, the discrete and the breakup probabilities on n , the principal quantum number of the state from which the atom was annihilated, broken-up, or in which it left the target. In figure 7.3 we show the result of the Monte-Carlo simulation with $n_{\text{max}} = 8$ for a sample of one million atoms using the *Born2* cross section set that also includes cross sections for the ionization (refer to section 7.3). For the annihilated atoms we can see that $P_{\text{anh}}(n)$ is negligible for values of $n \gtrsim 4$. The $P_{\text{dsc}}(n)$ dependence also shows a fast, but less drastic, decrease with n . Only the solution for the states with $n = n_{\text{max}} - 1$ or $n = n_{\text{max}} - 2$ is unstable under variation of n_{max} . For $n_{\text{max}} = 8$ this is a small contribution to the total P_{dsc} value. Finally, $P_{\text{br}}(n)$ decreases very slowly with n , showing that there is a significant fraction of atoms broken up from states with $n > n_{\text{max}}$. The probability of an atom to be excited into such a state with $n > n_{\text{max}}$ is also shown as a function of the principal quantum number of the last state before the excitation. Obviously, this effect is non-negligible.

For the cross section sets without breakup cross sections, we can only calculate directly the total probability for all electromagnetic processes and the probabilities for discrete transitions to states with $n' < n_{\text{max}}$. In these cases we cannot, therefore, dis-

tinguish whether an atom has been broken up or excited into a state with $n' > n_{\max}$, that is, we can only determine the *combination* of probabilities

$$p_{nlm}^{n' > n_{\max}} + p_{nlm}^{\text{br}} = p_{nlm}^{\text{em}} - \sum_{n' \leq n_{\max}, l'm'} p_{nlm}^{n'l'm'}. \quad (7.18)$$

This is, of course, equivalent to (7.17), but in this case p_{nlm}^{br} is unknown. Thus, for these cross section sets not even the breakup probability for low n states could be directly calculated and we are forced to use the procedure described below.

7.2.2 Calculation procedure

Based on the fast decrease of P_{anh} and P_{dsc} as a function of n we can assume that almost every atom excited to a state $n > n_{\max}$ will eventually be broken up. This is true even though the excitation probability per unit length of a given bound state is significantly larger than the breakup probability per unit length. We can explain it as follows. The mean free path of the excited atoms strongly decreases with increasing n . For $n \sim 8$ the mean free path is $\lesssim 0.1 \mu\text{m}$. An excited atom will thus interact many times within a very short distance. In every scattering event, the atom will have some small probability to break up, thereby terminating its evolution. In summary, the most probable evolution of an atom that has been excited to any state with $n \gtrsim 4$ is a sequence of excitations (and less frequent de-excitations) terminated by breakup.

However, while we are neglecting the atomic annihilation from states with $n > 8$ and thus setting $P_{\text{anh}} = P_{\text{anh}}(n \leq 8)$, we can estimate $P_{\text{dsc}}(n > 8)$ by means of a fit to the $P_{\text{dsc}}(n)$ histogram as recommended in [18]

$$P_{\text{dsc}}(n > 8) = \frac{a}{n^3} + \frac{b}{n^5}. \quad (7.19)$$

A simplified way to use (7.19) is to solve for the coefficients a and b with the values of $P_{\text{dsc}}(n_{\max} - 1)$ and $P_{\text{dsc}}(n_{\max} - 2)$ to obtain

$$a = \frac{(n-1)^5 P_{\text{dsc}}(n_{\max} - 1) - (n-2)^5 P_{\text{dsc}}(n_{\max} - 2)}{2n - 3}, \quad (7.20)$$

$$b = (n-1)^5 P_{\text{dsc}}(n_{\max} - 1) - a. \quad (7.21)$$

Now the sum over $P_{\text{dsc}}(n > n_{\max})$ can be performed and it can be written in terms of the polygamma function

$$\sum_{n=n_{\max}+1}^{\infty} P_{\text{dsc}}(n > n_{\max}) = -0.5a\Psi^2(n_{\max} + 1) - 1/24b\Psi^4(n_{\max} + 1), \quad (7.22)$$

which is defined as

$$\Psi^n(x) = \frac{d^n \ln(x)}{dx^n}. \quad (7.23)$$

Table 7.1: Results for the different probabilities defined in (7.16), as calculated with the *Born2* cross section set for a sample of ten million pionic atoms in a 95 μm thick Nickel target.

$\tau[10^{-15} \text{ s}]$	P_{br}	P_{anh}	$P_{\text{dsc}}(n \leq 8)$	$P_{\text{dsc}}(n > 8)$
1	0.2976	0.6527	0.0491	0.0006
2	0.3951	0.5287	0.0754	0.0008
3	0.4599	0.4451	0.0941	0.0009
4	0.5062	0.3848	0.1080	0.0010
5	0.5408	0.3392	0.1190	0.0010
6	0.5681	0.3029	0.1279	0.0011
7	0.5901	0.2740	0.1348	0.0011

Hence, taking into account (7.16) we obtain

$$P_{\text{br}} = 1 - P_{\text{dsc}} - P_{\text{anh}}, \quad (7.24)$$

where P_{dsc} consists of two parts,

$$P_{\text{dsc}} = P_{\text{dsc}}(n \leq 8) + P_{\text{dsc}}(n > 8), \quad (7.25)$$

of which $P_{\text{dsc}}(n \leq 8)$ is computed directly and $P_{\text{dsc}}(n > 8)$ is calculated from (7.19). In this manner, we can calculate the breakup probability even without ionization cross sections as input.

In table 7.1 and in figure 7.4 (top left) we show a few results for the probability for different lifetime values in a 95 μm Ni target. The target choice coincides with that of the DIRAC experiment. We observe that the result of $P_{\text{dsc}}(n > 8)$ adds only a small correction. In figure 7.4 we also show the ionization and annihilation distributions as a function of the target depth, and finally, the creation position for those atoms that managed to emerge from the target in a bound state. As emphasized in subsection 7.2.1, with increasing n only the atoms very near the target end will be able to leave the target in a discrete state.

7.3 Cross section sets

In our calculations of the breakup probability we employed three different sets of cross sections. The first two have been calculated in the framework of the Born approximation. We assign the labels *Born1* to the calculations made in reference [18] and *Born2* to those of [13, 14, 15]. The two sets differ in four main points:

- The *Born1* set neglects the contribution of incoherent scattering (collisions leading to an excitation of one or several electron(s) of the target atom), thus

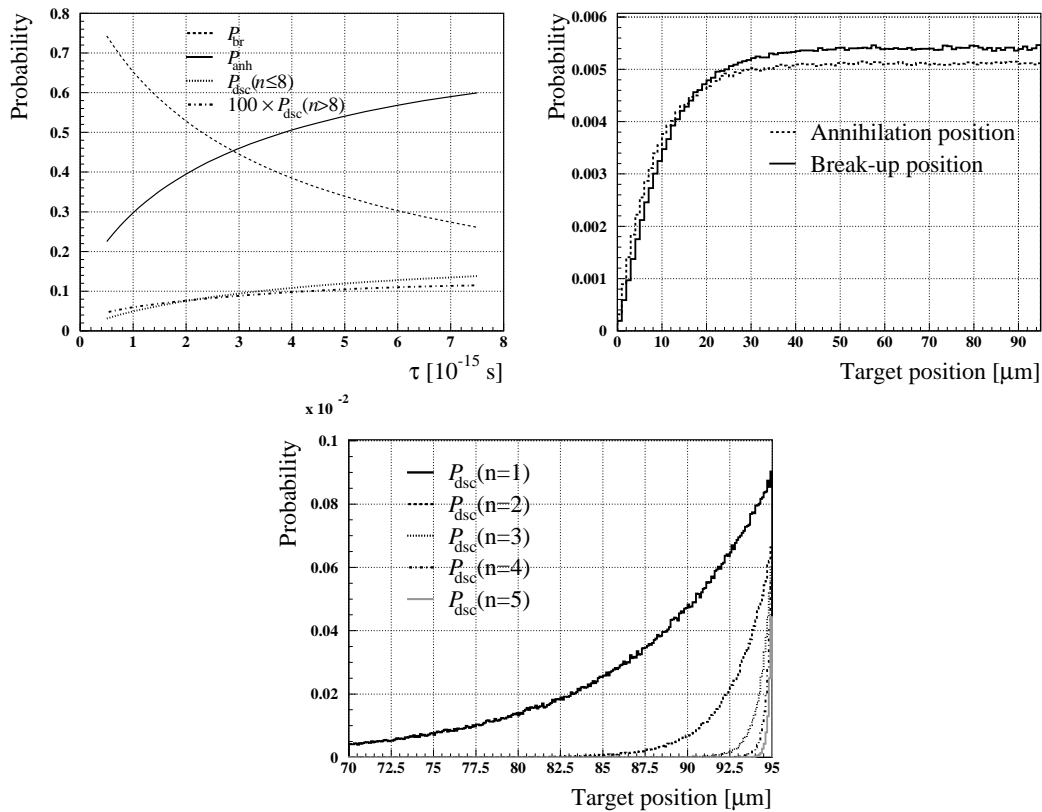


Figure 7.4: Top left: The breakup, annihilation, and discrete probabilities as a function of lifetime. Top right: Breakup and annihilation position distributions. Bottom: Creation position of those atoms that leave the target in a bound state (and contribute to P_{dsc}). Note that as n increases, only the atoms very near the target end can escape from it. All three plots refer to a 95 μm Ni target. In the last two, the lifetime is assumed to be $3 \cdot 10^{-15}$ s.

considering the coherent contribution only (collisions with the target atom as a whole), i.e. the leading term. By contrast the *Born2* set accounts for target excitations.

- The *Born1* set uses Molière’s parameterization [51] for the Thomas-Fermi equation solution as the target atom form factor of the pure electric interaction, whereas the *Born2* set takes electron orbitals determined numerically within the Hartree-Fock framework for the same purpose. The Thomas-Fermi-Molière parameterization of the atomic form factor is accurate for low momentum exchange, but gives a small excess for harder scattering.
- The *Born1* set considers the sudden approximation (no recoil energy for the target and the pionic atom) and neglects the energy difference between the initial and the final state, while the *Born2* set accounts for these two effects.
- Finally, the *Born2* set also considers the effect of magnetic and relativistic terms.

In principle it has been concluded [15] that accounting for second order effects like the magnetic terms of the Hamiltonian, the recoil energy of the atoms, or the relativistic terms, generally leads to an overall decrease of the sudden approximation pure electrostatic coherent cross section value due to destructive interference with the leading orders. Moreover, employing atomic orbitals obtained in the Hartree-Fock approach for the form factor used to compute these cross sections leads to lower values than those of the *Born1* set, since the Molière parameterization of the solution to the Thomas-Fermi equation is excessive for mean and large values of the photon momentum transfer. This last issue leads to discrepancies that increase for large n states and decrease for large Z target atoms. The difference appears to be balanced by neglecting the incoherent contribution to the cross section in the *Born1*. This results in a systematically smaller ground state cross section of the *Born1* set, whereas for larger n , the *Born1* cross sections are larger (up to $\sim 10\%$ discrepancy) or compatible with the *Born2* results. We show comparison of the different sets for three target materials in figure 7.5 and we shall analyze the disagreement in the breakup probability resulting from this effect.

Finally, we have also used a set of cross sections where the Glauber formalism has been applied to calculate the coherent contribution to the cross section value. The details are shown in [17]. This calculation technique accounts for multi-photon exchange in the pionium–target atom collision. Contrary to what one would expect, the consideration of more than one photon being exchanged diminishes the values of the cross sections due to a destructive interference of the n -photon exchange contributions (this happened also when accounting for magnetic terms in the *Born2* set). The leading order of the *Glauber* result matches the sudden approximation of the Born cross sections (since both neglect the difference between the initial and the final state energies). However, this cross section set uses a parameterization for the target atom form factors similar to the ones used in the *Born2* set. This explains the disagreement with respect to the *Born1* and the agreement with *Born2* set for low Z targets,

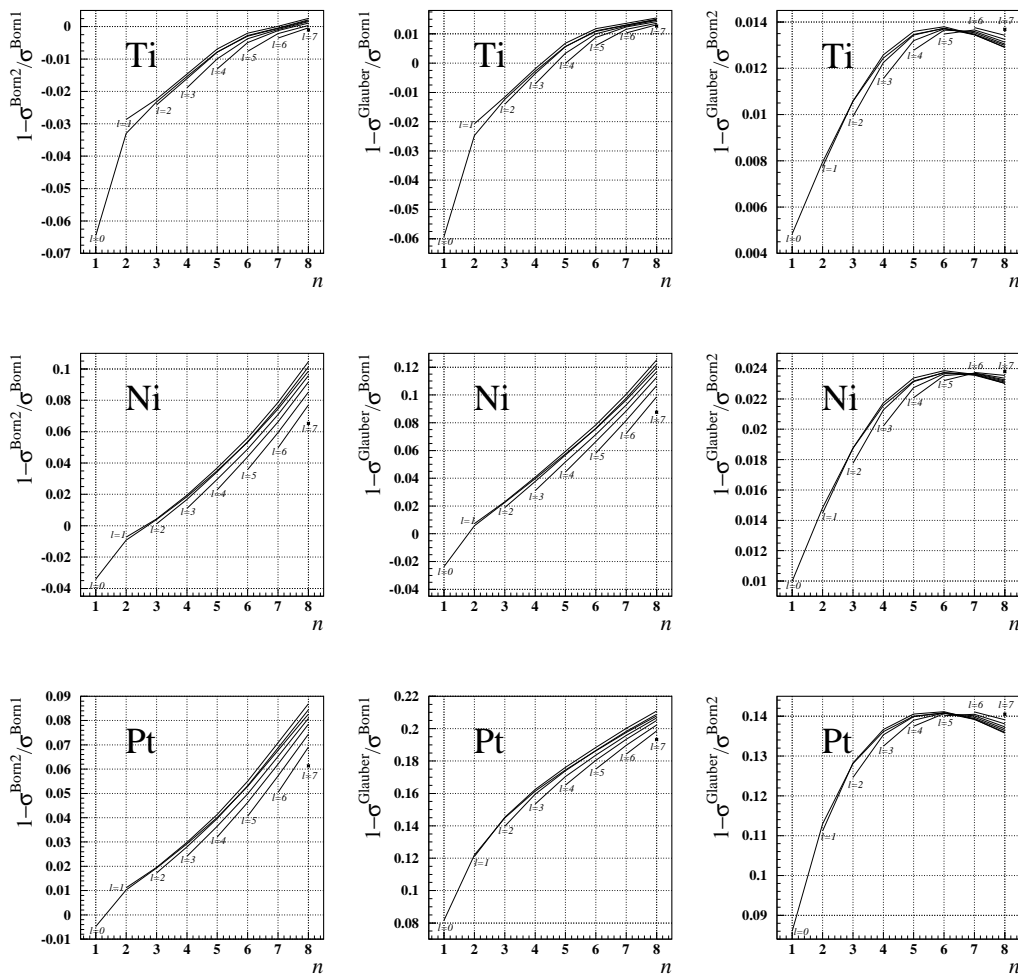


Figure 7.5: In the left column we compare the *Born1* and *Born2* cross section sets. The middle column shows a comparison of the *Born1* and *Glauber* sets and finally on the right we compare the *Born2* and *Glauber* sets. The comparison is made for Titanium ($Z = 22$), Nickel ($Z = 28$) and Platinum ($Z = 78$). The plots refer to total electromagnetic cross sections averaged over m for even z -parity states.

as can be seen in figure 7.5. The corrections due to multi-photon exchange are important for large Z targets [17] and this explains the large discrepancies obtained for Platinum.

7.4 Results and conclusions

After the discussions of the previous sections, we finally present the results of the breakup probability calculation. The DIRAC experiment has the possibility of choosing between several targets. These different targets have been designed to achieve the maximum breakup probability resolution in different lifetime ranges. Large Z targets with larger interaction cross sections are better suited for small lifetime values, whereas smaller Z materials are more sensitive to larger lifetime values. Three of these targets are the Pt 28 μm target, used for lifetime ranges $\tau < 1 \cdot 10^{-15}$ s, the Ni 95 μm target¹ for $\tau \sim 3 \cdot 10^{-15}$ s and the Ti 251 μm target for $\tau \sim 4 \cdot 10^{-15}$ s. The target thickness was chosen so as to have the same radiation length and hence equivalent multiple scattering effects for all three targets.

In figure 7.6, the breakup probability curves are shown for these three targets. The calculation has been carried out for samples of ten million events, with a statistical error less than 0.08%.

One can clearly see that for the Ti and Ni targets the *Glauber* and *Born2* sets lead to similar results whereas the *Born1* set shows an 8% disagreement. For the large Z target (Pt) both *Born1* and *Born2* are biased toward large values. In this case, the multi-photon contributions to the cross sections are significant. In any case, the discrepancies between the breakup probability results are at the level of the discrepancies between ground state cross sections and much smaller than the differences between the cross section sets for medium or highly excited states. We can understand this based on the fact that the probability for transitions to discrete states from states other than the ground state and maybe the first excited shell $P_{\text{dsc}}(n \gtrsim 2)$, is of the order of, or smaller than, 5%. Hence, even large uncertainties in this magnitude (up to 10 – 15%) lead to very small changes in the breakup probability result. Only discrepancies in the ground state population and maybe the first excited shell, where most of the atoms are created, would lead to significant differences between the breakup probability results of the different sets.

Graphically we can view the atom as a balloon being inflated in every collision with the target. The different sets will lead to similar size increase rates as long as the atom remains in a low excited state. However, as the atom grows (inflates), it will no longer be able to advance as easily in the target due to its large size and will finally break up (explode). Large discrepancies in the excitation and breakup rate of the excited atom will not be important given that the mean free paths for the excited states are very small compared to the target dimensions.

¹The Nickel target constitutes DIRAC's main target with which 90% of the data have been measured, as it is optimal for the theoretically predicted lifetime value.

Table 7.2: Comparison of the breakup probability results for the Ti 251 μm , the Ni 95 μm and the Pt 28 μm targets. The lifetime value is assumed to be $3 \cdot 10^{-15}$ s in the calculations.

Target	$P_{\text{br}}^{\text{Born1}}$	$P_{\text{br}}^{\text{Born2}}$	$P_{\text{br}}^{\text{Glauber}}$	$1 - \frac{P_{\text{br}}^{\text{Born2}}}{P_{\text{br}}^{\text{Born1}}}$	$1 - \frac{P_{\text{br}}^{\text{Glauber}}}{P_{\text{br}}^{\text{Born1}}}$	$1 - \frac{P_{\text{br}}^{\text{Glauber}}}{P_{\text{br}}^{\text{Born2}}}$
Ti	0.3026	0.3249	0.3232	-7.4%	-6.8%	0.5%
Ni	0.4425	0.4599	0.4555	-3.9%	-2.9%	1.0%
Pt	0.7137	0.7196	0.6924	-0.8%	3.0%	3.8%

In summary, the high precision measurement attempted by the DIRAC collaboration requires an accuracy to better than 1% in our theoretical breakup probability calculations. We note that the seemingly large discrepancies among our different cross section sets particularly for ponium transitions starting from highly excited states, do not lead to significant differences in the theoretical breakup probabilities. The discrepancies between breakup probabilities stem almost entirely from differences in the cross sections for the lowest lying states, where both the atomic structure of the target and the multi-photon transitions need to be treated as accurately as possible. This challenge, however, has already been mastered in our previous work [15, 17] where we showed that the required 1% accuracy can be achieved with our calculations, albeit only with the *Born2* and the *Glauber* sets for low Z and with the *Glauber* set for large Z targets. The important conclusion of the present investigation is the finding that the (infinitely many!) highly excited states of ponium do *not* limit the validity of our approach even though we can explicitly include only a moderate number of these states in our simulations.

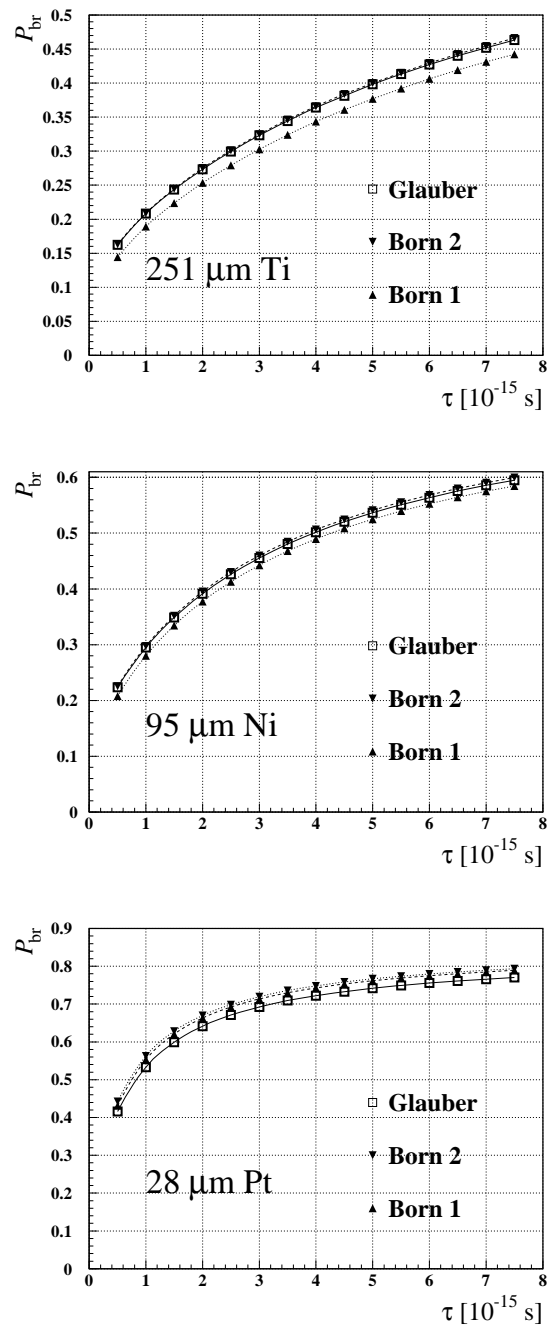


Figure 7.6: The breakup probability results for the three cross section sets and the three target materials.

8 Conclusions and outlook

For the success of the DIRAC experiment, the Coulomb interaction between target-atoms and ponium needs to be very well understood. The excitation, ionization, and total cross sections have been calculated in first order Born approximation to the highest level of accuracy. These calculations, at first, only included the major contribution due to the scalar potential. They were then extended to include target-excitations (incoherent scattering), which was seen to contribute quite strongly for targets with small nuclear charge Z . It was also shown that the corrections due to incoherent scattering cannot be estimated simply by scaling the coherent cross section with a factor $1 - 1/Z$. The first order Born calculations were completed by evaluating the terms containing the vector potential \mathbf{A} and relativistic corrections. The corrections due to terms containing one factor of \mathbf{A} turned out to be smaller than 1% and the others even smaller.

Higher order terms were evaluated in Glauber theory. As was known before for the total cross sections, they contribute significantly to the excitation cross sections, especially for targets with large Z . In fact, for Pt, e.g., the corrections can be about 24% for the excitation cross sections which is even larger than what had been found for the total cross sections. We compared the first few terms of the Glauber series to the full result. For small values of $Z < 10$ one can use the first order term only, for values up to $Z < 30$ including a second order correction is sufficient, and up to $Z < 60$ including third order terms is accurate enough. However, this procedure cannot be easily done for all transitions since second, third, etc., order corrections are already difficult to calculate for simple transitions. It seems best to do the full Glauber calculation and evaluate the higher order terms by the subtraction method that was presented in chapter 5.

Because the difference between first order Born and Glauber approximation is fairly large, we should be able to show in an independent calculation that the Glauber approximation indeed gives the correct result. The coupled channel approach was chosen. Including continuum states into the calculation was a problem that unfortunately could not be solved completely. The results that include only bound states as the basis for the wave function of ponium, already show that the Born approximation overestimates the transition probability. Using a rescaling procedure of the amplitudes lowers the transition probabilities even further so that they almost reach the Glauber transition probabilities. Including Weyl wave packets for the continuum basis states did not show any significant effect. From these results it is not conclusive that the Glauber approximation gives the most accurate values for the cross sections, but it could be shown that the Born approximation overestimates the correct results.

Finally, we calculated from the different cross sections the resulting relation between

the breakup probability and the lifetime, that is needed for the experiment DIRAC. A Monte Carlo simulation of ponium passing through the target was performed which shows that the differences between the cross section sets are significant. For light targets (Ti and Ni), the main contribution is the incoherent scattering, the relation between breakup probability and lifetime shows little effect if one includes the higher order corrections from the Glauber calculation. For the heavy target Pt, the main difference is due to the higher order corrections. It has been shown that the simulation can be performed even without information about the ionization cross sections. For the most accurate calculation of the relation between the lifetime of ponium and the breakup probability accessible by experiment, we suggest to use the very accurate coherent and incoherent first order Born results of [14, 15] together with the higher order corrections calculated in Glauber theory [17].

Further work should be done to clearly verify (or possibly reject) the Glauber results by a full coupled channel calculation. The evaluation of all the necessary matrix elements is very time consuming, however. One could also try to extend the Glauber approximation to include incoherent scattering and also to include the magnetic terms of the Hamiltonian. This does seem a formidable task, though, since one does not have a closed form for the eikonal in those cases. It would also be interesting to see how the results of the Monte Carlo simulation are affected by changing the cross sections systematically. This would give clearer information about how accurate they really need to be calculated. So far it is only stated that they need to be accurate to 1% or better.

It will be interesting to see the outcome of the experiment DIRAC in the next few years. Due to the experimental difficulties of extracting the ponium signal from the background, reaching the targeted accuracy of 10% for the lifetime (corresponding to about 4% for the breakup probability) will be a great achievement.

Bibliography

- [1] H. Fritzsche, M. Gell-Mann, and H. Leutwyler. *Phys. Lett. B*, 47:365, 1973. 1, 3
- [2] J. T. Friedman and H. W. Kendall. *Ann. Rev. Nucl. Science*, 22:203, 1972. 1, 3
- [3] J. C. Taylor. *Nucl. Phys. B*, 33:436, 1971. 1, 3
- [4] D. J. Gross and F. Wilczek. *Phys. Rev. D*, 8:3633, 1973. 1, 3
- [5] D. J. Gross and F. Wilczek. *Phys. Rev. Lett.*, 30:1343, 1973. 1, 3
- [6] S. Weinberg. *Phys. Rev. Lett.*, 17:616, 1966. 1, 4
- [7] Steven Weinberg. *Physica A*, 96:327, 1979. 1, 3
- [8] J. Gasser and H. Leutwyler. *Phys. Lett. B*, 125:325, 1983. 1, 3
- [9] J. Gasser and H. Leutwyler. *Ann. Phys. (N.Y.)*, 158:142, 1984. 1, 3, 4
- [10] J. Bijnens, G. Colangelo, G. Ecker, J. Gasser, and M. Saino. *Phys. Lett. B*, 374:210, 1996. 1, 4
- [11] G. Colangelo, J. Gasser, and H. Leutwyler. *Nucl. Phys. B*, 603:125, 2001. 1, 4
- [12] B. Adeva et al. Lifetime measurement of $\pi^+\pi^-$ atoms to test low energy QCD predictions. SP-SPC/P 284, CERN/SPSLC 95-1, 1994. <http://www.cern.ch/dirac>. 1, 3
- [13] Z. Halabuka, T. A. Heim, K. Hencken, D. Trautmann, and R. D. Viollier. *Nucl. Phys. B*, 554:86, 1999. 1, 25, 26, 32, 33, 34, 47, 49, 51, 55, 61, 66, 76, 78, 81
- [14] T. A. Heim, K. Hencken, D. Trautmann, and G. Baur. *J. Phys. B: At. Mol. Opt. Phys.*, 33:3583, 2000. 1, 25, 34, 35, 36, 39, 40, 42, 43, 47, 48, 56, 76, 78, 81, 90
- [15] Thomas A. Heim, Kai Hencken, Dirk Trautmann, and Gerhard Baur. *J. Phys. B: At. Mol. Opt. Phys.*, 34:3763, 2001. 1, 25, 46, 47, 48, 76, 78, 81, 83, 86, 90
- [16] L. G. Afanasyev, A. Tarasov, and O. Voskresenskaya. *J. Phys. G*, 25:B7, 1999. 2, 47, 50, 52, 57

- [17] Marc Schumann, Thomas A. Heim, Kai Hencken, Dirk Trautmann, and Gerhard Baur. *J. Phys. B: At. Mol. Opt. Phys.*, 35:2683, 2002. 2, 47, 76, 83, 85, 86, 90
- [18] L. G. Afanasyev and A. V. Tarasov. *Phys. At. Nuc.*, 59:2130, 1996. 2, 47, 76, 80, 81
- [19] Cibrán Santamarina Ríos. Monte Carlo calculation of ponium breakup probability. DIRAC 00-03, 2000. 2
- [20] C. Santamarina, M. Schumann, L. G. Afanasyev, and T. Heim. A monte carlo calculation of the ponium break-up probability with different sets of ponium target cross sections. submitted for publication in *J. Phys. B: At. Mol. Opt. Phys.*, 2003. 2
- [21] J. Uretsky and J. Palfrey. *Phys. Rev.*, 121:1798, 1961. 3, 4, 74
- [22] G. Colangelo, J. Gasser, and H. Leutwyler. *Phys. Lett. B*, 488:261, 2000. 3, 75
- [23] J. Gasser, V. E. Lyubovitskij, A. Rusetsky, and A. Gall. *Phys. Rev. D*, 64:016008, 2001. 3, 4
- [24] L. D. Landau and E. M. Lifshitz. *Quantum Mechanics (Non-Relativistic Theory)*. Pergamon Press, 3rd edition, 1976. 5
- [25] V. V. Uzhinskii. JINR preprint E2-96192, 1996. 5
- [26] B. Andersson et al. *Nucl. Phys. B*, 281:289, 1987. 5
- [27] B. Nilsson-Almquist and E. Stenlund. *Comp. Phys. Comm.*, 43:387, 1987. 5
- [28] L. G. Afanasyev et al. *Phys. At. Nucl.*, 60:938, 1997. 5
- [29] A. Lanaro. Highlights from DIRAC. Talk at CERN Seminar, Dec. 2001. 7, 9
- [30] Ch. P. Schuetz. The DIRAC experiment at CERN. preprint hep-ph/0305121, 2003. 8
- [31] J. Schacher. Double-exotic $\pi^+\pi^-$ atom and the CERN DIRAC experiment. http://www.lhep.unibe.ch/schacher/talks_03/ETH03.pdf, 2003. 9
- [32] R. J. Glauber. *Lectures in Theoretical Physics*, volume I, page 315. Interscience, New York, 1959. 15, 19, 50
- [33] Charles J. Joachain and C. Quigg. *Rev. Mod. Phys.*, 46(2):279, April 1974. 15, 50
- [34] C. J. Joachain. *Quantum Collision Theory*. North-Holland, Amsterdam, 1975. 15
- [35] R. J. Glauber. *Phys. Rev.*, 91:459, 1953. 19

- [36] R. J. Glauber. *Phys. Rev.*, 100(1):242, October 1955. 19
- [37] F. Salvat, J. D. Martínez, R. Mayol, and J. Parellada. *Phys. Rev. A*, 36:467, 1987. 26, 41, 49, 60
- [38] P. A. Amundsen and K. Ashamar. *J. Phys. B*, 14:4047, 1981. 28
- [39] M. Abramowitz and I. A. Stegun, editors. *Handbook of Mathematical Functions*. Dover, New York, 1965. 29, 30, 31, 32, 50, 62
- [40] D. Trautmann, G. Baur, and F. Rösel. *J. Phys. B*, 16:3005, 1983. 30, 31, 49, 61
- [41] I. Gradshteyn and I. Ryzhik. *Table of Integrals, Series and Product*. Academic Press, New York, 1964. 31, 44
- [42] R. Anhold. *Phys. Rev. A*, 31:3579, 1985. 34
- [43] J. H. McGuire, N. Stolterfoht, and P. R. Simony. *Phys. Rev. A*, 24:97, 1981. 34
- [44] J. A. Wheeler and W. E. Jr Lamb. *Phys. Rev.*, 55:858, 1939. 34
- [45] A. H. Sørensen. *Phys. Rev. A*, 58:2895, 1998. 34
- [46] A. B. Voitkiv, N. Grün, and W. Scheid. *Phys. Lett. A*, 260:240, 1999. 34
- [47] T. de Forest and J. D. Walecka. *Adv. Phys.*, 15:1, 1966. 34
- [48] F. Halzen and A. D. Martin. *Quarks and Leptons*. Wiley, New York, 1984. 34
- [49] W. Greiner and A. Schäfer. *Quantum Chromodynamics*. Springer, Berlin, 2nd edition, 1995. 34
- [50] K. Hencken, D. Trautmann, and G. Baur. *Z. Phys. C*, 68:473, 1995. 37
- [51] G. Molière. *Z. Naturforsch.*, 2a:133, 1947. 39, 41, 83
- [52] J. H. Hubbell, Wm. J. Veigele, E. A. Briggs, R. T. Brown, D. T. Cromer, and R. J. Howerton. *J. Phys. Chem. Ref. Data*, 4:471, 1975. 40
- [53] J. H. Hubbell and I. Øverbø. *J. Phys. Chem. Ref. Data*, 8:69, 1979. 40
- [54] H. A. Bethe and E. E. Salpeter. *Quantum Mechanics of One- and Two-Electron Atoms*. Plenum, New York, 1977. 43
- [55] A. B. Voitkiv, G. M. Sigaud, and E. C. Montenegro. *Phys. Rev. A*, 59:2794, 1999. 47
- [56] A. B. Voitkiv, N. Grün, and W. Scheid. *J. Phys. B: At. Mol. Opt. Phys.*, 33:3431, 2000. 47
- [57] H. Tai, R. H. Bassel, E. Gerjuoy, and V. Franco. *Phys. Rev. A*, 1:1819, 1970. 50

- [58] K. Alder and A Winther. *Electromagnetic excitation*. North-Holland, Amsterdam, 1975. 55
- [59] C. W. Gear. *Comm. ACM.*, 14:185, 1971. 64
- [60] C. W. Gear. *Comm. ACM.*, 14:176, 1971. 64
- [61] L. G. Afanasyev and C. Santamarina. DIRAC 00-04, CERN, 2000. 73
- [62] J. Gasser, V. E. Lyubovitskij, and A Rusetsky. *Phys. Lett. B*, 471:244, 1999. 74

Lebenslauf

Persönliche Daten

Marc Schumann
Neudorfstr. 26
8050 Zürich
Schweiz

Tel. (p): (++41 1) 3 11 54 92

Tel. (g): (++41 61) 2 67 37 53

Fax.: (++41 61) 2 67 13 49

E-Mail: Marc.Schumann@unibas.ch

Geb. am 27.03. 1972 in Hamm, Deutschland

Verheiratet, deutscher Staatsbürger

Schulbildung

- 08/1978–07/1982 Ludgeri Grundschule, Hamm
- 08/1982–07/1988 Gymnasium Hammonense, Hamm
- 08/1988–08/1989 Central Gwinnett High School, Lawrenceville, Georgia, USA,
High School Diploma
- 08/1989–06/1991 Gymnasium Hammonense, Abitur (Leistungskurse Mathematik
und Physik), Notendurchschnitt 1,7

Zivildienst

- 06/1991–10/1992 Zivildienst bei der Arbeiterwohlfahrt in Hamm, tätig im mobilen
sozialen Hilfsdienst

Studium

- 10/1992–01/1995 Technische Universität Clausthal, Vordiplome (10/1994) in Ma-
thematik und in Physik, Durchschnittsnoten jeweils 1,3
- 01/1995–12/1995 University of Cape Town, Südafrika,
Bachelor of Science (Honours) in Theoretical Physics (First
Class)
- 01/1996–03/1998 University of Cape Town, Südafrika,
Master of Science in Theoretical Physics (with distinction)
Titel der Arbeit: „Two-Gluon Exchange Graphs in Cavity QCD
to Order α_s^2 “
- 03/1998–12/1999 Univerisity of Cape Town, Südafrika,
Doktorand bei Prof. R.D. Viollier

01/2000–07/2003 Universität Basel, Schweiz,
Fortsetzung der Promotion bei Prof. D. Trautmann
Thema: „Excitation and Breakup of $\pi^+\pi^-$ -Atoms at High Energies“

Anstellungen

04/1994–02/1995 Assistent im Physikpraktikum der Drittsemester und System Administrator im CIP Pool des Physikinstituts an der TU Claus-thal

02/1995–12/1995 Übungsleiter im Physikpraktikum der Erstsemester in Kapstadt

02/1996–12/1997 Übungsleiter in den Vorlesungen Quantenmechanik und Statistische Mechanik im Honours Course

02/1998–12/1999 Übungsleiter in den Viertsemesterkursen Quantenmechanik und Klassische Mechanik, sowie Quantenmechanik im Honours Course

seit 01/2000 Assistent am Institut für Physik, Universität Basel, Übungsleiter in Physik III und Elektrodynamik

seit 04/2002 Systemadministrator für den Beowulf Cluster der theoretischen Physik mit Verantwortung für den Betrieb sowie der Planung und Einkauf von Erweiterungen

Stipendien und Auszeichnungen

02/1997–12/1999 Stipendium für ausländische Studenten von der Universität Kapstadt

2000 Research Associate an der Universität Kapstadt

seit 01/2000 Stipendium vom Schweizerischen Nationalfond

Fremdsprachen

Englisch (mehrjähriger Auslandsaufenthalt in den USA und in Südafrika)

Publikationen

1. M. Schumann, *Two-Gluon Exchange Graphs in Cavity QCD to Order α_s^2* , M.Sc. Thesis, University of Cape Town (1998).
2. R. Hofmann, M. Schumann, R.D. Viollier, *Calculation of the regularized vacuum energy in cavity field theories*, Eur. Phys. J. C **11**, 153–161 (1999).
3. M. Schumann, R.J. Lindebaum, R.D. Viollier, *Hadron masses in cavity quantum chromodynamics to order α_s^2* , Eur. Phys. J. C. **16**, 331–336 (2000).

4. R. Hofmann, M. Schumann, T. Gutsche, R.D. Viollier, *Vacuum structure of a modified MIT bag*, Eur. Phys. J. C. **16**, 677–681 (2000).
5. T. Heim, M. Schumann, K. Hencken, D. Trautmann, G. Baur, *Der elektromagnetische Aufbruch des Pionium für das DIRAC Experiment*, 22. Arbeitsbericht des Arbeitskreises Energiereiche Atomare Stöße, 142–146 (2001).
6. T. Heim, K. Hencken, M. Schumann, D. Trautmann, G. Baur, *Distribution of pions from breakup of pionium, Higher order corrections to the bound-bound excitation cross section of pionium, Calculation of electromagnetic breakup of pionium*, Proceedings of HadAtom01, arXiv:hep-ph/0112293, 13–15, (2001).
7. M. Schumann, T. Heim, K. Hencken, D. Trautmann, G. Baur, *Excitation cross-sections for pionium in the Glauber approximation*, J. Phys. B: At. Mol. Opt. Phys. **35**, 2683-2692 (2002).
8. M. Schumann, T. Heim, K. Hencken, D. Trautmann, G. Baur, *Anwendung der Glauber Theorie zur Berechnung der Anregungsquerschnitte von Pionium*, 23. Arbeitsbericht des Arbeitskreises Energiereiche Atomare Stöße, (2002).
9. T. Heim, K. Hencken, M. Schumann, D. Trautmann, G. Baur, *Coupled channel approach to breakup of pionium*, Proceedings of HadAtom02 (2002).
10. C. Santamarina, M. Schumann, L.G. Afanasyev, T. Heim, *A Monte Carlo calculation of the pionium breakup probability with different sets of pionium target cross sections*, submitted to J. Phys. B: At. Mol. Opt. Phys. (2003).

An der Ausbildung beteiligte Dozenten

TU-Clausthal	Prof. Dr. J. Albrecht, Prof. Dr. E. Bauer, Prof. Dr. H.-D. Doebner, Dr. K. Faulian, Prof. Dr. J. Hennig, Prof. Dr. V. Kempter, Dr. G. Lilienkamp, Prof. Dr. L. Lucht, Prof. Dr. D. Mayer, Prof. Dr. H.Pfnür, Dr. H. Roscher, Prof. Dr. H.J. Weinert
Univ. Cape Town	Prof. Dr. D. Ashman, Dr. N. Bilic, Dr. P. Cherenack, Prof. Dr. J. Cleymans, Prof. Dr. C. Dominguez, Prof. Dr. H. Driver, Prof. Dr. G. Ellis, Dr. G. Krychev, Prof. Dr. G. Robertson, Prof. Dr. R. Viollier
Univ. Basel	Prof. Dr. U. Aeschbacher, T. Ahrend, Prof. Dr. G. Baur, PD Dr. W. Breymann, PD Dr. T. Heim, PD Dr. K. Hencken, PD Dr. H. Mühri, Prof. Dr. D. Trautmann, PD Dr. H. Walser

Zürich, 9. Juli 2003

